UNIVERSIDAD COMPLUTENSE DE MADRID
FACULTAD DE CIENCIAS FÍSICAS

TESIS DOCTORAL

Statistical physics applied to population dynamics

Física estadística aplicada a la dinámica de Poblaciones

MEMORIA PARA OPTAR AL GRADO DE DOCTOR

PRESENTADA POR

Rodrigo Crespo Miguel

Director

Francisco Javier Cao García

Madrid

UNIVERSIDAD COMPLUTENSE DE MADRID
FACULTAD DE CIENCIAS FÍSICAS

TESIS DOCTORAL

STATISTICAL PHYSICS APPLIED TO POPULATION DYNAMICS
FÍSICA ESTADÍSTICA APLICADA A LA DINÁMICA DE POBLACIONES

MEMORIA PARA OPTAR AL GRADO DE DOCTOR

PRESENTADA POR

Rodrigo Crespo Miguel

DIRECTOR

Francisco Javier Cao García

UNIVERSIDAD COMPLUTENSE DE MADRID
FACULTAD DE CIENCIAS FÍSICAS
Departamento de Estructura de la Materia, Física Térmica y Electrónica

UNIVERSIDAD
COMPLUTENSE
MADRID

Statistical Physics applied to Population Dynamics
Física Estadística aplicada a la Dinámica de Poblaciones

Thesis by/Tesis por
Rodrigo Crespo Miguel

Submitted as part of the Doctoral Program in Physics
/Presentada dentro del Programa de Doctorado en Física

Thesis Director/Director de Tesis
Francisco Javier Cao García

Madrid, 2022

A todas las personas que han hecho más fácil poder escribir esta tesis

Agradecimientos

Y por fin estamos aquí. Y digo “por fin” no porque este tiempo haya sido un suplicio (aunque he de reconocer que hubo más de un momento de frustración, sobre todo cuando te pilla una pandemia de por medio y la lías en temas burocráticos) si no porque cuando empecé en este doctorado veía este momento como muy lejano, y siendo sincero, algo terrorífico: La idea de escribir una tesis desde cero es abrumadora y es un momento que en parte deseas que no llegue o que mágicamente se escriba sola (he de reconocer que he empezado escribiendo los agradecimientos como un inútil intento de aplazar lo inevitable), sobre todo por la redacción, que en mi caso particular no tenía ni idea de cómo empezar, mientras que la investigación, aún con sus momentos de atasco, fue bastante más amena y fuente de satisfacción cuando llegaba a buen puerto.

La pregunta ahora es qué hago hablando de mí mismo en el apartado de agradecimientos. La respuesta es sencilla, el camino, aunque merece la pena de por sí solo, a veces se hace un poco duro y tener gente apoyándote lo hace bastante más fácil.

Me vais a permitir empezar agradeciendo su ayuda a mi principal guía en el doctorado, que ha sido mi tutor Francisco Cao. Ha sido un placer que él aceptase supervisar mi tesis y le estoy muy agradecido por ello, y sin duda esto no se queda aquí, todo lo que me ha enseñado, tanto técnicas de investigación y trabajo, como conocimientos en sí, me ayudará a ser (espero) un buen investigador en el futuro. Pero Fran no ha sido el único que me ha ayudado académicamente hablando durante estos años, cuando llegué por primera vez al despacho en el que escribo estas líneas y estaba perdidísimo con cómo empezar pude contar con la ayuda de Javi y Elena, que comenzaron el doctorado antes que yo, dos personas maravillosas sin las cuáles no sé cómo me las habría apañado los dos primeros años, siempre dispuestas a echar una mano cuando lo necesité, lo que pasó varias veces. Además, quiero mostrar mi agradecimiento a Belén, Irene, Íñigo y el resto de gente del proyecto TRIATLAS, que fue mi sustento económico durante mi tercer año de doctorado. Y también a Borja Ibarra, ya que gracias a la colaboración que hice en su trabajo, aprendí muchas cosas sobre análisis e interpretación de datos y cómo afinar modelos.

Pero, aun siguiendo con lo académico, no todo empezó en el doctorado. El hecho de que esté aquí se debe en gran parte a grandes profesores, que ya desde el instituto me inspiraron un amor por el conocimiento y la ciencia en general y la física (y la biología, que también tiene mucho que ver en esta tesis) en particular (ya que es imposible mencionar a todos), como Manuel Fanlo y Olegario. Gracias, de no ser por vosotros quizá habría escogido otra carrera totalmente distinta. Y ya dentro de la facultad, cuando ya había decidido que quería ser físico, seguí encontrando algunos profesores magníficos que, quizá sin saberlo, avivaron un poco mis ganas de seguir con la física. En concreto quiero hacer una mención especial al profesor Luis Manuel González Romero, que aparte de ser uno de los mejores profesores que tuve en la carrera y el máster fue un excelente tutor de TFG y TFM y se portó de forma impecable conmigo durante ese tiempo.

Pero no solo de física vive Rodrigo, y aún quedan muchas personas que han influido en que ahora estéis leyendo esta tesis, empezando con mi familia: Padres, abuelos, tíos, primos y mi hermano Javier, y su novia Sara que ya es casi de la familia.

Aprovechando a Javier como punto de unión, continúo con mi banda, Last Whisper. Banda que ha sido quizá mi principal hobby durante estos años y que me ha hecho feliz, contribuyendo indirectamente a mi éxito profesional. Javier, Miguel, Iván y Javi "percuta" Romo (y también Gonzalo, que pasó por ahí al principio), sois muy grandes. Gracias por estos años de risas y Heavy Metal y por muchos más. Relacionado con ello, también quiero mencionar a Areh, uno de los mejores profesores que uno podría desear.

Tampoco puedo dejar de mencionar a grandes personas que conocí gracias a mi otra gran afición, Magic the Gathering, y que se han acabado convirtiendo en amigos, el "Team Tarados": Bube, "El Gallorrista", Manu, Dani "Tarado", Ángel, Berilio, Iñaki, Pinedo, Andrés, Juanlu, Javi "Tender", Potasio, Prote y otros que me dejo para más adelante. Gracias por esas tardes de Commander, o de cine, o de mil planes que ayudaron a desfogarme después del trabajo en el doctorado y que se aprecian de verdad. Hasta se os perdona el odio a los mazos de cementerio y que me liáseis para bajar a jugar.

Y cómo no acabar con más amigos cercanos, que o bien no entran en las categorías anteriores o bien quería extenderme más con ellos: "Los de antaño" de Berlanga: Raúl Aparicio, Jorge Blanco, "Comodoro" Gabriel y Gorka, que hicieron que estuviera deseando ir a un pueblecito de Soria cada fin de semana que me fuera posible solo por estar con ellos; o el grupo más cercano: Velas, con su eterno buen humor, Alex y Fer, con quien siempre sé que voy a poder contar, Gonzalo, que aunque la cosa no acabase muy bien con el grupo estuvo ahí todos estos años, y los dos de Fuenlabrada que conocimos jugando a las cartas y poco después hicieron tanta piña con nosotros, Checho y Guaza. Y también Gallito, que es de Getafe pero también hizo piña y es un cacho de pan. Y por supuesto Laura, Sandra, Rubén y Elena, que hace menos tiempo que se juntan con nosotros de fijo pero se les aprecia un montón.

Y no todos mis amigos (ni siquiera los más cercanos) se incluyen en estos dos grupos, también es necesario mencionar (aún a riesgo de extenderme en exceso en los agradecimientos) a Bonilla, que fue mi principal amistad de la carrera, Cristina, una de las mejores personas que he conocido y conoceré nunca, y que amenizó alguno de estos largos días de trabajo en la pausa para comer (y muchas cosas más), a Naiara, que apareció cuando ya estaba acabando todo esto, haciéndolo un poco más fácil, y a Óscar, Carmen, Pol, las Martas, Marina, Pablo, Carlos, Dani, Lisard, Ricardo, Jose y la gente de la peña en general, gracias por estos años de amistad, porque gracias a todos vosotros estoy donde estoy y soy quien soy. Al final, con gente como todos los que he mencionado, todo merece la pena.

Table of contents

Summary of the thesis

Introduction

Stochastic processes are a central issue in Statistical Physics (Gardiner 2009). In most real models, the deterministic prediction is only an estimate of the system's actual behavior since random factors affect it. Specifically, problems with significant historical relevance, such as Brownian motion (Brown 1828; Einstein 1905), could not be correctly studied until the development of the stochastic processes theory.

In this thesis, we study the effect of stochastic factors on populations within an ecosystem, classically modeled with deterministic growth equations (Cotgreave and Gotelli 2006). There are random fluctuations in natural ecosystems, which can change the model's behavior, even causing the extinction of an otherwise stable population in the deterministic case. The variability affecting a population can be modeled as a stochastic process with spatial and/or temporal correlation.

We begin by introducing the state of the art in ecology and stochastic processes. In Chapter 1, we introduce well-known deterministic dynamic equations for a single species, emphasizing on the Allee effect dynamic equation (Allee and Rosenthal 1949), for which the population has negative growth when its size is below a certain minimum threshold. Besides, we include metapopulation models to represent dispersal.

Chapter 2 introduces basic concepts about stochastic processes, random variables, and white noise. We also explain in this chapter the algorithm used for the numerical implementation of stochastic differential equations.

In Chapter 3, we apply the concepts of the previous chapter to growth equations describing population dynamics, including fluctuations present in real populations. In general, we can distinguish two types of fluctuations (Engen, Bakke, and Islam 1998): Environmental fluctuations are usually due to climate variability and affect the whole population, while demographic fluctuations represent individual variations in birth and death. Demographic fluctuations can be neglected for sufficiently large populations compared to environmental fluctuations (Lande, Engen, and Saether 2003).

Based on the models for metapopulations and environmental fluctuations, in Chapter 4, we define the spatial scale of population synchrony (Lande, Engen, and Sæther 1999). The spatial scale of population synchrony gives the characteristic distance at which two metapopulations remain correlated. This scale increases with the population dispersal distance and the spatial scale of synchrony of the environmental fluctuations.

Using the concepts introduced before, we study a model for a population affected by the Allee effect (Chapter 5). This model presents dispersal, which can alleviate the adverse effects of the localized Allee effect and sustain the species against environmental fluctuations (Dennis et al. 2016). In our study, we are interested in determining how the fluctuations affect population stability by using simulations and studying probability distributions.

Subsequently, we study the effect of habitat reduction on a population with Allee effect (Chapter 6). The partial destruction of a habitat can endanger a population's survival. It is especially harmful in populations that require more dispersal to be stable. This study consists

in modeling how habitat destruction affects the capacity of dispersal. For this aim, we will simulate the evolution of the species at long times for different dispersal distances and habitat sizes.

In Chapter 7, we study the predictability of population fluctuations under the influence of temporally autocorrelated environmental fluctuations. We found that the environmental-population correlation time is the largest, followed by the population autocorrelation time. They are greater than the environmental autocorrelation time. We also obtain the corresponding correlation functions, which provide additional information on the predictability of population fluctuations.

Objectives:

This thesis mainly studies the effect of environmental fluctuations on a population. The main questions to answer are:

Spatially extended stochastic population dynamics with Allee effect:

1. What are the main factors that affect the resilience of a population to environmental fluctuations?
2. How does the minimum viable population threshold affect the resilience of the population?
3. How and how much does dispersal affect the resilience of a population?
4. How does habitat size reduction affect the resilience of a population?

Predictability of population fluctuations:

1. Which are cross-correlation, autocorrelation functions, and correlation times for environmental and population fluctuations?
2. Which are the larger correlation times?
3. What do correlation functions and times tell us about the predictability of population fluctuations?

Results and conclusions:

The model we have developed for Allee effect and dispersal predicts how intense the environmental fluctuations must be to cause global population extinction. The resilience of a population depends on its threshold of minimum viable population and its dispersal. We show that more frequent and far-reaching dispersal is more effective in reducing the extinction risk, increasing population resilience of the species proportionally to the root of the dispersal rate. Conversely, the extinction risk increases for higher minimum viable population thresholds.

Once we have characterized the case for habitats much larger than the typical dispersal distances of the species, we next study the effect of the habitat size on a population with Allee effect. We show that a reduction of the habitat size affects the survival capacity of the population since it reduces the rescue mechanisms that prevent extinction (reducing the effective dispersal distance). Thus, we have studied how the size of the habitat, the dispersal rate, and the average distance of dispersal affect the extinction risk of a species. We obtain that increased dispersal ceases to be useful as a mechanism against extinction if the habitat size truncates its range. Thus, the resilience of the species increases with the size of the habitat in which this population is enclosed.

Finally, computing the correlations between the environment and populations allows us to study the predictability of population fluctuations. We obtained that the maximum influence of environmental fluctuations on the population is delayed. Furthermore, we have seen that the predictability of population fluctuations is greater than that of environmental fluctuations. These studies provide a deeper understanding of population dynamics affected by stochastic factors. This knowledge can be used to develop more efficient conservation strategies for vulnerable populations and to exploit species with economic interest.

Resumen de la tesis

Introducción

Los procesos estocásticos son un tema central en Física Estadística (Gardiner 2009). En muchos modelos reales, la predicción determinista solo es una estimación del comportamiento del sistema; al existir factores aleatorios. En concreto, problemas de relevancia histórica como el movimiento browniano (Brown 1828; Einstein 1905) no pudieron estudiarse correctamente hasta el desarrollo de la teoría de procesos estocásticos.

En esta tesis estudiamos el efecto de factores estocásticos sobre poblaciones en un ecosistema, clásicamente modeladas con ecuaciones de crecimiento deterministas (Cotgreave y Gotelli 2006). En ecosistemas reales existen fluctuaciones que cambian el comportamiento del modelo, llegando incluso a causar la extinción de poblaciones estables en el caso determinista. Esta variabilidad se modeliza como un proceso estocástico correlacionado espacial y/o temporalmente.

Comenzamos introduciendo los fundamentos necesarios de ecología y procesos estocásticos. En el Capítulo 1 presentamos las ecuaciones dinámicas deterministas para una especie, destacando la ecuación dinámica con Efecto Allee (Allee y Rosenthal 1949) que muestra decrecimiento cuando el tamaño de la población es menor que cierto umbral. Además, introducimos modelos de metapoblaciones para representar dispersión.

En el Capítulo 2 introducimos conceptos sobre procesos estocásticos, variables aleatorias y ruido blanco. También explicamos el algoritmo usado para la implementación numérica de ecuaciones diferenciales estocásticas.

En el Capítulo 3 aplicamos conceptos del capítulo anterior a ecuaciones de crecimiento que describen la dinámica de la población, incluyendo fluctuaciones presentes en poblaciones reales. En general distinguiremos dos tipos de fluctuaciones (Engen, Bakke y Islam 1998): Las fluctuaciones ambientales suelen deberse a variabilidad climática y afectan a toda la población, mientras que las demográficas representan variaciones individuales en natalidad y mortalidad. Para poblaciones suficientemente grandes, las fluctuaciones demográficas pueden despreciarse comparadas con las ambientales (Lande, Engen y Saether 2003).

Partiendo de modelos de metapoblaciones y fluctuaciones ambientales, en el Capítulo 4 definimos la escala espacial de sincronía de la población (Lande, Engen y Sæther 1999), que da la distancia característica a la que dos metapoblaciones permanecen correlacionadas. Esta escala aumenta con la distancia de dispersión de la población y la escala espacial de sincronía de las fluctuaciones ambientales.

Utilizando conceptos introducidos anteriormente, estudiamos un modelo para una población afectada por Efecto Allee (Capítulo 5). Este modelo presenta dispersión, que puede paliar los efectos negativos del Efecto Allee, y sostener la especie frente a fluctuaciones ambientales (Dennis et al. 2016). En este estudio buscamos determinar cómo estas fluctuaciones afectan a la estabilidad de la población, usando simulaciones y estudiando distribuciones de probabilidad.

Posteriormente abordamos la reducción del hábitat en una población con Efecto Allee (Capítulo 6). La destrucción parcial del hábitat puede hacer peligrar la supervivencia de una

población, siendo especialmente dañina en poblaciones que requieren mayor dispersión para ser estables. Este estudio consiste en modelar cómo la destrucción del hábitat afecta a la dispersión y estabilidad de la especie frente a fluctuaciones ambientales. Para ello, simularemos la evolución de la especie a tiempos largos para distintas distancias de dispersión y tamaños de hábitat.

En el Capítulo 7 estudiamos la predictibilidad de fluctuaciones poblacionales bajo la influencia de fluctuaciones ambientales temporalmente autocorrelacionadas. Hemos encontrado que el tiempo de correlación ambiente-población es el más largo, seguido por el tiempo de autocorrelación de la población. Ambos son mayores que el tiempo de autocorrelación ambiental. También obtenemos las funciones de correlación correspondientes, que dan información adicional de la predictibilidad de las fluctuaciones poblacionales.

Objetivos:

En esta tesis estudiamos el efecto de fluctuaciones ambientales sobre poblaciones. Las preguntas principales por resolver son:

Dinámica estocástica de poblaciones espacialmente extendidas con Efecto Allee:

1. ¿Cuáles son los factores principales que afectan a la resiliencia frente a fluctuaciones ambientales de una población?
2. ¿Cómo afecta el umbral de minima población viable a la resiliencia de la población?
3. ¿Cómo y en qué medida afecta la dispersión a la resiliencia de la población?
4. ¿Cómo afecta la reducción del habitat a la resiliencia de una población?

Predictibilidad de fluctuaciones poblacionales:

1. ¿Cuáles son las funciones de autocorrelación y correlación cruzada y tiempos de correlación de las fluctuaciones ambientales y poblacionales?
2. ¿Cuáles son los tiempos de correlación más largos?
3. ¿Qué nos dicen las funciones y tiempos de correlación sobre la predictibilidad de las fluctuaciones poblacionales?

Resultados y conclusiones:

El modelo para Efecto Allee y dispersión predice cuán intensas han de ser las fluctuaciones ambientales para causar la extinción de una población. La resiliencia de la población depende del umbral de mínima población viable y su dispersión. Demostramos que dispersiones más frecuentes y con mayor alcance son más eficaces reduciendo el riesgo de extinción, aumentando la resiliencia proporcionalmente a la raíz del ratio de dispersión. El riesgo de extinción, por otra parte, aumenta para umbrales de mínima población viable más altos.

Ya caracterizado el caso de hábitats mucho mayores que las distancias de dispersión de la especie, estudiamos el efecto de reducción del hábitat en poblaciones con efecto Allee. Mostramos que el tamaño del hábitat afecta a la capacidad de supervivencia de la población, reduciendo los mecanismos de rescate (capacidad efectiva de dispersión) que previenen la extinción. Así, estudiamos cómo el tamaño del hábitat, y el ratio y distancia media de dispersión afectan al riesgo de extinción de una especie. Obtenemos que el aumento de dispersión deja de ser efectivo si su alcance es truncado por el tamaño del hábitat. La intensidad mínima de las fluctuaciones ambientales que aseguran extinción aumenta cuanto mayor es el hábitat en el que se encuentra esta población.

Por último, obtener correlaciones entre ambiente y población nos permite estudiar la predictibilidad de las fluctuaciones poblacionales. Obtenemos que la influencia máxima de las fluctuaciones ambientales sobre la población está retardada. Además, hemos visto que la predictibilidad de las fluctuaciones poblacionales es mayor que la de las fluctuaciones ambientales. Estos estudios proporcionan un mayor entendimiento sobre las dinámicas de poblaciones sometidas a factores estocásticos. Este conocimiento puede ser empleado en el desarrollo de mejores estrategias de conservación para poblaciones vulnerables y de explotación de especies con interés económico

List of publications

Included in this thesis:

1. R. Crespo-Miguel, J.Jarillo, and F.J. Cao-García. 2022. "Dispersal-induced resilience to stochastic environmental fluctuations in populations with Allee effect." *Physical Review E 105* (1): 014413. https://doi.org/10.1103/PhysRevE.105.014413. Included in Chapter 5.
2. R. Crespo-Miguel, J.Jarillo, and F.J. Cao-García. 2022. "Scaling of population resilience with dispersal length and habitat size." *Journal of Statistical Mechanics: Theory and Experiment* 2022 (2): 023501. https://doi.org/10.1088/1742-5468/ac4982. Included in Chapter 6.
3. R. Crespo-Miguel and F.J. Cao-García. 2022. "Predictability of Population Fluctuations." *Mathematics* 10 (17):3176. https://doi.org/10.3390/math10173176. Included in Chapter 7.

Other publications related with this thesis:

4. R. Crespo-Miguel, I. Polo, C.R. Mechoso, Mª.B. Rodriguez-Fonseca, and F.J. Cao-García. 2022. "ENSO coupling to Tropical Atlantic: Analysis with an improved recharge oscillator model." Submitted for publication.
5. R. Crespo-Miguel and F.J. Cao-García. 2022. "Temporal correlations in a predator-prey ecosystem in the pressence of autocorrelated environmental fluctuations." Manuscript in preparation.
6. R. Crespo-Miguel and F.J. Cao-García. 2022. "Temporal correlations in two species ecosystems." Manuscript in preparation.
7. I.Plaza, K. M. Lemishko, R. Crespo-Miguel, T.Q Truong, L.S. Kaguni, F.J. Cao-García, G.L. Cielsieski, and B. Ibarra, 2022. "Mechanism of strand displacement DNA synthesis by the coordinated activities of human mitochondrial DNA polymerase and SSB." Preprint in https://doi.org/10.1101/2022.07.19.500644. Submitted for publication.

PART I:
Introduction and state of the art

Chapter 1: Growth equations for a single species.

The first and simplest population growth model was proposed by Malthus (Malthus 1798) with the exponential-growth equation

$$\frac{dN}{dt} = (b - d)N = rN \tag{1.1}$$

Where constants b and d are the birth and death rate (individuals/time), and $r = b - d$ is the resulting growth rate of the species. This growth equation yields the deterministic population evolution (blue line in Fig. 1.1)

$$N(t) = N_0 \cdot e^{rt} \tag{1.2}$$

Deterministic exponential evolution implies that a population stays constant if $r = 0$; it declines to extinction if $r < 0$, and it grows exponentially if the growth rate r is positive. This simple model does not explain the behavior of real populations accurately (except for small population size N) because some of its assumptions are poor. The assumption with the greatest impact on the unreal behavior is that birth and death rates are constant, which is impossible in the absence of infinite space and resources. In real cases, resources are limited, implying that birth and death rates cannot remain constant respect to the population densities, even when a population can temporally grow exponentially until the lack of resources begins.

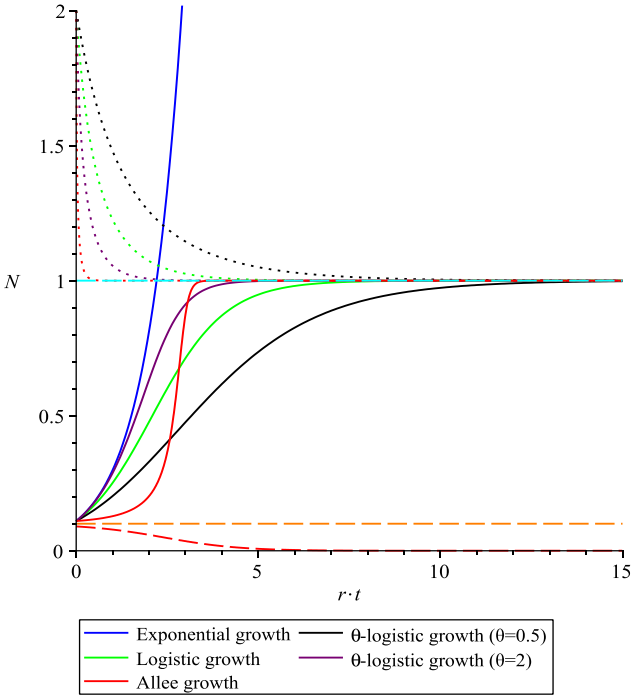

Figure 1.1: Deterministic population evolution for different growth models: Exponential (Malthus) equation in blue, logistic equation in green, θ-logistic equations in black ($\theta = 0.5$), and purple ($\theta = 2$), and Allee equation in red. We have chosen units such as $K = 1$ (cyan dashed line), and for the Allee equation, we have considered $A = 0.1$ (orange dashed line). Solid lines are for an initial population density of $N_0 = 0.11$, whereas dotted lines are for an initial population $N_0 = 2$. The red dashed line is for an initial population $N_0 = 0.09$.

To solve this problem, Verhulst suggested that limited resources could modify the birth and death rates depending on the population size (Verhulst 1838). In his logistic model, there is a linear increase with the population size N in the death rate d. On the other hand, the birth rate b linearly decreases with N as

$$b = b_0 - b_1 N \tag{1.3}$$
$$d = d_0 + d_1 N \tag{1.4}$$

Substituting Equations (1.3) and (1.4) in the growth equation, Eq. (1.1), we get

$$\frac{dN}{dt} = (b_0 - b_1 N - d_0 - d_1 N)N = (b_0 - d_0)N\left(1 - \frac{(b_1 + d_1)}{(b_0 - d_0)}N\right) = rN\left(1 - \frac{N}{K}\right) \tag{1.5}$$

Where $K = \frac{(b_0 - d_0)}{(b_1 + d_1)}$ is the carrying capacity, which is the stable population size, i.e., the number of individuals that the system has at equilibrium. The logistic growth equation, i.e., Eq. (1.5), gives the following deterministic population evolution

$$N(t) = \frac{K}{1 + \left(\frac{K}{N_0} - 1\right)e^{-rt}} \tag{1.6}$$

Equation (1.6) has an exponential-like behavior for a small population size N. However, the growth becomes slower for greater populations. Provided that the growth rate r is positive, the population asymptotically reaches the carrying capacity K at long times (see green line in Fig. 1).

The assumption of linear dependence on the population size N of birth and death rates can be generalized by the theta-logistic model (Gilpin and Ayala 1973; Clark et al. 2010)

$$\frac{dN}{dt} = rN\left(1 - \left(\frac{N}{K}\right)^{\theta}\right) \tag{1.7}$$

And its solution is a generalization of Equation (1.6) (black and purple lines in Fig.1)

$$N(t) = \frac{K}{\left(1 + \left(\left(\frac{K}{N_0}\right)^{\theta} - 1\right)e^{-\theta rt}\right)^{\frac{1}{\theta}}} \tag{1.8}$$

All the models described above assume that the effective growth rate $\frac{dN}{dt} \cdot \frac{1}{N}$ decreases (or remains constant) when the population size N grows (see Fig.1.2). Nonetheless, there are many species whose effective growth rate decays at small population densities. The tendency of some species to extinction al low population densities, caused by this decay of the effective growth rate, is named Allee Effect (Allee and Rosenthal 1949). Allee Effect has been observed in field research in ecology and conservation biology. It can have many different causes, such as difficulties in finding a breeding partner or the need for cooperation in a herd to overcome difficulties. For example, an isolated individual is easier to be hunted by a predator than another that is defended by its mates. Another possible cause of Allee Effect is the higher efficiency in searching for resources by groups compared to isolated individuals. Any of these causes (at small population densities) may imply an increasing birth rate or decreasing death

rate with N.

This low (or more likely negative) growth rate for small populations can be modeled by adding quadratic terms on the population density in the birth and death rates, Eqs. (1.3) and (1.4), to get the Allee growth equation

$$\frac{dN}{dt} = rN\left(1 - \frac{N}{K}\right)\left(\frac{N}{A} - 1\right) \tag{1.9}$$

Equation (1.9) tells us that the deterministic behavior of a population affected by the Allee effect is such that it will evolve to reach the carrying capacity if the initial population size is greater than the Allee threshold ($N_0 > A$). In contrast, if the initial population N_0 is smaller than the threshold Allee A, it will eventually become extinct. In contrast, if the initial population is equal to A, it will remain constant in an unstable equilibrium.

We can notice in Fig. 1.1 and 1.2 that for a deterministic Allee effect, the population growth is slower than the one given by other growth equations when the population size is slightly bigger than the Allee Threshold A. Such behavior is a consequence of difficulties of recovery when the population decreases to sizes close to this threshold.

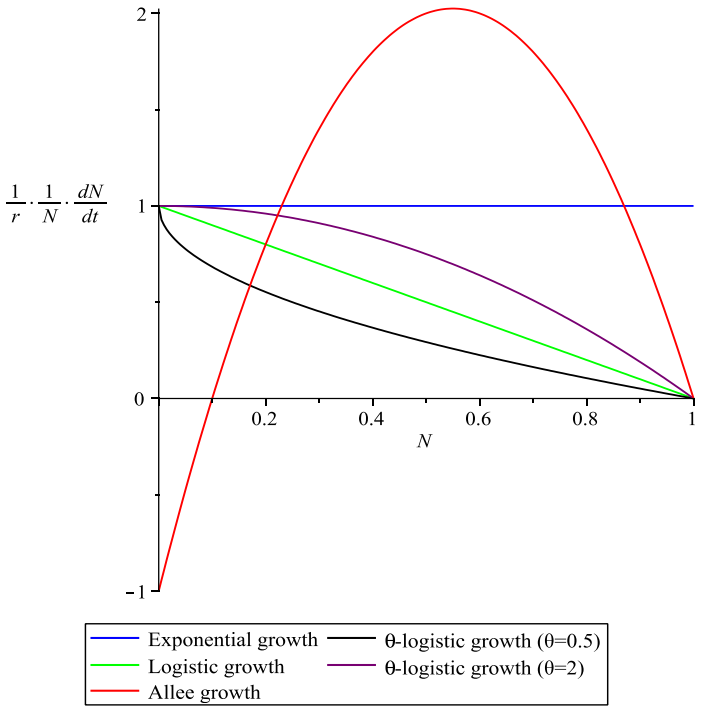

Figure 1.2: Effective growth rate $\frac{dN}{dt} \cdot \frac{1}{N}$ divided by the growth rate r (constant) as a function of the population size N. Here, we have chosen units such as the carrying capacity K is equal to 1, representing the Allee growth equation with $A = 0.1$ as an example. The color code is the same as in Figure 1.1. We can see that the effective growth rate is constant for the exponential model and decreases with the population size N in logistic and theta-logistic models. In contrast, the only model that has an increasing effective growth rate (at low N) is the one proposed by Allee.

1.1. Spatial models

The above models study the evolution of the population in a single point, ignoring the effects of individuals in its neighborhood. However, ignoring the populations that inhabit the surrounding zones is simplistic and, in most cases, an inaccurate approach. In some ecosystems, a population spread along a vast area can be viable and stable even if subpopulations in some smaller areas of the habitat disappear, meaning that the local risk of extinction is always higher than the global risk. Metapopulation models (Lande, Engen, and Saether 2003; Cotgreave and Gotelli 2006) are usually the simplest way to approach this problem. These models study populations as several local populations, that stay in zones usually called patches, linked by dispersal. The simplest metapopulation models only predict whether the local populations inside a patch exist or are extinct, with no concern about the population size in each patch.

Levins (Levins 1970) studied the evolution of the fraction of occupied patches by defining the following continuous-time equation

$$\frac{dp}{dt} = c \cdot p(1-p) - e \cdot p \tag{1.10}$$

Here p is the fraction of occupied patches, c is the colonization rate, and e the extinction rate. The dependence of the first term in this equation in $(1-p)$ is explained by the fact that we cannot colonize an occupied patch, and the dependence in p means that the colonizers must come from an occupied patch. However, c and e are not always constant and may depend on the number of occupied patches (Gotelli and Kelley 1993; Hanski and Gyllenberg 1993), so Equation (1.10) becomes

$$\frac{dp}{dt} = c(p) \cdot p(1-p) - e(p) \cdot p \tag{1.11}$$

The most important implication of this equation is that individuals disperse from occupied patches and can move to others, colonizing them(if they were unoccupied)with a certain effectivity. Equation (1.11) does not tell us how many individuals live in every patch, but only if there are individuals or not. In any case, starting from the same principle of dispersal, we can think of a general model of dispersal for continuous-time and space that yields the size of the population in each patch

$$\frac{dN(x,t)}{dt} = \left.\frac{dN(x,t)}{dt}\right|_{local} + \left.\frac{dN(x,t)}{dt}\right|_{dispersal} \tag{1.12}$$

$$\left.\frac{dN(x,t)}{dt}\right|_{dispersal} = -mN(x,t) + m\int N(x-y,t)f(y)dy \tag{1.13}$$

Where m is the dispersal rate, and f is a (normalized) function that describes how individuals disperse along space (usually a gaussian, and almost always a symmetrical function with a global maximum in zero and decreases with the absolute value of y). Besides, $\left.\frac{dN}{dt}\right|_{local}$ is the local growth equation, which can be any growth equation presented in the previous subsection (depending on the model). See that in Equation (1.13), individuals leave from a certain point and disperse to other points in space (which can lead to colonization of local-extinct areas). This dispersal usually means that areas that had suffered from a local extinction

can recover by repopulation from nearby patches (this recovery is commonly named rescue effect in metapopulation models). Nonetheless, dispersal can also drag a whole system to extinction if the harmed area is large enough, especially in populations with Allee effect, which need a minimum population density to persist.

Chapter 2: Stochastic Processes.

The deterministic models mentioned in the previous chapters are ideal simplifications of the real behavior of ecological systems in Nature. Natural populations are often affected by non-deterministic circumstances such as temporal and variable climate changes (environmental fluctuations) or variability in individual reproduction or mortality (demographic fluctuations). Such fluctuations can cause the extinction of a population that would be stable in its absence. Thus, we need to implement those events in our mathematical models. They are represented by stochastic processes included in the deterministic growth equation, which becomes a stochastic differential equation. To understand this kind of model, we will have to introduce some basic concepts about stochastic processes and Gaussian white noise in this chapter.

2.1. Random variables

Fluctuations, unpredictability, or both can cause random events, so they represent functions instead of quantities because we must interpret them as the probability that certain possibility happens. Because of that, a random variable X is characterized by a range Ω containing all the possible values of the variable, and a probability distribution $P_X(x)$ that assigns a probability to each element $x\epsilon\Omega$. If X is a continuous variable, $P_X(x)$ is called the probability density function (pdf). The probability distribution (both for discrete and continuous variables) must satisfy the following two conditions:

-Positivity: $P_X(x) \geq 0 \ \forall \ x \in \Omega$

-Normalization: $\sum_\Omega P_X(x) = 1$ if X is discrete, and $\int_\Omega P_X(x) = 1$ if X is continuous.

For some experiments, named deterministic, we always get the same result (or output) if we repeat the same input. Nonetheless, not all experiments are deterministic, and the same input can produce different outputs. Then, the experiment is said to be random, and each measurement of the outputs of a random experiment is a random variable. The collection of all these measurements of a random experiment is what we call a **stochastic process**.

Let us introduce three principal probability distributions:

-Normal distribution:

$$P_X(x) = \frac{1}{\sqrt{2\pi\sigma^2}} e^{\frac{-(x-\mu)^2}{2\sigma^2}} \tag{2.1}$$

Where μ is the mean value of the random variable X (i.e., $< X >$) and $\sigma^2 = < X^2 > - < X >^2$ is its variance.

-Exponential distribution:

$$P_X(x) = \lambda e^{-\lambda x} \tag{2.2}$$

if the random variable is definite positive or

$$P_X(x) = \frac{\lambda}{2} e^{-\lambda|x|} \tag{2.3}$$

if it can take negative values

-Dirac Delta:

$$P_X(x) = \delta(x - x_0) \tag{2.4}$$

Which is equal to zero in all x except x_0, where it diverges. The Dirac Delta satisfies the following property

$$\int_\Omega f(x)\delta(x - x_0)\, dx = \begin{cases} f(x_0) & if\ x_0 \in \Omega \\ 0 & if\ x_0 \notin \Omega \end{cases} \tag{2.5}$$

2.2. Fluctuations

The non-deterministic parts of an evolving system are usually called fluctuations (or noise). Fluctuations are a set of random variables, one for each point of space and time $X = \{X(S), S \in \Omega_S\}$ (Ω_S is the range of space and time considered). This set of random variables is defined by its pdf and its autocorrelation. For example, when we speak about Gaussian white noise, these fluctuations have a Gaussian (normal distribution) stationary probability distribution (spd) and are uncorrelated on time

The autocorrelation function measures the dependence of the noise on itself in another point of space or time. It is usually defined for temporal autocorrelations

$$c_{XX}(t') =< X(x,t)X(x,t+t') >, \tag{2.6}$$

and for spatial autocorrelations

$$c_{XX}(y) =< X(x,t)X(x+y,t) >. \tag{2.7}$$

In general, correlations are defined as

$$c_{XY}(y,t') =< X(x,t)Y(x+y,t+t') >. \tag{2.8}$$

For example, the kind of environmental fluctuations that appear when we are studying Allee effect are Gaussian with mean zero, uncorrelated in time (white noise), and exponentially correlated in space:

$$c_{\xi\xi}(t',y) = \sigma^2\delta(t')e^{-\sqrt{2}|y|/l_e} \tag{2.9}$$

Here, σ is the amplitude of the fluctuations (which is the square root of the variance), and l_e the characteristic distance at which the environmental fluctuations remain correlated, named spatial scale of synchrony of the fluctuations (see Chapter 4 for more details).

Note that when the variable X has mean zero (such as for fluctuations around equilibrium presented in Chapter 7 (Crespo-Miguel and Cao-García 2022)), its autocorrelation at time and space equal to zero is equal to its variance, i.e., $Var(X) =< X(t)^2 >= c_{XX}(0,0)$

2.3. Wiener Process

A Wiener process $W(t)$ is a stochastic process depending on a real variable $t \geq 0$, whose increments for t_i , $W(t_{i+1}) - W(t_i)$, follow a Gaussian distribution with mean 0 and variance $\sigma^2 \Delta t$ and are independent of any other combination of times. These properties mean that the Wiener Process is the sum of independent Gaussian increments. A Wiener process also verifies $W(0) = 0$. Thus, Wiener Processes have the following properties:

- $< W(t) >= 0, < W(t_i) W(t_j) >= \sigma^2 \min(t_i, t_j)$, particularly $< W(t)^2 >= \sigma^2 t$
- $W(t + \Delta t) - W(t)$ is independent of $W(t)$ for $\Delta t > 0$

White noises are usually introduced as the derivative of the Wiener Process (Méndez, Campos, and Bartumeus 2014)

$$\frac{dW(t)}{dt} = \xi(t) \tag{2.10}$$

Equation (2.10) can be shown by defining $Y(t) = \int_0^t \xi(s) ds$ and calculating its autocorrelation

$$\begin{aligned} < Y(t_2) Y(t_1) >= & \int_0^{t_2} ds_2 \int_0^{t_1} ds_1 < \xi(s_2) \xi(s_1) > \\ & = \sigma^2 \int_0^{t_2} ds_2 \int_0^{t_1} ds_1 \delta(s_2 - s_1) = \sigma^2 \min(t_2, t_1) \end{aligned} \tag{2.11}$$

Then, the autocorrelation of $Y(t)$ is the autocorrelation of a Wiener Process. Moreover, by definition, $Y(0) = 0$, so $Y(t)$ is a Wiener Process because it satisfies its defining properties.

2.4 Stochastic Differential Equations

Deterministic systems are often modeled by differential equations, which have the general form

$$\frac{dx}{dt} = f(x(t), t) \tag{2.12}$$

For example, growth equations in Chapter 1 (Eqs. (1.1), (1.5), (1.7), (1.9) or (1.12)). Nonetheless, in many natural situations, external events affect the system, which can be described as stochastic processes (such as climate changes affecting a population, described as environmental noise). In that case, the differential equation becomes a stochastic differential equation, with the general form

$$\frac{dx}{dt} = f(x(t), t, \xi(t)) \tag{2.13}$$

Where $\xi(t)$ is a (usually, but not always white) noise or stochastic process. A notable stochastic equation is the Langevin Equation, in which the stochastic process appears as a linear term (i.e., the equation has a linear dependence on $\xi(t)$),

$$\frac{dx}{dt} = F(x(t), t) dt + G(x(t), t) \xi(t) \tag{2.14}$$

The function G can be independent of $x(t)$ and t (i.e., it is a constant), then we say that the noise is additive; otherwise, the noise is multiplicative. Provided that $\xi(t)$ can be white noise, it can be uncorrelated, driving us to a formal problem: If the right hand of the equation is non-differentiable, then the left side should not be differentiable either so that this equation can be incoherent. That problem is solved by transforming Eq. (2.14) to a more rigorous form

$$dx = F(x(t), t)dt + G(x(t), t)dW(t) \tag{2.15}$$

This equation has an integral form, which is much more useful for simulation purposes

$$x(t) = x(t_0) + \int_{t_0}^{t} F(x(t'), t')\, dt' + \int_{t_0}^{t} G(x(t'), t')dW(t') \tag{2.16}$$

The main problem with this expression is that, due to the stochasticity of the Wiener Process $W(t)$, the interpretation is not unique. There are two main descriptions used for stochastic integration: Itô and Stratonovich.

2.5. Itô and Stratonovich integrals.

For the integration of a stochastic process, we must begin by dividing the time interval into n subintervals $[t_0, t_1), [t_1, t_2), \dots, [t_{n-1}, t]$. When n is big enough, we can interpret the integral as the following summation, where we evaluate the functions at the initial point of each subinterval

$$\int_{t_0}^{t} G(x(t), t)dW(t) = \sum_{i=1}^{n} G(x(t_{i-1}), t_{i-1}) \cdot (W(t_i) - W(t_{i-1})) \tag{2.17}$$

This is the Itô integral, while we get the Stratonovich integral by evaluating the function G at the mean of the positions in t_i and t_{i-1} instead of at the initial point

$$\int_{t_0}^{t} G(x(t), t) \circ dW(t) = \sum_{i=1}^{n} G\left(\frac{x(t_i) + x(t_{i-1})}{2}, t_{i-1}\right) \cdot (W(t_i) - W(t_{i-1})) \tag{2.18}$$

The small circle is just a notation telling us that the integration is done in the Stratonovich prescription. In the case of additive noise, both interpretations are the same, but generally, the solution of the stochastic differential equation depends on the prescription we are using (Gardiner 2009). Then, we have two different kinds of stochastic differential (or integral) equations, using Itô prescription (Eq. (2.15) and (2.16)) or Stratonovich prescription

$$d\tilde{x} = \Phi(\tilde{x}(t), t)dt + \Gamma(\tilde{x}(t), t) \circ dW(t) \tag{2.19}$$

$$\tilde{x}(t) = \tilde{x}(t_0) + \int_{t_0}^{t} \Phi(\tilde{x}(t), t)\, dt + \int_{t_0}^{t} \Gamma(\tilde{x}(t), t) \circ dW(t) \tag{2.20}$$

Nonetheless, a solution of a stochastic equation in the sense of Itô integration is also a solution to a different equation in the Stratonovich prescription. To prove that, we introduce the Itô chain rule; this is, if $q(s)$ is an arbitrary function and $x(t)$ satisfies the Itô equation, then $q[x(t)]$ satisfies the Itô equation as well, and

$$dq[x(t)] = \left[F(x(t),t)\frac{dq}{ds}\Big|_{x(t)} + \frac{1}{2}G(x(t),t)^2\frac{d^2q}{ds^2}\Big|_{x(t)}\right]dt + G(x(t),t)\frac{dq}{ds}\Big|_{x(t)}dW(t), \quad (2.21)$$

while Stratonovich prescription follows the standard chain rule.

Then, if $x(t)$ verifies Itô stochastic differential equation, Eq. (2.15), it also verifies the following Stratonovich equation

$$dx = \left(F - \frac{\sigma^2}{2}G\frac{dG}{dx}\right)dt + G \circ dW \quad (2.22)$$

Or conversely, if $\tilde{x}(t)$ satisfies Stratonovich stochastic differential equation, Eq.(2.19), it also satisfies the following Itô SDE

$$d\tilde{x} = \left(\Phi + \frac{\sigma^2}{2}\Gamma\frac{d\Gamma}{d\tilde{x}}\right)dt + \Gamma dW \quad (2.23)$$

Because after applying some calculations and the Itô chain rule, we get

$$\int_{t_0}^{t}\Gamma(x(t'),t') \circ dW(t') = \int_{t_0}^{t}\Gamma(x(t'),t')dW(t') + \frac{\sigma^2}{2}\int_{t_0}^{t}\Gamma(x(t'),t')\frac{d\Gamma(x(t'),t')}{dx}dt' \quad (2.24)$$

Even if we can transform the equations, there is still a dilemma: we must choose a prescription to solve our stochastic problems because the interpretation can lead to different solutions. For continuous systems (that is the case of real physical systems), Stratonovich prescription is more suitable. In contrast, Itô prescription has better results for discontinuous ones, like the evolution of the economy or the dynamics of biological populations (Mannella and McClintock 2012). Nonetheless, the two prescriptions seem to yield the same results for growth equations with environmental noise if we take care of the conditions in the growth equation, i.e., the deterministic part of the equation is well defined (Braumann 2007).

2.6. Numerical implementation of stochastic differential equations: The Euler Algorithm.

Consider that we have a Langevin equation that we want to integrate with the expression of Equation (2.15) where $dW(t)$ is the differential of a Wiener Process $W(t)$. Then, we can divide the whole simulation time into n intervals of length Δt, where n tends to infinity, and then Δt→0.

By integrating Equation (2.15) between some time t_i and the previous time step, we obtain

$$x(t_i) = x(t_{i-1}) + \int_{t_{i-1}}^{t_i}F(x,t')\,dt' + \int_{t_{i-1}}^{t_i}G(x,t')dW(t'). \quad (2.25)$$

In the limit $\Delta t \to 0$ and the Itô prescription, Equation (2.25), expanding to the lowest order, equals

$$x(t_i) = x(t_{i-1}) + F(x, t_{i-1})\,\Delta t + G(x, t_{i-1}) \cdot \big(W(t_i) - W(t_{i-1})\big). \tag{2.26}$$

Nonetheless, by definition, successive increments of a Wiener Process are gaussian random variables with mean zero and $< \big(W(t_i) - W(t_{i-1})\big)^2 >= \sigma^2 \Delta t$. Then, we can express this increment by

$$W(t_i) - W(t_{i-1}) = \sigma\sqrt{\Delta t}\,\zeta(t_{i-1}) \tag{2.27}$$

Where ζ is a time uncorrelated random variable following a gaussian distribution of zero mean and variance one.

Then, we can get the value of x at a particular time t_i from its value at the previous time step by using the equation

$$x(t_i) = x(t_{i-1}) + F(x, t_{i-1})\,\Delta t + G(x, t_{i-1})\sigma\sqrt{\Delta t}\,\zeta(t_{i-1}) \tag{2.28}$$

Note that this expression was obtained for Itô prescription. However, we can also simulate an evolution given by the Stratonovich prescription. To do that, we should transform the Stratonovich SDE by applying Eq. (2.23) and then applying Eq. (2.28) to the resulting Itô SDE.

We follow Itô numerical integration to get results in parts II and III of this thesis. In part II (which studies a spatially extended population), we implement spatially autocorrelated white noise affecting the population dynamics. This means that a set of normally distributed random numbers (a number for each spatial point) is generated for each time step. That set of numbers presents an autocorrelation function decreasing (exponentially) with the distance, and each set is uncorrelated with the set generated at the previous time step.

Chapter 3: Noise in population dynamics. Environmental and demographic fluctuations.

Once we have understood the fundaments of stochastic processes, we are interested in implementing them in the growth equation that describes population dynamics. In Chapter 1, we studied deterministic growth equations for populations of living beings, which do not include the effects of environmental variability (environmental stochasticity). Other important possibilities are also ignored: For example, some individuals may not have the same offspring as others, or they can die sooner or later than another individual (demographic stochasticity).

This kind of event is random, and because of that, stochastic processes are great tools to describe them. In ecology, there are two essential sources of stochasticity: environmental and demographic fluctuations (Engen, Bakke, and Islam 1998; Lande, Engen, and Saether 2003). These events are crucial in the conservation of species because these fluctuations can cause the extinction of an otherwise stable population.

Some of these fluctuations are cyclic (such as seasonal environmental changes or breeding seasons) and somehow correlated along space and time. In any case, we can include fluctuations just as white noise when we are studying evolution during long times with long time steps (about the duration of these cycles). Approximating environmental fluctuations as white noise can be done because temporal correlation (typically of the scale of days) is measured to be very short in relation to the time scales: For example, the inverse of the growth rate (that has a typical duration of years or even greater) is usually a much longer time than the typical correlation times of the fluctuations.

3.1. Environmental fluctuations.

These fluctuations are usually caused by environmental variability and affect the probability of death and reproduction of all the individuals in a particular location. Nonetheless, individuals far from the zone where the fluctuation happened can be unaffected (unless there is intense long-range dispersal). Weather is one of the most important forms of that variability, but other causes such as diseases are sources of environmental fluctuations. On the one hand, if at a given time, there is some adverse condition, such as a cold snap or a drought, we can expect that more individuals will die. On the other hand, individuals tend to have more offspring when the climate is more favorable. These fluctuations affect the population's evolution proportionally to the population size.

Even when climatic catastrophes (tornados, earthquakes, and fires, among others) are usually studied as a different kind of stochasticity, they can be appropriately approximated as extreme cases of environmental fluctuations (this is, environmental fluctuations with very large amplitudes) (Shaffer 1987). This approximation can be made because the mean extinction time of a population suffering from a catastrophe scales with the carrying capacity in a similar way that it does with environmental fluctuations. In both cases, the extinction time scales proportionally to the carrying capacity K raised to the power of a function that depends on the intensity of the fluctuations or the catastrophe. Thus, for both environmental fluctuation and catastrophes, the mean extinction time decreases for more intense events (Lande 1993). This also means that a population does not become extinct by the effect of a single, short-termed catastrophe because extinction times are usually longer than the duration of these events.

3.2. Demographic fluctuations

Demographic fluctuations are caused by individual variations in natality and mortality that are generally unrelated to variations in other individuals. For every unit of time, an individual can die with a certain probability. Also, there is a probability of mating or not, and the size of the offspring follows a certain probability distribution. Those probabilities depend on factors such as sex or age structure. Since it works on every individual separately, it can be averaged (and neglected compared to environmental fluctuations, as we will explain in the next subsection) in large populations, having a more profound impact on smaller ones.

3.3. Mathematical formulation of environmental and demographic fluctuations.

To obtain a formulation of the effects of the fluctuations on the growth equations, we begin defining the population dynamics as a diffusion process (Dennis 2002; Dennis et al. 2016; Karlin and Taylor 1967) that has the form

$$dN = F(N)dt + \sqrt{Var(N)}dB, \tag{3.1}$$

where B is a Wiener Process, $F(N)$ is a deterministic growth term (Chapter 1), and $Var(N)$ is the variance of the population size N.

Then, we consider a population, focusing only on the female individuals (it is an excellent approximation provided that in most cases, males are non-limiting), for which we measure its size after every time step (typically a year, usually after the breeding season). Then we define individual fitness as the individual viability for the next breeding season plus the number of female offspring surviving the first time step, and we can represent it by the following equation

$$w_i = \mu_w + \delta_i \tag{3.2}$$

Where μ_w is the expected individual fitness and δ_i is the deviation from that expected individual fitness for the individual i. Both μ_w and δ_i are independent random variables (they vary from some time step to another), and the expected value of δ_i is zero. Given that the expected fitness is independent of the population density, its variation is related to environmental fluctuations, while the variation of individual fitness is related to demographical fluctuations.

Then, we define the multiplicative growth rate λ (this means $N(t+\Delta t) = \lambda(t)N(t)$) as the mean individual fitness (Lande, Engen, and Saether 2003)

$$\lambda = \frac{1}{N}\sum_{i=1}^{N} w_i = \mu_w + \frac{1}{N}\sum_{i=1}^{N} \delta_i \tag{3.3}$$

Then, defining $\sigma_e^2 = Var(\mu_w), \sigma_d^2 = \frac{1}{N}\sum_{i=1}^{N} Var(\delta_i)$ the variance σ_λ^2 that has the form (May 1973; Lande, Engen, and Saether 2003)

$$\sigma_\lambda^2 = Var(\mu_w) + \frac{1}{N^2}\sum_{i=1}^{N} Var(\delta_i) = \sigma_e^2 + \frac{\sigma_d^2}{N} \tag{3.4}$$

From this equation, we can see that, for large sizes of the population ($N \gg \sigma_d^2/\sigma_e^2$), demographical fluctuations can be neglected with respect to environmental fluctuations. Typical critical population size above which demographical fluctuations are negligible is $N_c = 10\sigma_d^2/\sigma_e^2$. Depending on the species, this critical population size may vary from 10 to 1000, and it is often around 100.

Then the variance of the population size N is $Var(N) = N^2\sigma_\lambda^2 = N^2\left(\sigma_e^2 + \frac{\sigma_d^2}{N}\right)$, and replacing this variance in Eq. (3.1), the stochastic growth equation becomes

$$dN = F(N)dt + N\sqrt{\sigma_e^2 + \frac{\sigma_d^2}{N}}dB \tag{3.5}$$

In the Growth Equation (3.5), we see that the effect of environmental fluctuations scales with the population size N. In contrast, the effect of the demographical fluctuations scale with the square root of the population, so if the population is large enough,[1] the demographical fluctuations can be neglected, and the growth equation has the form

$$dN = F(N)dt + N\sigma_e dB \tag{3.6}$$

Equation (3.6) is the general dynamical population growth equation. Considering Allee Effect dynamics,

$$F(N) = rN\left(1 - \frac{N}{K}\right)\left(\frac{N}{A} - 1\right) - mN + m\int N(x-y,t)f(y)dy \tag{3.7}$$

In Figure 3.1, we have represented two relevant cases introduced in Chapter 1, Allee equations without dispersal starting both above and under the Allee Threshold A, including environmental fluctuations as a noise term. It is essential to notice that fluctuations, if they are large enough, cause a very different behavior with respect to the deterministic case. For example, on the one hand, there is a simulation in which we started above the Allee threshold A, and the population finally decreases to zero. On the other hand, we can see that it is possible to start below the Allee Threshold and recover to finally fluctuate around equilibrium

[1] Given that in our works about Allee effect (Chapters 5 and 6) we assume $K = 1$ it may seem like the population is not large enough to neglect demographic fluctuations, even when we are close to the equilibrium. This confussion is only about the system of units we are using. Regular stochastic Allee growth equation (without neglecting demographic fluctuations) has the form

$$dN = \left(rN\left(1 - \frac{N}{K}\right)\left(\frac{N}{A} - 1\right) - mN + m\int N(x-y,t)f(y)dy\right)dt + N\sqrt{\sigma_e^2 + \frac{\sigma_d^2}{N}}dB$$

If we perform the change that yields the units for which $\widetilde{K} = 1$, i.e. $\widetilde{N} = N/K$, $\tilde{A} = A/K$, $\widetilde{K} = K/K = 1$, then the equation becomes:

$$d\widetilde{N} = \left(r\widetilde{N}\left(1 - \frac{\widetilde{N}}{\widetilde{K}}\right)\left(\frac{\widetilde{N}}{\tilde{A}} - 1\right) - m\widetilde{N} + m\int \widetilde{N}(x-y,t)f(y)dy\right)dt + \widetilde{N}\sqrt{\sigma_e^2 + \frac{\sigma_d^2}{K\widetilde{N}}}dB$$

Where, if the "real" $N = K\widetilde{N}$ is big enough we can neglect demographic fluctuations and then we get the growth equation used in our work and valid for $\widetilde{K} = 1$. In our work (chapters 5 and 6) we eliminated the tilde notation.

at the carrying capacity K, even when populations with these initial conditions end up in extinction in the deterministic dynamics.

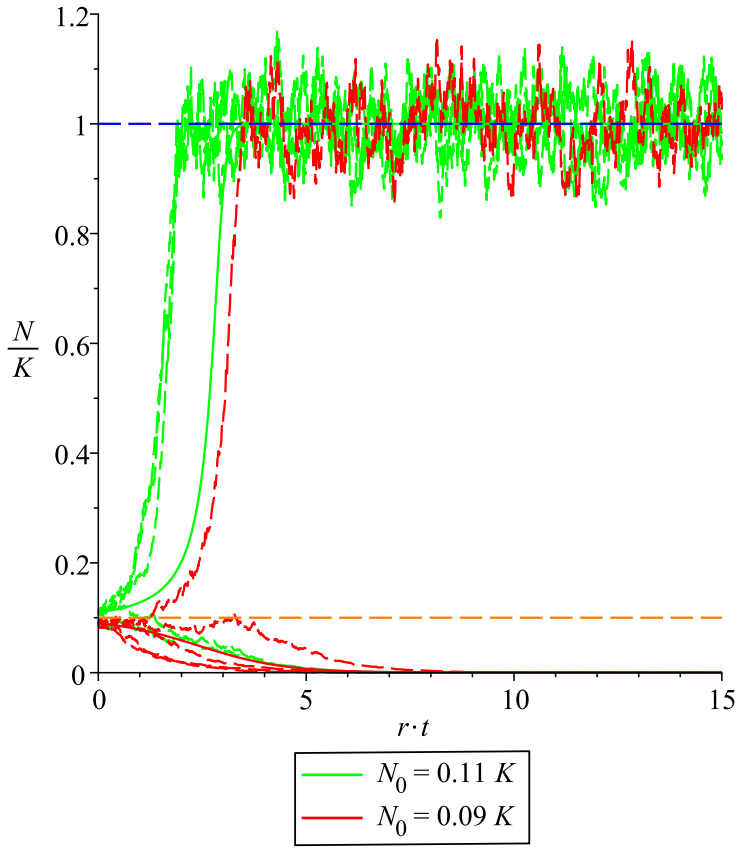

Figure 3.1: Population evolution for Allee growth models with different initial conditions. We have chosen a vast carrying capacity ($K = 10^6$, blue dashed line), so demographic fluctuations can be neglected. We have considered an amplitude of the environmental fluctuations σ_e=0.2, and for the Allee equation, the Allee Threshold has a value $A = 0.1\,K$(orange dashed line). Green lines indicate an initial population $N_0 = 0.11K$, while the red lines start at $N_0 = 0.09K$. Dashed lines indicate different realizations of the stochastic dynamics, while the solid ones show the deterministic dynamics for comparing purposes.

Chapter 4: Population synchrony.

In Chapter 1, we have introduced the main concepts of metapopulations and dispersal (Lande, Engen, and Saether 2003; Cotgreave and Gotelli 2006). The fluctuations affecting two distant metapopulations can be correlated. The spatial correlation between metapopulations is called population synchrony, which has a crucial role in population dynamics, for example, by affecting the probability of regional extinction. Some causes of population synchrony are weather, predation, and individual dispersal between the synchronized populations (Moran 1953; Jarillo et al. 2020; Ranta et al. 1995).

The first of those three references was one of the first and most important studies about population synchrony (Moran 1953), where Moran studied two closed Canadian Lynx populations without individual dispersal. In that paper, he established that in a simple linear model with small fluctuations around the equilibrium, the correlation between the two populations is proportional to the environmental correlation. Moran effect has been studied by many authors, and the assumption of a linear structure can be relaxed in many cases to non-linear functions as well (Ranta et al. 1997; Hansen et al. 2020).

4.1. Population synchrony with individual dispersal.

Let us assume a population dynamics model with dispersal that has a population dynamics equation such as

$$dN(x,t) = dN(x,t)|_{local} + dN(x,t)|_{dispersal} + N\sigma_e dB(x,t) \tag{4.1}$$

Where the local term $dN(x,t)|_{local}$ has the form of an effective per-capita growth rate β multiplying the number of individuals N (and can be one of the deterministic, not dispersing growth equations in chapter one, such as logistic or Allee), i.e.,

$$dN(x,t)|_{local} = \beta(N,x,t)N(x,t)dt \tag{4.2}$$

The dispersal term describes that individuals tend to move along the habitat. In the simplification in which there is no external migration, this term is

$$dN(x,t)|_{dispersal} = \left(-mN(x,t) + m\int N(x-y,t)f(y)dy\right)dt \tag{4.3}$$

Where individual dispersal $f(y)$ is symmetric with mean 0 (it is usually a gaussian distribution), which means $f(y) = f(-y)$. To study population synchrony, it is useful to linearize equation 4.1 around equilibrium provided small fluctuations. We define the proportional deviation from deterministic equilibrium as $\varepsilon = N/K - 1$, which has an expected value of 0 on each location, then equation 4.1 becomes

$$d\varepsilon(x,t) = -(\gamma + m)\varepsilon(x,t)dt + m\,dt\int \varepsilon(x-y,t)f(y)dy + \sigma_e dB(x,t) \tag{4.4}$$

Where γ is the linearized rate of return to equilibrium in the absence of dispersal (equal to r in logistic growth), and the gaussian white noise dB is exponentially autocorrelated in space with

correlation longitude or spatial scale of environmental synchrony l_e(the typical distance at which the fluctuations remain correlated). Note that the same linearization around equilibrium (for a local population without dispersal, i.e., $m = 0$) is used for our model in Chapter 7.

Then, the spatial autocorrelation of population fluctuations is defined by

$$c(z) =< \varepsilon(x,t)\varepsilon(x+z,t) > \tag{4.5}$$

And the spatial autocorrelation of the environmental fluctuations is

$$\rho_e(z)dt =< dB(x,t)dB(x+z,t) > \tag{4.6}$$

Then, let us assume that $\varepsilon(x,t+dt) = \varepsilon(x,t) + d\varepsilon(x,t)$. Then, for the stationary distribution, we have $< \varepsilon(x,t)\varepsilon(x+z,t) >=< \varepsilon(x,t+dt)\varepsilon(x+z,t+dt) >$, so applying these assumptions and Eq. (4.4) to the definition of $c(z)$ (Eq. (4.5)) and neglecting terms of second order in dt we obtain the following expression:

$$2(\gamma+m)c(z) = 2m\int c(z-y,t)f(y)dy + \sigma_e^2\rho_e(z) \tag{4.7}$$

In the absence of dispersal, the equation verifies Moran Effect, which is

$$c(z) = \frac{\sigma_e^2\rho_e(z)}{2\gamma} \tag{4.8}$$

Because $\rho(z) = \frac{c(z)}{c(0)} = \rho_e(z)$. Also, from (Lande, Engen, and Sæther 1999), we have the following bound for the autocorrelation of the population in $z = 0$:

$$\frac{\sigma_e^2}{2(\gamma+m)} < c(0) < \frac{\sigma_e^2}{2\gamma} \tag{4.9}$$

So dispersal significantly decreases the lower bound if it is big enough. Furthermore, Lande et al. defined the spatial scale of population synchrony for a single dispersed species, which has been extended recently to study population synchrony in systems of two species (Jarillo et al. 2018; 2020).

The standard deviation of individual dispersal distance l_m, which is the characteristical spatial scale traveled by an individual, is defined as $l_m^2 = \int z^2 f(z)dz \,/\, \int f(z)dz$. Conversely, l_e is the spatial scale of environmental synchrony, which can be calculated by $l_e^2 = \int z^2\rho_e(z)dz \,/\, \int \rho_e(z)dz$.

Then, an analogous definition is used for the spatial scale of population synchrony l

$$l^2 = \frac{\int z^2 c(z)dz}{\int c(z)dz} \tag{4.10}$$

Population synchrony can be computed using Fourier transforms to integrate Equation (4.7), getting the result

$$l = \sqrt{l_e^2 + \frac{m l_m^2}{\gamma}} \tag{4.11}$$

Meaning that both higher dispersal or weaker regulation (lower rate of return to equilibrium) on a species imply a greater spatial scale of population synchrony, which is also the typical size of an area affected by regional extinction (Lande, Engen, and Saether 2003). Thus, populations with larger spatial scales of synchrony have a higher risk of regional extinction (Heino et al. 1997; Heino 1998; Heino, Ripa, and Kaitala 2000), which depends on the intensity of population fluctuations as well. However, dispersal can also act by increasing the effective rate of return of local fluctuations to the mean population size. Dispersal also increases this local mean population size (Engen, Lande, and Sæther 2002), which decreases the extinction risk. However, the overall effect of dispersal is to decrease local extinction risk. As we show in Chapters 5 and 6, dispersal is even more useful as a tool to avoid regional extinction if the total area inhabited by the population is substantially larger than the scale of population synchrony (Engen, Lande, and Sæther 2002).

PART II:
Spatially extended stochastic population dynamics with Allee Effect

Chapter 5: Dispersal-induced resilience to stochastic environmental fluctuations in populations with Allee effect

Many species are unsustainable at small population densities (Allee effect); i.e., below the so-called Allee threshold, the population decreases instead of growing. In a closed local population, environmental fluctuations always lead to extinction. Here, we show how, in spatially extended habitats, dispersal can lead to a sustainable population in a region, provided the amplitude of environmental fluctuations is below an extinction threshold. We have identified two types of sustainable populations: high-density and low-density populations (through a mean-field approximation, valid in the limit of large dispersal length). Our results show that patches, where population is high, low, or extinct, coexist when the population is close to global extinction (even for homogeneous habitats). The extinction threshold is maximum for characteristic dispersal distances much larger than the spatial scale of synchrony of environmental fluctuations. The extinction threshold increases proportionally to the square root of the dispersal rate and decreases with the Allee threshold. The low-density-population solution can allow understanding of difficulties in non-recovery events after harvesting. This theoretical framework provides a unique approach to address other factors, such as habitat fragmentation or harvesting, impacting population resilience to environmental fluctuations.

5.1. Introduction

Many species need a minimum population density to be viable, for example, the island fox (Angulo et al. 2007), the polar bear (Molnár et al. 2008), American ginseng (Hackney and McGraw 2001) and the Atlantic codfish (Kuparinen and Hutchings 2014) among others. This minimum viable population density is named the Allee threshold (Allee 1931), and below it, the population declines toward extinction, a phenomenon called the (strong) Allee effect.

Field research has characterized the impact for plants and animals of reaching population densities below the Allee threshold. The strength of the impact depends on the strength of the Allee effect (Kumar and Dubey 2020), the presence of harvest (Liz and Ruiz-Herrera 2015), and the absence of positive human intervention (Crates et al. 2017; McDermott and Finnoff 2016). Many of these depleted populations never recover and become extinct in some years. Some depleted populations take many years (much more than the average lifetime of the species) to get out of this situation and eventually recover. In animals, monogamous species with long lifetimes are more likely to show the Allee effect (Sæther, Ringsby, and Røskaft 1996; Angulo et al. 2007), in addition to solitary species with difficulties for finding a breeding mate or an unbalanced male-female ratio (Molnár et al. 2008). Another causes that explain Allee effect in animals are nonefficient feeding (Way and Banks 1967), difficulties surviving in an environment with predators, competitors or human harvest (Moynihan and Kruuk 2010; Kenward 2006); or inbreeding depression (Ralls, Frankham, and Ballou 2013; Frankham and Ralls 1998). In plants, less efficient pollination or fruit production (decreasing at small populations) (Hackney and McGraw 2001) seem to be the principal causes providing the Allee effect. Most of the articles cited above qualitatively describe how a certain species in a low-population-density situation has difficulties surviving due to the Allee effect.

Theoretical papers have addressed the general question of the eradication of alien species (Liebhold and Bascompte 2003), and of spatial patterns' influence on the spread of invading species (Lewis and Kareiva 1993), observed in the gypsy moth (Vercken et al. 2011). These papers show that both the Allee effect and environmental variability can contribute to the

extinction of a population. Other works have studied the effects of stochasticity in species vulnerable to the Allee effect (Dennis 2002; Engen, Lande, and Sæther 2003; Lee, Sæther, and Engen 2011; Méndez et al. 2019) describing mean time to extinction, or probability of extinction after a given time, for a single location. Migration between locations increases the mean time to extinction, as it has been shown in a metapopulation model with a 3x3 grid (Brassil 2001). Studies of a locally endangered butterfly sustain the important role of immigration in the regional dynamics to counterbalance the Allee effects (Bonsall et al. 2014). Recently, Dennis et al. (Dennis et al. 2016) showed that an external constant migration term can sustain the population in the presence of stochastic environmental fluctuations. Here, we go a step further and show that a spatially extended population with dispersal between the locations can be sustainable. We compute the stationary population probability distributions in the mean-field limit (large dispersal distance), which elucidates the spatially extended population dynamics for finite dispersal distance. This results clarify the conditions for sustainability in spatially extended habitats, quantifying the effects of dispersal in the resilience to stochastic environmental fluctuations.

We have studied a one-dimensional model, which is a good approach for some ecological systems such as rivers or oceanic water columns (Villa Martín et al. 2015). One-dimensional models also allow a more straightforward yet accurate study of many characteristics of interaction-based population dynamics (Ribeiro and Ribeiro 2015).

The results we present here provide insight on how natural or human-induced changes in the species' dynamical parameters would influence its extinction risk due to environmental fluctuations. In particular, they provide information on how an increase in the amplitude of environmental fluctuations can affect the sustainability of a population. This problem is of particular present relevance as several regions of the Earth are increasing its climate variability (IPCC 2012).

5.2. Spatially extended population model

We introduce here a spatially extended, one-dimensional population model, including Allee effects, environmental fluctuations, and dispersal. This model allows us to assess the resilience of populations to environmental fluctuations and the role played by dispersal in this resilience.

The deterministic Allee model (Allee and Rosenthal 1949; Odum and Allee 2006), introduced in the first chapter of this thesis, gives the local deterministic dynamics of the population density $N(x,t)$ at location x and time t. This dynamics is determined by a characteristic extinction rate r, a carrying capacity K (stable viable population density), and an Allee threshold A (minimum viable population density). Note that the population density $N(x,t)$ is defined as the local number of individuals per unit of length at a given time. Additionally, environmental stochasticity is introduced through an additional stochastic contribution $\sigma\, N\, dB$, proportional to the population density, as explained in Chapter 3. The amplitude of these environmental fluctuations is given by σ, and $dB(x,t)$ is a normalized Gaussian random field (Chapter 2) with a spatial scale of synchrony l_e, giving the spatial scale of synchrony of the environmental fluctuations (Chapter 4), which is the characteristic distance at which environmental fluctuations remain correlated (Jarillo et al. 2018). Therefore, the local dynamics of a population density $N(x,t)$ in the stochastic Allee model is given by

$$dN(x,t)|_{local} = r\, N(x,t) \left(\frac{N(x,t)}{A} - 1\right) \left(1 - \frac{N(x,t)}{K}\right) dt + \sigma\, N(x,t)\, dB(x,t). \qquad (5.1)$$

The first term corresponds to the deterministic Allee model (Allee and Rosenthal 1949; Odum and Allee 2006; Lewis and Kareiva 1993). This equation implies a rate of return to extinction for populations close to extinction of $\gamma_0 = r$ and a rate of return to the carrying capacity for populations close to the carrying capacity of $\gamma_K = r\,(K/A - 1)$. The second term in Eq. (5.1) gives the contribution of stochastic environmental fluctuations to the changes in the local population, with an amplitude of the environmental fluctuations σ. The random field $dB(x,t)$ is given by increments of standard Brownian motions in each position with zero mean and variance dt, and it is spatially correlated with an exponential autocorrelation of length l_e, which is the spatial scale of synchrony of environmental fluctuations (Jarillo et al. 2018).

The dispersal couples the dynamics in the different locations. We consider a dispersal model (as done in Chapter 1) for which individuals disperse away with a rate m to a characteristic distance l_m. Thus, dispersal gives an additional contribution to the dynamics of

$$dN(x,t)|_{dispersal} = -m\,N(x,t)\,dt + m\,dt \int N(x-y,t)\,f(y)\,dy\,, \tag{5.2}$$

which makes the dynamics nonlocal. The first term represents the population decrease at position x due to individuals that disperse away with probability $m\,dt$. The second term gives the population increase due to individuals that disperse to position x from a position displaced a distance y where the population is $N(x-y,t)$. Therefore, m is the rate of random dispersal to a position at a distance y with probability $f(y)$, where $f(y)$ has been taken as a Gaussian with variance l_m^2 and zero mean. Dispersal rate m is the same in both terms in Eq. 5.2 because our model assumes no external migration: Every individual leaving a patch moves to another within the ecosystem, whereas every individual arriving at a patch must have come from the same ecosystem. Furthermore, we consider a homogeneous habitat, so neither the dispersal rate m nor the dispersal profile $f(y)$ (nor any other parameter of the model) depends on position x. Hence, individuals disperse at a rate m to typical distances of the order of l_m. As the dispersal term in Eq. 5.2 is proportional to the population density $N(x,t)$, depleted regions will receive a net population flux from nearby nondepleted regions.

The combination of local and dispersal contributions to the change in population density gives the complete spatially extended dynamics,

$$dN = dN|_{local} + dN|_{dispersal}\,. \tag{5.3}$$

Typical late time population distributions given by this dynamical equation can be seen in Fig. 5.1 (panels A, C, and E). Table 5.1 gives a summary of the variables and parameters used and their units.

Variables	Description
$N(x,t)$	Population density at a given position x and a time t. Units of length^{-1}.
A	Allee threshold of the species, below it, the species has negative growth. Units of length^{-1}.
K	Carrying capacity of the species, meaning stable, viable population density. Units of length^{-1}.
r	Extinction rate (at very low population densities). Units of time^{-1}.
γ_0	Rate of return to extinction. Units of time^{-1}.
γ_K	Rate of return to carrying capacity. Units of time^{-1}.
m	Dispersal rate of the species. Units of time^{-1}.
l_e	Spatial scale of synchrony of environmental fluctuations. Units of length.
l_m	Mean distance traveled by the dispersed individuals (characteristic width of the Gaussian dispersion function). Units of length.
σ	Amplitude of the environmental fluctuations, giving the standard deviation of the environmental fluctuations. Units of time$^{-1/2}$.
$\sigma_{extinction}$	Extinction threshold for the amplitude of environmental fluctuations (Minimum amplitude of the fluctuations that ensures global extinction). Units of time$^{-1/2}$.

Table 5.1: Variables used in this chapter (definitions and units).

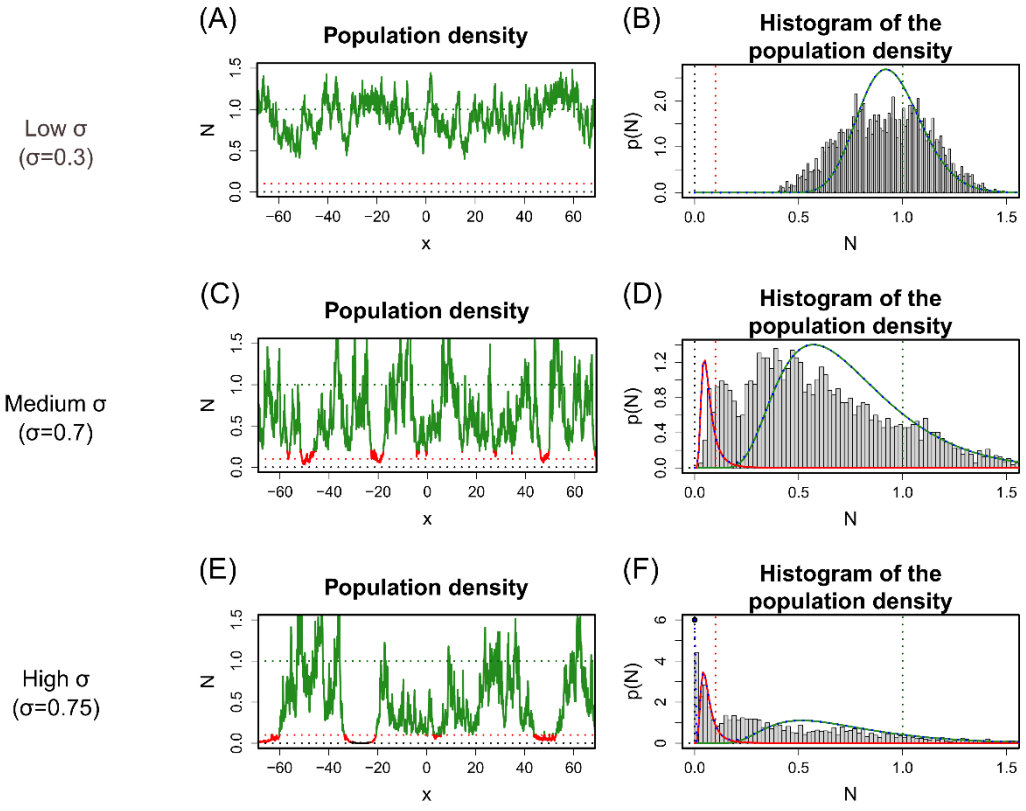

Figure 5.1: Spatial profiles of population density, and their associated averaged population density histograms compared with mean-field population probability distributions. Panels A, C and E: spatial profile of the population density for simulation at long time, $t = 1000$, with extinction rate $r = 0.1$, Allee threshold $A = 0.1$, carrying capacity $K = 1$, dispersal rate $m = 1$, and dispersal distance equal to the spatial scale of synchrony of environmental fluctuations $l_m = l_e = 1$. Panels B, D, and F: population density histograms for the spatial profiles of

population densities shown in Panels A, C, and E, respectively. The curves in Panels A, C, and E show the patches in extinction (black) high-population (green), and low-population states (red), according to the histograms in Panels B, D, and F. Panels B, D, and F also show the fit to a linear combination of the mean-field population probability distributions. The results for these fits are $p(N) = p_{high}(N)$ *in Panel B,* $p(N) = 0.08p_{low}(N) + 0.92p_{high}(N)$ *in Panel D and* $p(N) = 0.06p_0(N) + 0.22p_{low}(N) + 0.72p_{high}(N)$ *in Panel F. Each contribution is represented with its fitted weight.* $p_{low}(N)$ *(red line) and* $p_{high}(N)$ *(green line) correspond, respectively, to the low- and high-density mean-field population probability distribution solutions. They are given by the two non-zero branches of solutions of the mean-field equations for values of σ below the extinction threshold (see also Fig. 5.2).* $p_0(N)$*(black point) is the zero population density solution (i.e., extinction). Red dashed lines indicate Allee threshold value* $A = 0.1$*, green dashed lines indicate carrying capacity* $K = 1$*, and black dashed lines indicate* $N = 0$*. Note the similarities between the population density histograms obtained from direct numerical simulation and the fit to the linear combination of the population probability distributions obtained with the mean-field limit approximation (i.e., the large migration distance limit,* $l_m/l_e \to \infty$*). However, the real histograms are displaced to the left due to the border effects, which are effects beyond the mean-field approximation (i.e., due to finite migration distance, in this case* $l_m/l_e = 1$*). Note also that increasing the environmental fluctuations σ increases the presence of regions where the population is depleted or extinct, as σ approaches the extinction threshold (*$\sigma_{extinction} = 0.80$ *for the parameter values in this figure).*

5.3. Numerical simulations

The numerical simulations of the previously described dynamical equation are performed taking the scale of synchrony of environmental fluctuations, l_e, as reference length, *i.e.,* $l_e = 1$, and 20 lattice nodes per unit length. The total length of the simulation box was 140 times the maximum of l_e and l_m, and we consider periodic boundary conditions (aiming to obtain results for infinite habitat). The time resolution was 50 times smaller than the minimum of the characteristic times of the dynamics (*i.e.*, the minimum of the inverses of the rates r and m). These resolutions, simulations boxes, and boundary conditions guarantee that the dynamics is well-resolved (in time and space) and mimics an infinite habitat for better comparison with the results found with the mean-field approximation (Law, Dieckmann, and Metz 2000; Morozov and Poggiale 2012) described below. In this way, we performed numerical simulations of spatially extended populations, starting from a population density equal to the carrying capacity in each node of the simulation box. We ran several simulations for each set of parameters with different amplitudes of the environmental fluctuations. See Appendix 5.C for further details on the simulation algorithm.

We define the extinction threshold, $\sigma_{extinction}$, as the characteristic amplitude of environmental fluctuations above which the environmental fluctuations leads to the global extinction of the population. The environmental fluctuation extinction threshold $\sigma_{extinction}$ is obtained from long time simulation ($t = 1000 = 100\, r^{-1}$) as the center of the transition interval from the never extinct to the always global extinct final case.

Besides, relevant information of a spatially extended population is how probable it is to find a given population density in a given location, *i.e.*, to determine the population probability distribution. We have assumed homogeneous habitat conditions, which is represented by location-independent population dynamics parameters (extinction rate r, carrying capacity K, Allee threshold A, and amplitude of environmental fluctuations σ). Thus, the population

probability distribution $p(N)$ does not depend on location and gives the probability to find the population density N in any site. The population probability distribution $p(N)$ is computed from numerical simulations doing population density histograms, like those shown in Fig. 5.1 Panels B, D, and F.

5.4. Analytical population probability distribution

Additionally, we can get further insight into the population dynamics through a more analytical approach for the computation of the population probability. The stochastic differential equations for the stochastic Allee model with and without dispersal, Eqs. (5.1) and (5.3), have the form $dN = F(N)\,dt + \sqrt{v(N)}\,dB$. For equations of this form, if a stationary population probability distribution exists it is given by (Karlin and Taylor 1967)

$$p(N) = \frac{n}{v(N)} \cdot \exp\left(2\int \frac{F(N)}{v(N)}\,dN\right), \tag{5.4}$$

where n is a normalization factor.

Therefore, for the stochastic Allee model without dispersal, Eq. (5.1), the stationary population probability distribution is

$$p(N) = \frac{n \cdot \exp\left(\frac{1}{\sigma^2}\left(\frac{2rN}{K} + \frac{2rN}{A} - \frac{rN^2}{AK}\right)\right)}{\sigma^2 N^{2+2r/\sigma^2}}, \tag{5.5}$$

This population distribution has a divergence in $N = 0$ and is not normalizable, which means that a population with an Allee-type growth will always become extinct in the absence of dispersal ($m = 0$). (The extinction is faster for larger environmental fluctuations. See Appendix 5.B.)

Only populations with dispersal may be stable in the long term. For the stochastic Allee model with dispersal, Eq. (5.3), the stationary population probability distribution with dispersal is

$$p(N) = \frac{n \cdot \exp\left(\frac{1}{\sigma^2}\left(\frac{2rN}{K} + \frac{2rN}{A} - \frac{rN^2}{AK} - \frac{2mI}{N}\right)\right)}{\sigma^2 N^{2+2(r+m)/\sigma^2}}, \tag{5.6}$$

where the coupling term $I(x) = \int N(x-y)\,f(y)\,dy$ makes the population probability in one location depending on the values of the population density in the surrounding region. This additional dispersal term makes the population distribution normalizable and with no-zero mean for certain ranges of values of m and σ.

5.5. Mean-field approximation

We propose here to combine the analytic expression in Eq. (5.6) with the mean-field approximation to deal with the coupling term $I(x)$. When the dispersal length is much larger than the spatial scale of synchrony of environmental fluctuations, $l_m \gg l_e$ (for example, the case of long-distance migrant birds), the mean-field approximation is a good approximation. The mean-field approximation assumes the stationary population density is approximately

equal in all points of space. (Long-distance dispersal, $l_m \gg l_e$, makes the population density more homogeneous, recolonizing low-populated points from those that are "overpopulated"). The mean-field approximation implies that the coupling term I in Eq. (5.6) can be treated as position independent, $I(x) = I$, and we can approximate it by the mean value of the population density

$$I = \int_0^\infty N\, p(N)\, dN\,. \tag{5.7}$$

This approximation mimics the dynamics of long-distance dispersal (see Fig. 5.A2 in Appendix 5.A). The extinction threshold, $\sigma_{extinction}$, was defined here as the amplitude of environmental fluctuations above which the environmental fluctuations lead to the global extinction of population. In the mean-field approximation, the extinction threshold can be computed directly obtaining the value of the environmental amplitude where there is no longer a solution of the system of equations formed by Eqs. (5.6) and (5.7) (*i.e.*, the point where the green and the red curves merge in Fig. 5.2A), except the extinction in the all space solution, (non-normalizable divergence in N=0). Thus, when the amplitude of environmental fluctuations exceeds the extinction threshold, the only possible solution implies global extinction (we find population at $N = 0$ for long times with probability 1, $p(N = 0) = 1$), and it is not normalizable. Therefore, the mean-field approximation allows us to compute the stationary probability distribution and to estimate the extinction threshold for a particular set of parameters (which is a close upper limit of the real extinction threshold when the dispersal distance of the species is large enough). We get two branches of solutions, which represent two different equilibria: the high mean population density solution, p_{high}, and low mean population density solution, p_{low}. See Figs. 5.1 and 5.2.

The diagram of the mean population densities I for the two branches of solutions depends on the parameters of the model (Fig. 5.2). Lower Allee thresholds A displace the diagram toward higher amplitudes of environmental fluctuations σ, but lower the mean population I and make more prominent the minimum of the lower branch. Higher dispersal rates m displace the diagram to higher amplitudes of environmental fluctuations σ and slightly to higher mean population densities I, marking the role of dispersal as a stabilizing factor of the population. (See Fig. 5.2 and Fig. 5.A1 in Appendix 5.A.)

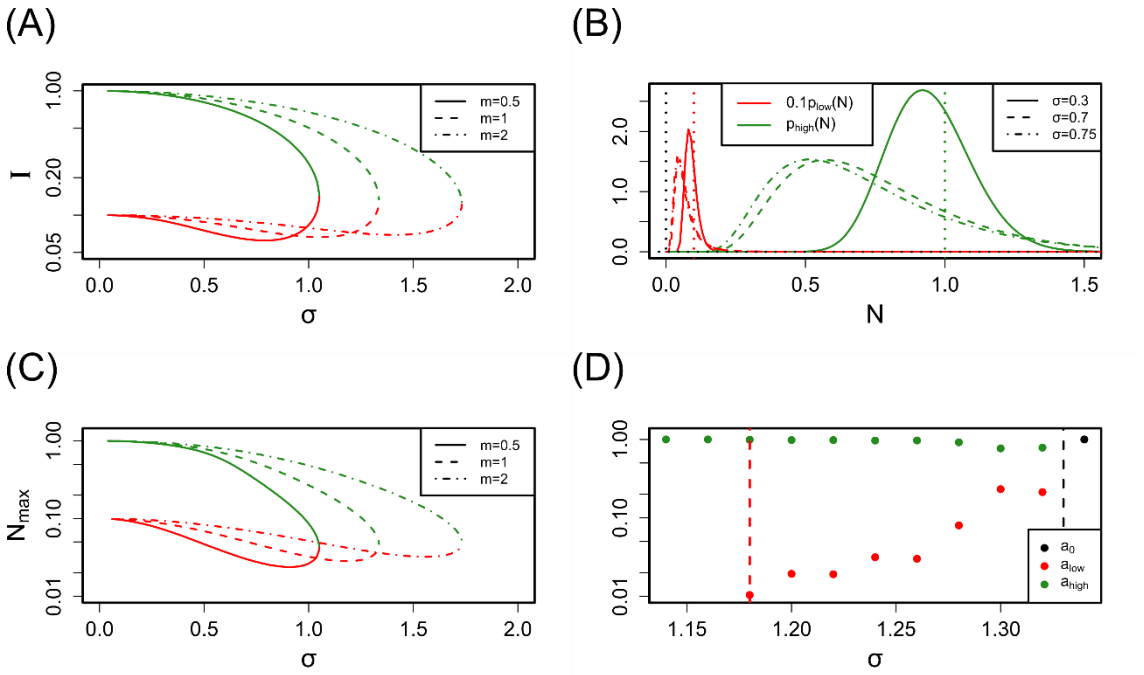

Figure 5.2: Solutions in the mean-field approximation. (Panel A) Mean population density I as a function of environmental noise amplitude σ for the two nonzero branches of solutions at the mean-field approximation ($l_m \gg l_e$): high-density (green) and low-density (red) branches (shown in logarithmic scale). Extinction rate $r = 0.1$, carrying capacity $K = 1$, Allee threshold $A = 0.1$, and dispersal rate $m = 0.5$ (solid line), $m = 1$ (dashed line), and $m = 2$ (dash-dotted line). (Panel B) High-density (green) and low-density (red, divided by 10 to make the figure more visible) population probability distributions, phigh and plow, respectively. They are calculated at the mean-field approximation for the same parameters of Panel A and $m = 1$, for values of the environmental fluctuations amplitude $\sigma = 0.3$ (solid line), $\sigma = 0.7$ (dashed line) and $\sigma = 0.75$ (dash-dotted line). Vertical lines show $N = 0$ (black), $N = A = 0.1$ (red) and $N = K = 1$(green). (Panel C) Position of the maximum of mean-field distributions N_{max} as a function of environmental noise amplitude σ, for the two nonzero branches of solutions at the mean-field approximation (shown in logarithmic scale) with the same parameters as in Panel A. (Panel D) Fitted contribution of each mean-field distribution in stationary distributions simulated by population dynamics assuming mean-field limit (see appendix 5.C) such as $p(N)_{simulated} = a_{low}\ p_{low}\ (N) + a_{high}\ p_{high}\ (N) + a_0\ p_0\ (N)$, where $p_0(N)$ is the zero population density solution (i.e., extinction) and $a_{low} + a_{high} + a_0 = 1$, for extinction rate $r = 0.1$, carrying capacity $K = 1$, Allee threshold $A = 0.1$, and dispersal rate $m = 1$. Vertical red dashed line shows the amplitude of environmental fluctuations which gives the position of the minimum in the lower branch of N_{max} (panel C), and vertical black dashed line shows the extinction threshold σextinction calculated in the mean field limit. The vertical axis is shown in logarithmic scale and values below 0.01 are not represented. The figure shows that contributions of $p_{low}\ (N)$ start to appear for sigmas equal or greater than the position of the minimum in the lower branch of N_{max}. Additionally extinction appears for amplitudes of environmental fluctuations greater than $\sigma_{extinction}$.

5.6. Maximum approximation

The maximum approximation assumes the extinction threshold is the value of the amplitude of environmental fluctuations σ that locates the maximum of $p_I(N)$ [where $p_I(N)$ *is* is the population probability for a given I] at the Allee threshold A. This estimation gives for the extinction threshold,

$$\sigma_{extinction} = \sqrt{m\left(\frac{I}{A} - 1\right)}. \tag{5.8}$$

This expression points out that the extinction threshold approximately increases with the square root of the migration rate and decreases with the Allee threshold A (Fig. 5.3). In order to obtain the value of $\sigma_{extinction}$ estimated with the mean-field and maximum approximations, we must simultaneously solve numerically Eqs. (5.6), (5.7), and (5.8). It should be noted that the maximum approximation is only an additional approximation, which can be added to the method introduced in the previous section [$\sigma_{extinction}$ is the value of the environmental amplitude where there is no longer a solution for the set of equations Eqs. (5.6) and (5.7)]. The maximum approximation allows a faster estimation of the extinction threshold and shows that the extinction threshold approximately grows with the root of the dispersal rate m. However, the method described in the previous section is more accurate and is preferred to compute the extinction threshold in the mean-field limit.

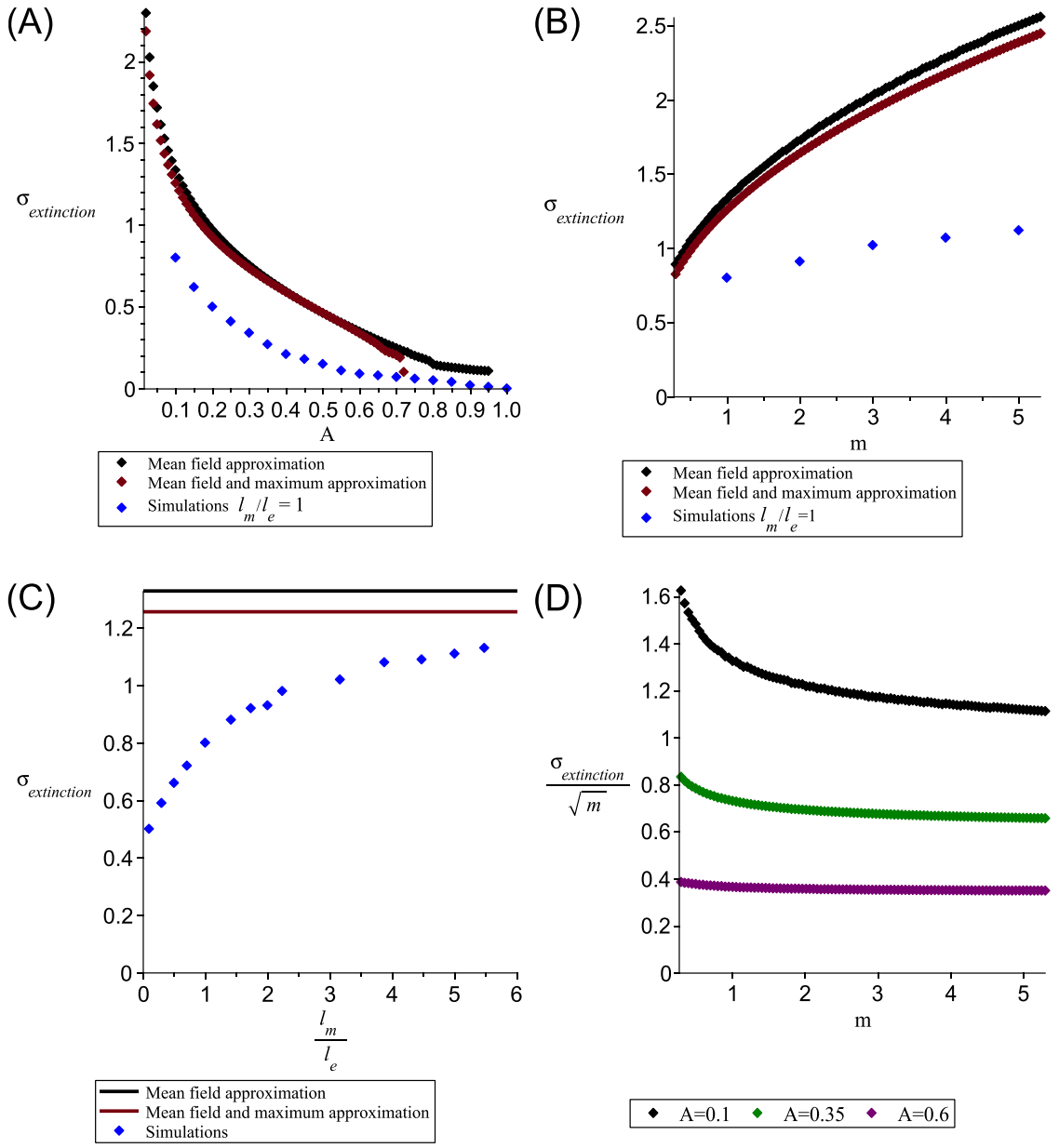

Figure 5.3: Extinction threshold $\sigma_{extinction}$ versus different parameters. (Panel A) Extinction threshold versus Allee threshold for the mean-field approximation (black dots) (i.e., large dispersal length, $l_m \gg l_e$), for the mean-field and maximum approximations (red dots), and for a simulation with $l_m = l_e$ (i.e., dispersal length l_m equal to the spatial scale of synchrony of environmental fluctuations l_e), all with dispersal rate $m = 1$. (Panel B) Extinction threshold versus dispersal rate using the same color code as the previous panel, all with Allee threshold $A = 0.1$. The dispersal rates considered, m =0.3 to 5.3, are similar or higher than the characteristic extinction rate considered in this simulations $r = 0.1$, providing a significant contribution to population recoveries. (Panel C) Extinction threshold $\sigma_{extinction}$ as a function of the ratio between the characteristic dispersal distance and the spatial scale of synchrony of environmental fluctuations l_m/l_e, using the same color codes as the previous panels, all with $m = 1$ and $A = 0.1$. (Panel D) Scaling of the extinction threshold at large dispersal rate verified plotting the ratio $\sigma_{extinction}/\sqrt{m}$ versus the dispersal rate m (in the same interval as in Panel B) for Allee thresholds $A = 0.1$ (black), $A = 0.35$(green), and $A = 0.6$(purple) obtained for the

mean-field approximation. For all panels, the extinction rate is $r = 0.1$ *and the carrying capacity* $K = 1$.

5.7. Dispersal makes the population resilient to environmental fluctuations

In a closed local population, environmental fluctuations lead to extinction in the presence of environmental fluctuation, because environmental fluctuations eventually lead the population density below the Allee threshold A, and to extinction. Our results show that dispersal allows the recovery of a region with a depleted population thanks to population arriving from nearby nondepleted regions. This dispersal-induced population recovery makes the species resilient to population depletion caused by environmental fluctuations. Resilience to environmental fluctuations is enhanced increasing dispersal (either by increasing dispersal rate or by increasing dispersal length), stressing the relevance of the rescue effect of dispersal. See Fig. 5.3, where the extinction threshold $\sigma_{extinction}$ is represented. When environmental fluctuations are larger than the extinction threshold, the population becomes globally extinct.

From the mean-field approximation, we obtain that in the absence of dispersal, $m = 0$, the population probability, Eq. 5.5, diverges in $N = 0$ as $N^{-2\left(1+\frac{r}{\sigma^2}\right)}$, indicating that the population always goes extinct (after a certain transition time). However, when dispersal is present, the dispersal term with I suppress the divergence at zero population density, and the species can be sustained. Then, dispersal (or migration) is necessary to sustain a population at long times. This result is consistent with previous results found with a constant migration term in (Dennis et al. 2016). They considered a constant external migration in the growth equation, instead of spatial extended dispersal within the habitat that we considered. In the case with dispersal, the system of equations formed by Eqs. (5.6) and (5.7) is numerically found to have either two roots or no root (different from the zero root). (See Panel A of Fig. 5.2.) The two regimes are separated by a critical value of the amplitude of environmental fluctuations, $\sigma_{extinction}$. (The results obtained with the mean-field approximation are shown with black dots in Fig. 5.3). For values above this extinction threshold, $\sigma_{extinction}$, populations become extinct in all the locations. In contrast, for values below the extinction threshold, there is an equilibrium between extinction and recovery from extinction due to dispersal from other regions. The two branches of solutions represent two different equilibria. The high mean population density solution, p_{high} (green curves in Panels B, D, and F of Fig. 5.1) has most regions of space with population densities above the Allee threshold, and local extinction is rare. The regions above the Allee threshold have population densities below the carrying capacity due to the cost of recovering areas with local extinction. The low mean value solution p_{low} (red curves in Panels B, D, and F of Fig. 5.1) has most of the regions below the Allee threshold, and they are just prevented from extinction due to the dispersal contributions from the regions with population densities above the Allee threshold. These two ideal solutions have been obtained in the mean-field approximation, which assumes large dispersal lengths *(*$l_m \gg l_e$*)*. Nonetheless, this approximation is a limit case that can be useful to understand populations with shorter dispersal lengths, because their extinction thresholds have similar parameter dependences (Panels A and B of Fig. 5.3).

For finite dispersal length (Fig. 5.1), a much more common situation, simulations may present low and high-density solutions at different regions of the same habitat, together with regions of extinction (regions of zero population density in Panel E of Fig. 5.1, reflected as peaks at zero in the histogram of Panel F of Fig. 5.1).

The additional maximum approximation explained in section 5.6 works well for low values of A, reproducing the results of the mean-field approximation ($l_m \gg l_e$), as shown in Fig. 5.3.

On the one hand, the extinction threshold is found to decrease as the Allee threshold increases (Panel A of Fig. 5.3), as both simulations and mean-field approximation show. On the other hand, increasing the dispersal rate increases the extinction threshold, which at large values of the dispersal rate grows as

$$\sigma_{extinction} \sim \sqrt{m}\,, \tag{5.9}$$

as we expected from Eq. (5.8), obtained by the mean-field and maximum approximations (See Panels B and D of Fig. 5.3.). This dependence of the extinction threshold with the square root of the dispersal rate is related to the stochastic nature of the environmental fluctuations (which is here modeled with a Wiener process). Finally, maximum values of the extinction threshold are found in the mean-field limit, where characteristic dispersal distance is much larger than the spatial scale of environmental synchrony, $l_m \gg l_e$ (right-hand side of Panel C of Fig. 5.3). For values of the dispersal distance of the order of the spatial scale of environmental synchrony, the extinction threshold is reduced (for example, to half the value given by the mean-field approximation in the simulation shown in the blue dots of Panel C of Fig. 5.3). Therefore, resilience to environmental noise is reduced when dispersal is less frequent (lower m) or more local (lower l_m).

5.8. Discussion

We have shown that dispersal can make a population with an Allee threshold more resilient to environmental noise-induced extinction. This resilience can be characterized by the extinction threshold $\sigma_{extinction}$ for the amplitude of environmental fluctuations, above which the species becomes extinct. This extinction threshold increases if the dispersal rate m increases, or if the relative dispersal length l_m/l_e increases. This result is consistent with the relevance of the rescue effect of dispersal, which is proven to be an effective mechanism reducing local and global extinction risk in spatially extended populations (Brown and Kodric-Brown 1977; Gotelli 1991) and has been studied in Allee effect dynamics (Kanarek et al. 2015; Kent, Patrick Doncaster, and Sluckin 2003). The rescue effect entails that dispersal or migration can help repopulate extinct patches, reduce extinction risk, and improve the long-term sustainability of a species (Eriksson et al. 2014).

Mean-field approximation leads us to identify two branches of sustainable population distributions. For one of the branches, the high-density-population state, the population distribution has most regions above the Allee threshold and some regions below it. (See green curve in panel F of Fig. 5.1.) For the other branch, the low-density-population state, the population distribution has most regions with a population below the Allee threshold but is sustained by dispersal from the regions above the Allee threshold. (See red curve in Panel F of Fig. 5.1.) Dennis et al. (Dennis et al. 2016) already identified the two branches, of low- and high- population density states, but for one location with external migration. Here, this analysis has been done for a spatially extended population with only internal dispersal, allowing recolonization of regions with local extinction by neighboring populations. We also show that the path to global extinction is a path through the emergence of local depletions and extinctions, which spatially coexist with nondepleted regions (even for homogeneous habitats). In this path to global extinction, low-density and extinct regions cover a more

significant fraction of the area as the amplitude of environmental fluctuations increases toward the extinction threshold. Different spatial domains are close to different mean-field steady state solutions, as shown in Fig. 5.1 (Panels A, C, and E). Finite dispersal length decouples distant regions allowing for the coexistence of different solutions in different regions. However, the migrations between regions through the borders modifies the distribution in each region from the ideal mean field distributions. A linear combination of both mean-field distributions appears in finite dispersal simulations and in mean-field simulations (with theoretically infinitely large spatial scales of population synchrony, see Appendix 5.A), suggesting that low- and high-density metapopulations may coexist in neighboring regions. In the mean-field limit, the zero population density solution (i.e., extinction) does not coexist with low- and high-density solutions, while for finite dispersal length, extinct regions coexist (with low- and high-density solutions) for amplitudes of environmental fluctuations close to global extinction.

The typical size of the population depleted zones is given by the spatial scale of population synchrony (Moran 1953; Russell Lande, Engen, and Saether 2003). The spatial scale of population synchrony arises by environmental fluctuation synchrony and can be modulated by dispersion and trophic interactions (Liebhold, Koenig, and Bjørnstad 2004; Lande, Engen, and Sæther 1999; Jarillo et al. 2020; 2018). The characteristics of the spatial and temporal environmental correlations can modulate the characteristics of the transition to extinction (Barghathi, Tackkett, and Vojta 2017). Identifying the causes of population synchrony in natural populations is a challenge for ecologists due to the complexity and amount of data, which are sometimes incomplete and inaccurate, and thus, it is difficult to identify all the factors involved (Liebhold, Koenig, and Bjørnstad 2004). Additionally, spatial scales of population synchrony give the typical size of the areas affected by local extinction, and seem to be related to transitions to extinction in population dynamics (Heino et al. 1997; Engen, Lande, and Sæther 2002; Engen 2007). In the case of infinitely long dispersal distances (i.e., mean-field approximation) we would have also infinitely large spatial scales of population synchrony, and thus, infinitely large areas with local extinction (i.e., the whole habitat). This infinite typical size of areas affected by extinction is coherent with our results in the mean-field limit, where either the population becomes globally extinct or no regions present local extinction after long times.

The low-density-population state may be related to the absence of recovery seen in some ecosystems after halting harvesting (Lotze et al. 2011). In those ecosystems, the species seems to be trapped in a low population state, where they have been led by harvesting. They do not recover to the previous high-density population state unless harvesting is stopped during long periods, usually taking tens of generations. Our additional simulations with an initial population in the low-population distribution show that the low-population-density state alone is unstable in our model. After enough time, it evolves toward a high-density population state, a coexistence of regions with low- and high-population states, or global extinction, depending on the parameter values. The transitory dynamics presents moving fronts between the low and the high-population density state, which could provide clues on recovery dynamics (Kessler, Ner, and Sander 1998; Panja 2004; Hagberg and Meron 1994). The low-population-density state might be a separatrix between extinction and nonzero population state, because initial conditions close to the low-density state seem to be particularly sensible to stochasticity. However, the low-population-density state seems to be locally stable when it is close to a high-population density state. Dennis et al. (Dennis et al. 2016) also showed that external migration can stabilize the low-population-density state, and lead to basin hopping between low- and

high-population density states. Similar behavior can be present in our model due to dispersal from a neighboring high-population region. Simulations with amplitudes of environmental fluctuations close to the extinction threshold show the stochastic emergence of extinction regions inside low-population-density regions, even if initially the population density was at the carrying capacity in all points in space. (See Fig. 5.A4 in Appendix 5.A.) Studies concerning similar growth equations and demographic (instead of environmental) fluctuations (Weissmann and Shnerb 2014; Villa Martín et al. 2015) show a catastrophic transition between a high-density state and extinction. However, they did not find contributions of a low-density state in the stationary distribution of the population. This difference in the presence (or absence) of this contribution can be due to environmental fluctuations or the different dispersal terms, which are the main differences with our models. In addition, Villa Martín et al. (Villa Martín et al. 2015) suggest that smoother transitions appear in smaller spatial dimensions, and catastrophic shifts are prevented, which could explain the contribution of a low-population-density state in one-dimensional models, as the one studied here.

Further studies of transitions between low- and high-density-population states have to be done to deeply understand the implications of the two states presented here for these ecosystems. Our current results already suggest that the repopulation of an area can lead to a change from the low- to the high-density-population state, if it is intense enough to lead to a change in the regime of the dynamics in this area. Further studies could provide clues to optimize repopulation strategies.

It would be also interesting to address also the problem from the particular case where the Allee effect arises due to a population-density-dependent mating rate, as in the studies with lattice models done in Refs. (Windus and Jensen 2007; Pires and Duarte Queirós 2019). Our results have similarities (and differences) with the results obtained in these studies with lattice Monte Carlo simulations in an agent-based approach. They studied the mortality resilience and found three equilibrium values for the mean site population in the mean-field limit: high, low and extinct. Their low-population state was characterized as an unstable separatrix between the high and the extinct state in the mean-field limit. Here we have gone a step beyond and shown this low population state can be locally stable in the presence of a nearby high-population state (as was done in Ref. (Dennis et al. 2016) by external migration). These results stimulate further research beyond the mean-field limit to get a deeper understanding of the spatially extended population dynamics in the presence of environmental fluctuations.

Additionally, the individual-based model in Ref.(Surendran, Plank, and Simpson 2020) supports the crucial role of dispersal to sustain a population. This model shows that local competition or cooperation among neighbor individuals lowers the effective Allee threshold compared to global competition or cooperation. Analogously our study considers local density regulation showing that coupling through dispersal can lead to recovery of patches close to or below the Allee threshold. (Note we only consider mean-field dynamics in dispersal and only for comparison with limited-range dispersal.) All these results stress the relevance of population spatial structure.

Our results compute the extinction threshold, providing an approach for assessing extinction risk under an increase of the amplitude of environmental fluctuations. (An increase in climate variability was reported for several Earth regions (IPCC 2012).) The numerical analysis we performed here indicates toward the low-density state being an unstable state appearing only at high amplitudes of the environmental fluctuations, close to the transition to extinction. This low-density state is locally and transitorily stabilized, probably by dispersal, and it might play a

relevant role in (or be a good indicator of) the dynamics of populations close to the Allee threshold. These results seem in accordance with the three types of patches observed in a locally endangered butterfly(Bonsall et al. 2014), where this effect is probably enhanced and fixed in space due to habitat heterogeneities. The solutions identified, high- and low-density-population states, require a future, more detailed analysis of stability and transitions between them and to extinction, and factors that influence these transitions, such as harvesting and habitat suitability (which in nature are generally heterogeneous and stochastic in space and time).

This theoretical framework also allows studying the impact of fragmentation (i.e., the effects of finite-sized habitats), which introduces an effective limit in dispersal. Therefore, fragmentation decrease the potential of dispersion to recover populations and reduce the resilience to environmental fluctuations, with further details in Chapter 6 (Crespo-Miguel, Jarillo, and Cao-García 2022b). This analysis in the theoretical framework proposed here will provide information on the resilience of low- and high-population states in finite-size habitats, assessing the impact of these states and transitions for the species sustainability on a scenario of increasing climate variability (IPCC 2012).

The model presented here could shed new light on source-sink dynamics by including external migration and variations in habitat quality (e.g., adding position dependence of the parameters) in this model (Pulliam 1988; Dias 1996). In source-sink dynamics, some patches (sources) are more suitable and allow populations to increase, while others (sinks) have low quality and cannot sustain populations independently. However, populations in sinks can be sustained by excess individuals coming from sources. The source-sink effect has been observed in endangered populations, which present the Allee effect (in some patches) mitigated by inmigration (from other patches) (Bonsall et al. 2014). Heterogeneous patches coupled through dispersal can give a nonmonotonic dependence of the extinction probability with the dispersal rate (Agranov and Bunin 2021).

5.A. Appendix: Supplementary figures

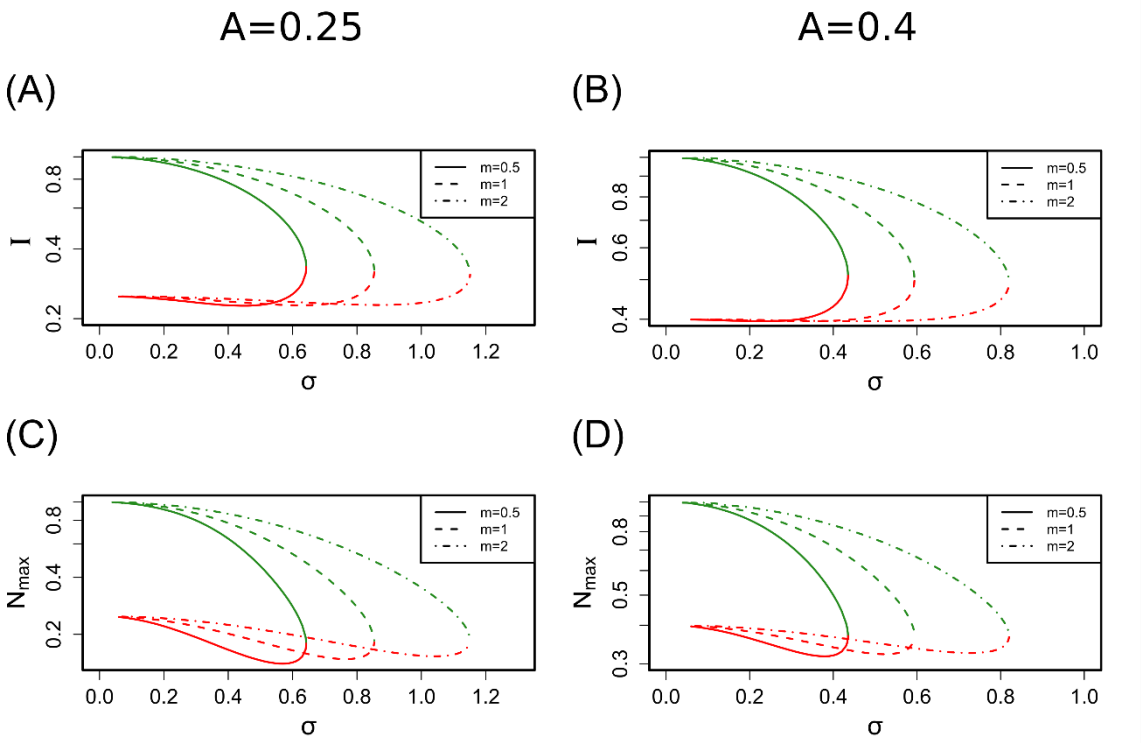

Figure 5.A1: Solutions in the mean-field approximation: Mean population density I as a function of environmental noise amplitude σ for the two nonzero branches of solutions at the mean-field approximation, with extinction rate $r = 0.1$, carrying capacity $K = 1$, dispersal rate $m = 0.5$ (solid line), $m = 1$ (dashed line), and $m = 2$ (dash-dotted line), for Allee threshold $A = 0.25$ (Panel A) and $A = 0.4$ (Panel B). Position of the maximum of mean-field distributions N_{max} as a function of environmental noise amplitude σ for the two nonzero branches of solutions at the mean-field approximation, with the same parameters as Panels A and B, and for Allee threshold $A = 0.25$ (Panel C) and $A = 0.4$ (Panel D).

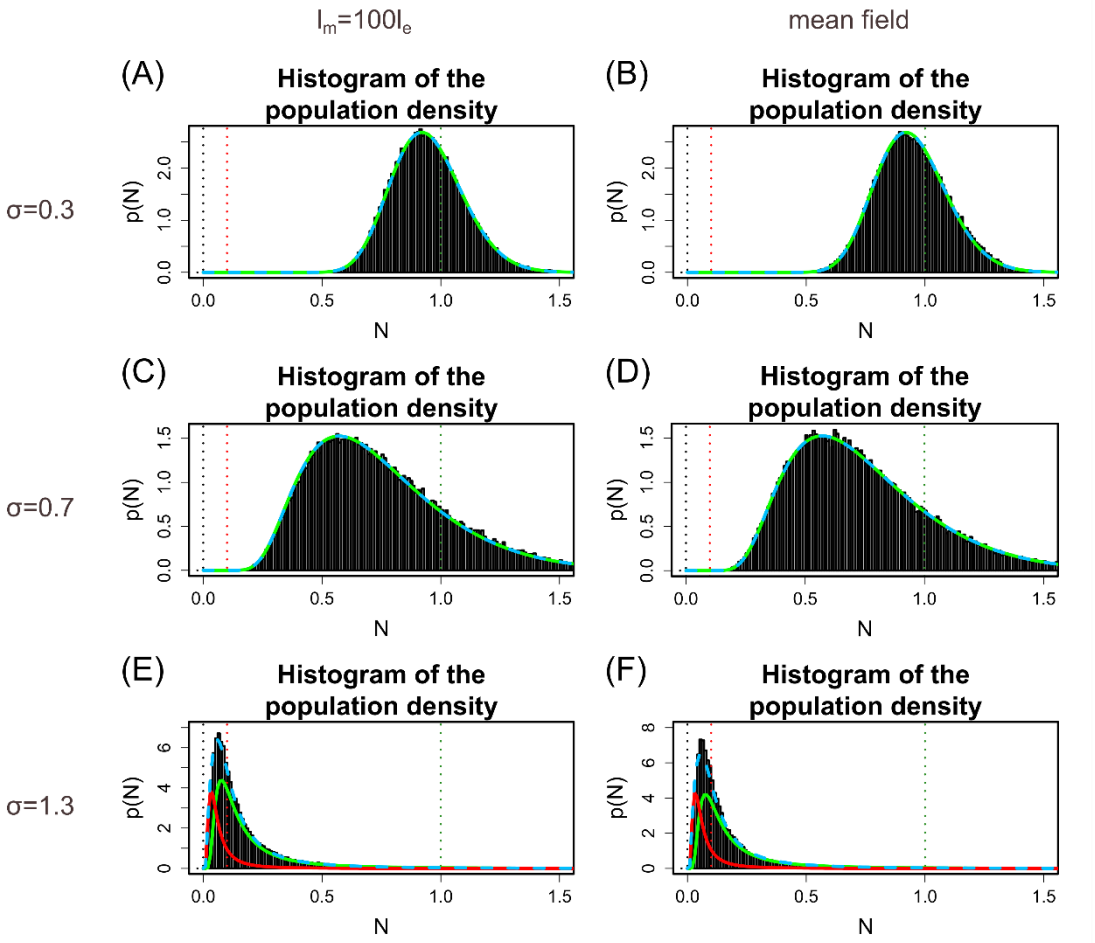

Figure 5.A2: Simulated population density histograms compared with mean-field population probability distributions. Panels A, C, and E show the histograms obtained for the spatial profile of the population density for simulation at a long time, $t = 1000$, with dispersal distance equal to 100 times the spatial scale of synchrony of environmental fluctuations, $l_m = 100l_e$, and periodic boundary conditions. Panels B, D, and F show the histograms obtained for the spatial profile of the population density for simulation at a long time, $t = 1000$, and mean-field approximation. For every panel we considered extinction rate $r = 0.1$, Allee threshold $A = 0.1$, carrying capacity $K = 1$, dispersal rate $m = 1$, spatial scale of synchrony of environmental fluctuations $l_e = 1$, and a total length of the simulation box $L = 4000$. Panels also show the fit (purple dashed line) to a linear combination of the mean-field population probability distributions. The results for these fits are $p(N) = p_{high}(N)$ in Panels A to D, $p(N) = 0.20p_{low}(N) + 0.80p_{high}(N)$ in Panel E and $p(N) = 0.23p_{low}(N) + 0.77p_{high}(N)$ in Panel F. Each contribution is represented with its fitted weight. $p_{low}(N)$ (red line) and $p_{high}(N)$ (green line) correspond, respectively, to the low and high-density mean-field population probability distribution solutions. They are given by the two nonzero branches of solutions of the mean-field equations for values of σ below the extinction threshold ($\sigma_{extinction} = 1.33$, close to $\sigma = 1.3$ in Panels E and F; see also Fig. 5.2). Red dashed vertical lines indicate Allee threshold value $A = 0.1$, green dashed lines indicate carrying capacity $K = 1$, and black dashed lines indicate $N = 0$. Note the similarities between the population density histograms obtained from direct numerical simulation and the fit to the linear combination of the population probability distributions obtained with the mean-field limit approximation.

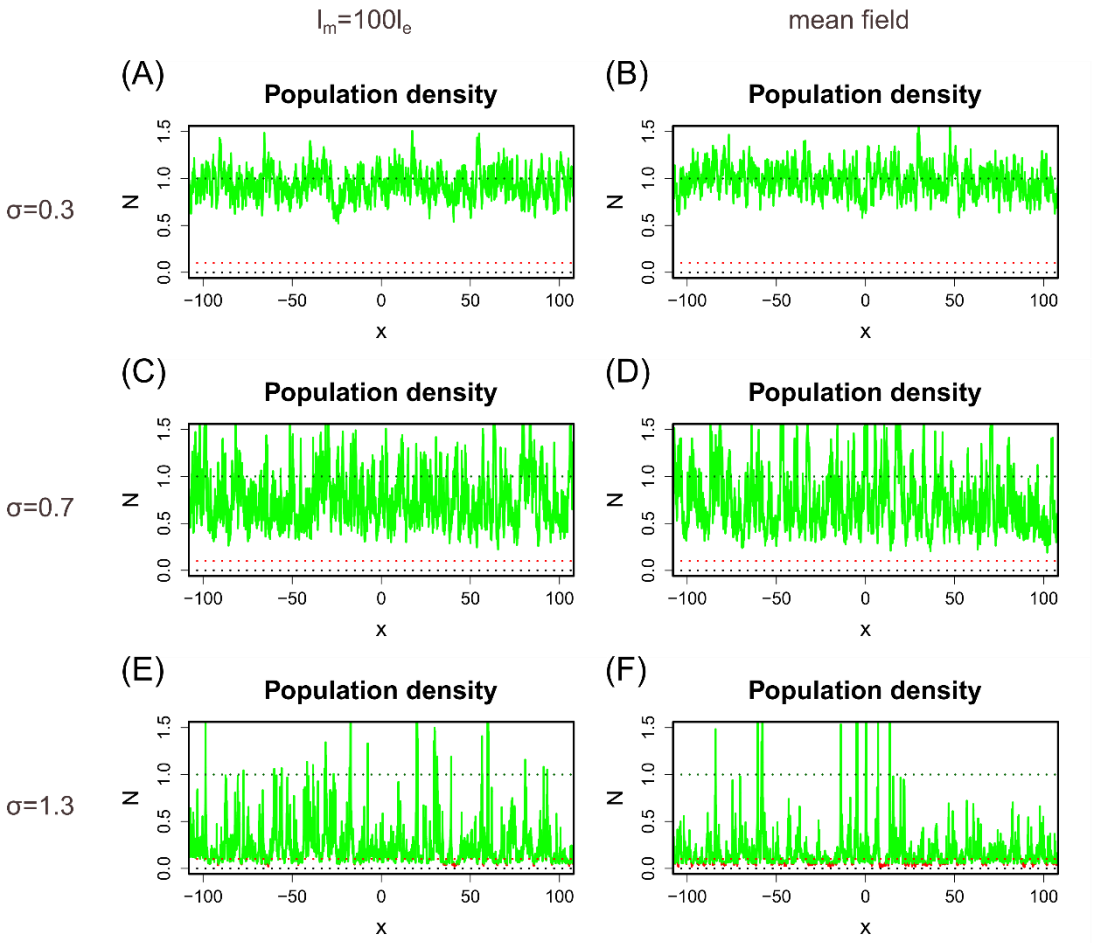

Figure 5.A3: Simulated population densities compared with mean-field population probability distributions, for different amplitudes of environmental fluctuations σ. Panels A, C, and E show the spatial profile of the population density at late time, $t = 1000 = 100r^{-1}$, with dispersal distance $l_m = 100l_e$, and spatial scale of synchrony of environmental fluctuations $l_e = 1$, and periodic boundary conditions. Panels B, D, and F show the spatial profile of the population density for simulation at late time, $t = 1000 = 100r^{-1}$, and mean field approximation. Every panel gives the associated histogram in the same panel in Figure 5.A2. For every panel we considered extinction rate $r = 0.1$, Allee threshold $A = 0.1$, carrying capacity $K = 1$, dispersal rate $m = 1$, spatial scale of synchrony of environmental fluctuations $l_e = 1$, and a total length of the simulation box $L = 4000$ (we only represent from $x = -100$ to $x = 100$ to improve visualization of spatial structure). The curves represented show the patches in high-population (green), and low-population (red) states according to which distribution dominates in the respective panel of figure 5.A2. Here, $\sigma_{extinction} = 1.33$, close to $\sigma = 1.3$ in Panels E and F; see also Fig. 5.2. Red dashed vertical lines indicate Allee threshold value $A = 0.1$, green dashed lines indicate carrying capacity $K = 1$, and black dashed lines indicate $N = 0$.

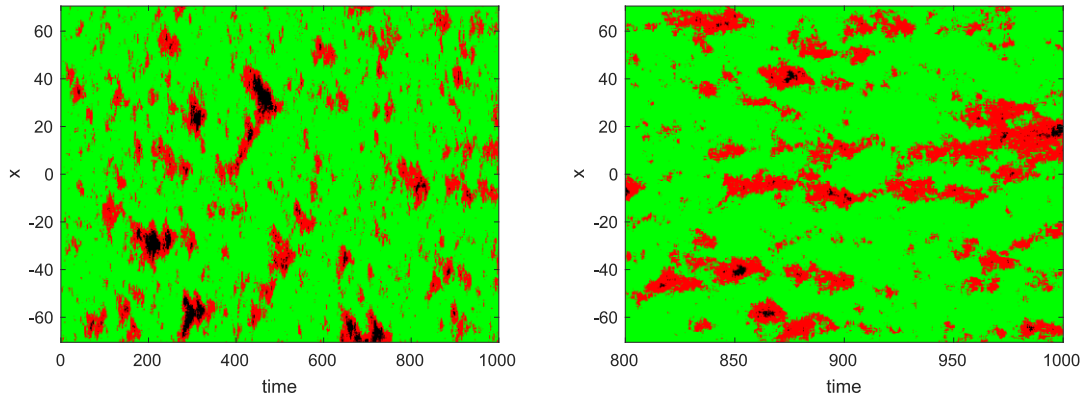

Figure 5.A4: Evolution of the spatial profile of population density from $t = 0$ to $t = 1000 = 100r^{-1}$ (left), and zoom on the late evolution from $t = 800 = 80r^{-1}$ to $t = 1000 = 100r^{-1}$ (right). Extinction rate $r = 0.1$; Allee threshold $A = 0.1$; carrying capacity $K = 1$; dispersal rate $m = 1$; dispersal distance equal to the spatial scale of synchrony of environmental fluctuations, $l_m = l_e = 1$; and amplitude of the environmental fluctuations $\sigma = 0.75$ (while the extinction threshold is $\sigma_{extinction} = 0.80$). The colors in the figure correspond to patches in high-population (green, $N > 0.1$), low-population (red, $0.01 < N \leq 0.1$), and extinction states (black, $N \leq 0.01$), the criterion used in Fig. 1E. These states correspond to high-density, low-density, and extinction distribution in Fig. 1F.

5.B. Appendix: Time to extinction in the absence of dispersal

The stationary population density distribution, $p(N)$, without dispersal is given by Eq. 5.5. This equation shows that the population distribution in the absence of dispersal is not normalizable, because it diverges at zero population density with $N^{-2\left(1+r/\sigma^2\right)}$. Therefore, the population will die out at long times. However, Eq. 5.5 does not indicate when this extinction will occur. Divergence at zero being greater for smaller environmental fluctuations may suggest that extinction happens faster for lesser environmental variability, but this is not the case as we show below.

Mean first passing time (Gardiner 2009; Dennis et al. 2016) can be used to study the expected time to extinction of the population. Hence, the expected time taken for a population starting at a specific initial population density N_0 to reach a smaller population density N_f is described by

$$\tau_{N_0 \to N_f} = 2 \int_{N_f}^{N_0} \frac{\int_N^\infty p(z)dz}{v(N)p(N)} dN, \tag{5.B1}$$

where $p(N)$ is described by Eq.5.5, $v(N) = \sigma^2 N^2$, and N_0 is the initial population density. Replacing $p(N)$ and $v(N)$ we obtain

$$\tau_{N_0 \to N_f} = \frac{2}{\sigma^2} \int_{N_f}^{N_0} N^{2r/\sigma^2} \frac{\int_N^\infty \left(\frac{\exp\left(\frac{1}{\sigma^2}\left(\frac{2rz}{K} + \frac{2rz}{A} - \frac{rz^2}{AK}\right)\right)}{z^{2+2r/\sigma^2}} dz \right)}{\exp\left(\frac{1}{\sigma^2}\left(\frac{2rN}{K} + \frac{2rN}{A} - \frac{rN^2}{AK}\right)\right)} dN. \tag{5.B2}$$

Exact time to extinction is reached when the chosen extinction threshold reference N_f tends to zero. However, the numerical computation becomes very slow in this case, and we chose instead a small nonzero value of N_f, for example, the Allee threshold A, or populations 10 or 100 times smaller, which in many cases is equivalent to extinction (because it is of the order of one or a few individuals, unable to survive). Fig. 5.B shows that the time needed to reach such a small population (starting from the carrying capacity K) decreases with the amplitude of environmental fluctuations σ. Smaller final population sizes N_f imply slightly longer first passing times. However, considering for N_f the Allee threshold A, or 100 times fewer individuals, yields almost no difference in the extinction time.

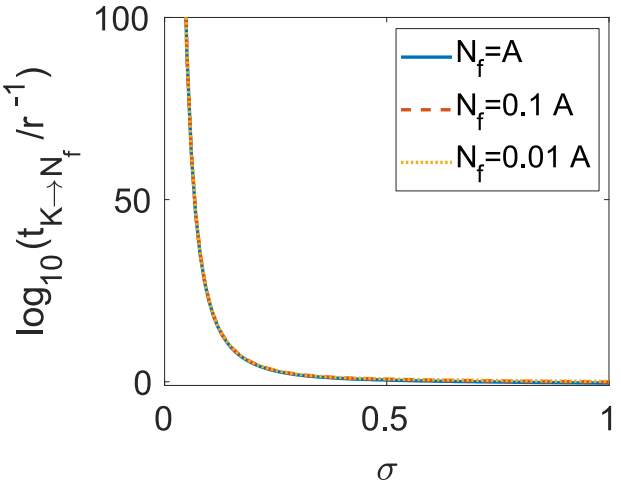

Figure 5.B: Approximation of the extinction time in the absence of dispersal. Decimal logarithm of the expected time taken for a population starting from the carrying capacity K to reach a final population N_f , divided by the inverse extinction rate r^{-1}. We have considered a carrying capacity $K = 1$, Allee threshold $A = 0.1$, and an extinction rate $r = 0.1$. We can see in the figure that choosing the Allee threshold A as final population density yields a very similar extinction time compared to choosing a final population density 100 times smaller.

5.C. Appendix: Simulation algorithm

We begin by setting the parameters for the simulation: Allee threshold A, carrying capacity K, extinction rate r, migration rate m, mean dispersal distance l_m, the amplitude of environmental fluctuations σ, and spatial scale of environmental synchrony l_e.

Space and time are discretized. The spatial grid is an array of length n (a natural, odd number) from $x = -L_{end}$ to $x = L_{end}$ (representing a box of size $2L_{end}$). The characteristic spatial scales are the dispersal distance l_m, and the spatial scale of synchrony of the environmental fluctuations l_e. We chose L_{end} (at least) 20 times the larger characteristic timescale (for example, 20 times l_m in Figs. 5.A2 and 5.A3, where $l_m = 100l_e$, while for most of the other simulations, 70 times the maximum spatial scale). The spatial vector length n is chosen such as the distance between neighbor nodes $\Delta L = 2L_{end}/(n-1)$ and is (at least) 20 times smaller than the minimum spatial scale. This spatial resolution and box size have been shown to provide an accurate description of the population dynamics in an infinite habitat (results are independent of L_{end} and ΔL).

The temporal grid is an array from $t = 0$ to $t = t_{end}$, with a distance between nodes of Δt, which is taken as 50 times the minimum temporal scale, and t_{end} is 100 times the maximum temporal scale. The characteristic temporal scales are $1/r$ and $1/m$.

The initial conditions at $t = 0$ are all spatial nodes with a population density equal to the carrying capacity, $N(x_i, t = 0) = K$, unless stated otherwise.

Once the grid has been defined, and the initial conditions set, we begin the simulation. The differential equation that governs the model is defined by Eq. (5.3). To implement it numerically, we can calculate the population density at a specific point in time and space, by using the Euler algorithm such as

$$N(x_i, t_{j+1}) = N(x_i, t_j) + \Delta N(x_i, t_j)\Delta t + \sigma N(x_i, t_j)\zeta(t_j)\sqrt{\Delta t}\,. \qquad (5.C1)$$

Where $\zeta(t_j)$ is an exponentially autocorrelated Gaussian field with zero mean, variance equal to 1, and correlation distance equal to l_e, and $\Delta N(x_i, t_j)$, the deterministic contribution, is

$$\begin{aligned}\Delta N(x_i, t_j) = r \cdot N(x_i, t_j)\left(\frac{N(x_i, t_j)}{A} - 1\right)\left(1 - \frac{N(x_i, t_j)}{K}\right)\cdot \Delta t - m \cdot N(x_i, t_j)\cdot \Delta t \\ +m \cdot \Delta t \cdot \sum_{k=-\frac{n-1}{2}}^{\frac{n-1}{2}} N(x_{i-k}, t_j)\cdot \frac{1}{\sqrt{2\pi l_m^2}} e^{\frac{-(k\cdot\Delta L)^2}{2l_m^2}}\cdot \Delta L\,.\end{aligned} \qquad (5.C2)$$

Note that in the sum x_{i-k} can have values outside of the spatial grid. We can solve that by setting periodic boundary conditions, which means that the first and the last point of the grid behave as neighboring nodes, implying that an individual which disperses beyond the last patch appears at the beginning of the grid (and vice versa), i.e.:

$$N(x_{i-k}, t_j) = \begin{cases} N(x_{i-k+n}, t_j)\ if\ 1 > i - k \\ N(x_{i-k}, t_j)\ if\ 1 \le i - k \le n \\ N(x_{i-k-n}, t_j)\ if\ i - k > n \end{cases} \qquad (5.C3)$$

In case we want to simulate the dispersal dynamics in the mean-field limit (as done in the simulations for Figures 5.2, 5.A2 and 5.A3), we change the last term of Eq. (5.C2), the dispersal term, and we use instead

$$\begin{aligned}\Delta N(x_i, t_j) = r \cdot N(x_i, t_j)\left(\frac{N(x_i, t_j)}{A} - 1\right)\left(1 - \frac{N(x_i, t_j)}{K}\right)\cdot \Delta t - m \cdot N(x_i, t_j)\cdot \Delta t \\ +m \cdot \Delta t \cdot \frac{\sum_{k=1}^{n} N(x_k, t_j)}{n}.\end{aligned} \qquad (5.C4)$$

(For mean-field simulations we have set $L_{end} = 2000\ l_e$.)

We have verified the results for these algorithms with different spatial and temporal resolutions and we found the results are accurate, stable, and consistent.

Chapter 6: Scaling of population resilience with dispersal length and habitat size

Environmental fluctuations can create population-depleted areas and even extinct areas for the population. This effect is more severe in the presence of the Allee effect (decreasing growth rate at low population densities). Dispersal inside the habitat provides a rescue effect on population-depleted areas, enhancing the population resilience to environmental fluctuations. Habitat reduction decreases the effectiveness of the dispersal rescue mechanism. We report here how the population resilience to environmental fluctuations decreases when the dispersal length or the habitat size are reduced. The resilience reduction is characterized by a decrease of the extinction threshold for environmental fluctuations. The extinction threshold is shown to scale with the ratio between the dispersal length and the scale of environmental synchrony, i.e., it is the dispersal connection between non-environmentally-correlated regions that provides resilience to environmental fluctuations. Habitat reduction also decreases the resilience to environmental fluctuations, when the habitat size is similar to or smaller than the characteristic dispersal distances. The power laws of these scaling behaviors are characterized here. Alternative scaling functions with spatial scales of population synchrony are found to fit the simulations worse. These results support the dispersal length as the critical scale for extinction induced by habitat reduction.

6.1. Introduction

Habitat reduction is one of the main causes of danger for population stability (Fahrig 1997). The extinction risk is higher for species that experience (strong) Allee Effect (decreasing growth rate at low population densities) (Allee and Schuett 1927; Allee 1931) because habitat reduction emphasizes the harmful phenomena for small population densities. Genetic variability is reduced due to the increasing inbreeding in small habitats (Wagenius, Lonsdorf, and Neuhauser 2007; Bruggeman, Wiegand, and Fernández 2010). The weakest individuals of strongly territorial or intra-competing species can be displaced and die because they cannot find a place to settle down without being attacked by their congeners (Jager, Carr, and Efroymson 2006). Other possible consequences of habitat reduction include species that suffer from lack of food and are forced to change their diet (Araújo et al. 2014). Several studies also prove the detrimental effect of fragmentation on populations. For example, stochastic simulations in a bidimensional space in which each individual moves, dies, or procreates randomly every time step (Fahrig 1997) show that fragmentation and even more habitat loss imply a greater extinction risk. Stochastic logistic growth models have also proven that fragmentation reduces population abundance (Herbener, Tavener, and Hobbs 2010), i.e., the sum of the population size in two separate patches is always lower than the population when the patches are together. Here, we will mainly explore the impact of habitat size reduction by decreasing the effective dispersal length.

Environmental fluctuations represent stochastic external factors (as weather fluctuations) influencing the population dynamics. Environmental fluctuations typically have spatial synchrony and lead to spatial synchrony on the population fluctuations. These spatially synchronized population fluctuations imply simultaneous population depletions or even local or global extinctions (Heino et al. 1997; Engen, Lande, and Sæther 2002; Engen 2007). The spatial scale of population synchrony is equal (Moran 1953) or larger, due to dispersal (Lande, Engen, and Sæther 1999), than the spatial scale of synchrony of environmental fluctuations.

Interspecies interactions can further increase the spatial scale of population synchrony (Bjørnstad, Ims, and Lambin 1999; Blasius, Huppert, and Stone 1999; Cazelles and Boudjema 2001; Jörgen Ripa and Ranta 2007; Jarillo et al. 2018; 2020; Fernández-Grande and Cao-Garcia 2020). Here, we describe the risk of extinction in terms of population resilience to environmental fluctuations. In the previous chapter we defined the extinction threshold (for the environmental fluctuations) as the value of the amplitude of environmental fluctuations above which environmental fluctuations cause a global extinction of the population (Crespo-Miguel, Jarillo, and Cao-García 2022a). The extinction threshold provides a measure of the resilience to extinction.

In spatially extended populations (also known as metapopulations), dispersal provides a rescue mechanism to prevent local extinction from becoming global. Dispersal allows repopulating depleted regions with individuals from the non-depleted areas. Theoretical studies have shown that dispersal is much more effective as a mechanism to enhance resilience to environmental fluctuation if the area occupied by the population is much larger than the scale of population synchrony (Engen, Lande, and Sæther 2002). In addition, habitat fragmentation or habitat reduction effectively decreases dispersal as it has been observed in field studies for animals such as squirrels (Antolin et al. 2001) and in simulations that mimic the natural growth of populations of different species of plants (Collingham and Huntley 2000; Dullinger et al. 2015).

Here, we study the impact on resilience to environmental fluctuations due to reducing the dispersal length. We also investigate the harmful consequences of habitat reduction as an effective limiter of dispersal length. See Section 6.3. The study is performed with the spatially extended population model (with Allee effect, dispersal, and stochastic environmental fluctuations) introduced in Section 6.2.

6.2. Methods: Spatially extended population model for finite and infinite habitats

To study the effects of fragmentation in populations we introduce here a spatially extended population model with Allee effect, dispersal and environmental stochasticity. Dispersal provides the population with resilience to environmental stochasticity, as show for example in the previous chapter of this thesis for infinite habitats. Here, we check how this resilience is limited when the population is confined to a finite habitat, which is implemented through a finite simulation box with reflecting boundary conditions.

6.2.1. Infinite habitat

The evolution equation has both a deterministic and a stochastic part (caused by environmental stochasticity) giving the dynamics of the population density $N(x,t)$ as a function of the spatial point x for future times t. The local deterministic dynamics is described by an Allee growth equation (Allee and Rosenthal 1949), described in Chapter 1. Additionally, environmental stochasticity is added as a multiplicative noise, so the local dynamics of the population is described by

$$dN|_{local} = rN\left(\frac{N}{A}-1\right)\left(1-\frac{N}{K}\right)\,dt + \sigma N dB\,. \tag{6.1}$$

Here, r is the population's characteristic extinction rate (at low populations), and K is the population's carrying capacity (the stable, viable population density). A is the population's Allee threshold, the minimum viable population density (i.e., the minimum local population density that gives a deterministic positive growth). The environmental stochastic term $\sigma N dB$ is

proportional to the population density N, as we are considering only environmental fluctuations (Chapter 3). The amplitude of environmental fluctuations is given by σ, and dB is a normalized Gaussian random field (further details in Chapter 2) with zero mean $\langle dB(x,t)\rangle = 0$, and with spatial scale of synchrony of the fluctuations equal to l_e, which means that the environmental fluctuations are correlated within a length l_e (Lande, Engen, and Saether 2003). This Gaussian field is uncorrelated in time and has an exponentially decreasing spatial correlation function

$$c_{dBdB}(y) = e^{-\sqrt{2}|y|/l_e}. \tag{6.2}$$

This means $\langle dB(x,t)dB(x+y,t+\tau)\rangle = \begin{cases} c_{dBdB}(y)dt & if\ \tau = 0 \\ 0 & if\ \tau \neq 0 \end{cases}$.

Dispersal is also considered as it plays a crucial role in the long-term stability of a spatially extended population(Chapter 5). If we consider individuals dispersing at a mean characteristic distance equal to l_m with a migration rate m, then the dispersal term, as introduced in Chapter 1, can be described by

$$dN|_{dispersal} = -\,m\,N\,dt + m\,dt \int N(y,t) f(x-y)dy\,, \tag{6.3}$$

where the function $f(x-y)$ is a Gaussian function with mean zero and variance equal to l_m^2. This equation describes that individuals leave from a particular point y with probability $m\,dt$, and they disperse with probability $f(x-y)$ to a distance $x-y$, usually of the order of l_m, coupling the population densities along space.

Combining Eqs. (6.1) and (6.3), we get the dynamical equation of a spatially extended, non-confined population,

$$dN = rN\left(\frac{N}{A}-1\right)\left(1-\frac{N}{K}\right)dt - \,m\,N\,dt + m\,dt \int N(y,t) f(x-y)dy + \sigma N dB\,. \tag{6.4}$$

This non-confined population equations are used to simulate a population on an infinite habitat, corresponding to an infinite confinement size, $L = \infty$. In practice, this corresponds to cases where the size of the habitat is much larger than the characteristic scales of the systems (in particular, larger than the population synchrony scales). Numerically, we considered large confinement size L, and periodic boundary conditions to reduce the border effects. (Our results revealed that border effects are negligible for values of $L \gg l_m$ as we discuss later in detail in the results section.)

The deterministic local term, the first term in Eq. (6.4), has two stable population densities $N = 0$ (extinction) and $N = K$ (carrying capacity). We see that the rates of return to extinction or to the carrying capacity for small population fluctuations are given by $\gamma_0 = r$ and $\gamma_k = r\left(\frac{K}{A}-1\right)$, respectively (Chapter 5). For populations close to a stable equilibrium point, small environmental fluctuations lead to a spatial scale of population synchrony l (as introduced in Chapter 4) greater than the spatial scale of synchrony of environmental fluctuations l_e, with $l = \sqrt{l_e^2 + m l_m^2/\gamma}$ and γ the rate of return to the stable equilibrium (Lande, Engen, and Sæther

1999). Therefore, in the present case, we can define two characteristic scales of population synchrony around extinction and around carrying capacity, l_0 and l_K, respectively, defined as

$$l_0 = \sqrt{l_e^2 + \frac{m \cdot l_m^2}{\gamma_0}}, \tag{6.5}$$

$$l_K = \sqrt{l_e^2 + \frac{m \cdot l_m^2}{\gamma_K}}, \tag{6.6}$$

due to the different rates of return to extinction and to carrying capacity, γ_0 and γ_K respectively (Chapter 5).

6.2.2. Finite habitat

Here we aim to address the effects of habitat size on the ecosystem resilience to environmental fluctuations. This provides very relevant information on the impact of habitat fragmentation in ecosystems.

We consider a population confined between the frontier positions $x = a$ and $x = b$, i.e., in the interval $x \in [a, b]$, which means a confinement length of $L = b - a$. We consider reflecting boundary conditions in these two frontier positions. One of the possible ways to introduce these reflecting boundary conditions is to generalize the convolution $\int N(y,t) f(x-y) dy$ in Eq. (6.4) to a convolution $F_\infty^{[a,b]}(x)$ defined by the following iterative process. We start computing

$$F_0^{[a,b]}(x) = \int_a^b N(y,t) f(x-y) dy \tag{6.7}$$

in an interval wider than $[a, b]$ by several l_m, for example $[a - 3l_m, b + 3l_m]$. Then, we alternatively reflect the dispersal tails outside each of the sides of the interval to the interior. Alternatively applying the right frontier reflection transformation

$$F_{2n+1}^{[a,b]}(x) = \begin{cases} F_{2n}^{[a,b]}(x) + F_{2n}^{[a,b]}(2b - x) \; if \; x \leq b \\ 0 \qquad\qquad\qquad\qquad if \; x > b \end{cases}, \tag{6.8}$$

and the left frontier reflection transformation

$$F_{2n+2}^{[a,b]}(x) = \begin{cases} F_{2n+1}^{[a,b]}(x) + F_{2n+1}^{[a,b]}(2a - x) \; if \; x \geq a \\ 0 \qquad\qquad\qquad\qquad if \; x < a \end{cases}. \tag{6.9}$$

The process finally converges to a convolution $F_\infty^{[a,b]}(x)$, which gives the dispersal of the population confined in the interval $[a, b]$ with reflecting boundary conditions. The dynamical equations for the population confined in this interval is given by

$$dN = rN\left(\frac{N}{A} - 1\right)\left(1 - \frac{N}{K}\right) dt - m\, N\, dt + m\, F_\infty^{[a,b]}\, dt + \sigma N dB\,. \tag{6.10}$$

Numerical simulations have been performed for finite habitat (finite L) using Eq. (6.10) with reflecting boundary conditions, and for infinite habitat ($L = \infty$) using Eq. (6.4), with periodic boundary conditions. Spatial and temporal resolutions are implemented in the same way for both cases. We consider the environmental synchrony scale, l_e, as the reference length, and set the spatial resolutions to have at least 20 lattice nodes per minimum parameter length (i.e., the smallest parameter among l_e, l_m, and L). The time resolution has been set as 50 times smaller than the minimum of r^{-1} and m^{-1} (the inverses of the extinction rate r and of the migration rate m respectively). (The extinction threshold mildly depends on the logarithm of the maximum simulation time as discussed in Appendix 6.C. Increasing the maximum simulation time one order of magnitude, from $t = 100r^{-1}$ to $t = 1000r^{-1}$, only implies a change of the order of 10% in the extinction threshold.) Table 6.1 summarizes the variables used in this article, their definitions and units.

Variables	**Description**
$N(x,t)$	Population density at a given position x and time t. Units of space^{-1}
A	Allee threshold of the species. Species with a population density lower than A has negative growth in a deterministic system. Units of space^{-1}
K	Carrying capacity of the species. Units of space^{-1}
r	Extinction rate of the species (at low population). Units of time^{-1}
γ_0	Rate of return to extinction, $\gamma_0 = r$. Units of time^{-1}
γ_K	Rate of return to carrying capacity, $\gamma_K = r\,(K/A - 1)$. Units of time^{-1}
m	Dispersal rate of the species. Units of time^{-1}
l_e	Spatial scale of synchrony of environmental fluctuations. Units of length
l_m	Characteristic dispersal distances of the population. Units of length
L	Confinement size. Units of length
σ	Amplitude of the environmental fluctuations. It is equal to the standard deviation of the environmental fluctuations. Units of time$^{-1/2}$
$\sigma_{extinction}$	Extinction threshold for the amplitude of environmental fluctuations (Minimum amplitude of the environmental fluctuations that ensures global extinction). Units of time$^{-1/2}$

Table 6.1: Variables used in this chapter, definitions, and units.

6.3. Resilience to environmental fluctuations

Environmental fluctuations can lead an otherwise stable population to global extinction. Here, we address how large are the environmental fluctuations that a population can endure without going extinct. We define the extinction threshold $\sigma_{extinction}$ as the minimum amplitude of environmental fluctuations that ensures global extinction (See Appendix 6.D). The extinction threshold provides a measure of the resilience of the population to environmental fluctuations.

As described in Chapter 5, dispersal plays an important role in making the populations more resilient to environmental fluctuations, recovering depleted or extinct populations in one location through the dispersal of the individuals from nearby non-depleted locations (Crespo-Miguel, Jarillo, and Cao-García 2022a; Hanski and Gyllenberg 1993; Gotelli 1991). Habitat reduction (or habitat fragmentation) confines the population to a smaller region, where therefore the population fluctuations are more correlated. This higher population correlation reduces the effectiveness of this dispersal recovery mechanism. As a result, habitat reduction decreases the resilience of the population to environmental fluctuations. See Figs. 6.1 and 6.2. Reductions in the dispersal length l_m also lead to reductions in the resilience of the population to environmental fluctuations, as we see in Fig. 6.2, and we study below in more detail in Section 6.3.1, where we show the scaling of the extinction threshold $\sigma_{extinction}$ with the dispersal length l_m. In Section 6.3.2, we characterize the scaling of the extinction threshold $\sigma_{extinction}$ with habitat size L. Finally, in Section 6.3.3, we show how we can define an effective dispersal length $l_{m,effective}(L)$ to describe how the dispersal length l_m is effectively reduced as the habitat size L decreases. This effective reduction in l_m leads to earlier saturation of the extinction threshold as a function of l_m for smaller confinement sizes L, as Fig. 6.2. shows

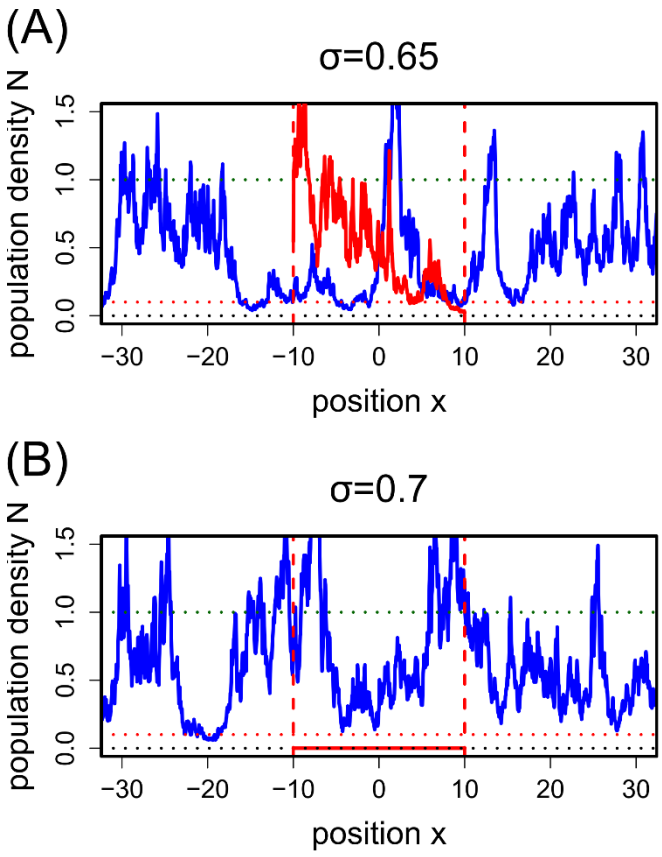

Figure 6.1: Habitat reduction can lead to extinction, as it reduces the resilience to environmental fluctuations. Population density $N(x)$ at long times ($t = 100\, r^{-1}$) for a huge confinement size, $L = 142$ (blue solid line) and for a medium confinement size, $L = 20$ (red solid line), and for two amplitudes of the environmental noise $\sigma = 0.65$ (upper panel) and $\sigma = 0.70$ (bottom panel). The figure shows an example of how the reduction of confinement size reduces the resilience to environmental fluctuations, leading to extinction of the more confined

population when environmental noise is increased (red solid line of the bottom panel). Horizontal dotted lines represent extinction $N = 0$ (black), Allee threshold $N = A = 0.1$ (red) and carrying capacity $N = K = 1$ (green) population density values. These parameter values are common to all the cases represented in this figure, and also the extinction rate $r = 0.1$, the dispersal rate $m = 1$, and the dispersal length $l_m = l_e$ (with the spatial scale of environmental synchrony l_e chosen as unit of length $l_e = 1$). Huge confinement size $L = 142$ (blue solid line) was simulated with Eq. (6.4) and periodic boundary conditions, while medium confinement size $L = 20$ (red solid line) was simulated with Eq. (6.10) and reflecting boundary conditions.

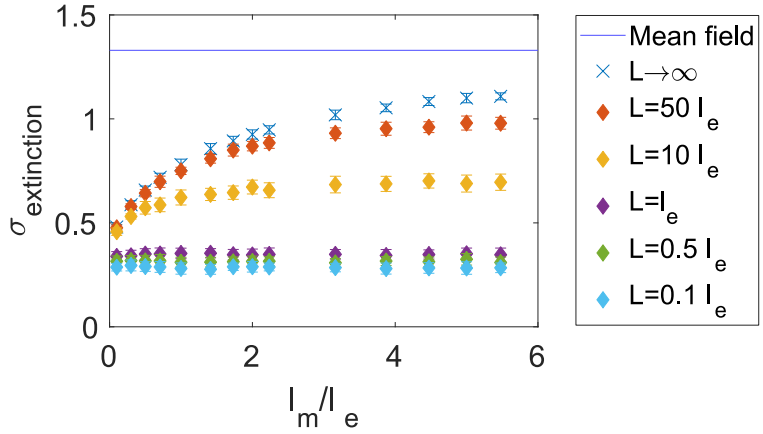

Figure 6.2: Extinction threshold $\sigma_{extinction}$ as a function of the ratio l_m/l_e for different confinement sizes L. X-shaped points indicate simulations with a huge confinement size $L = 100\sqrt{l_e^2 + l_m^2}$ and periodic boundary conditions, whereas diamond-shaped points indicate simulations with a finite confinement size and reflecting boundary conditions. Vertical bars indicate uncertainty in the simulation result (see Appendix 6.D). All simulations are for Allee threshold $A = 0.1$, carrying capacity $K = 1$, extinction rate $r = 0.1$, migration rate $m = 1$, and spatial scale of synchrony of environmental fluctuations $l_e = 1$. The blue solid line represents the result in the limit of infinite habitat size and characteristic dispersal length, $L = \infty, \frac{l_m}{l_e} = \infty$ and it has been obtained using the mean field approximation as described in the previous chapter.

6.3.1. Greater dispersal lengths increase the resilience to environmental fluctuations

Increasing the dispersal length increases the dispersal rescue effect in the population. This enhanced rescue effect increases the extinction threshold $\sigma_{extinction}$ (see Fig. 6.2), until it saturates to the mean field value ($l_m \to \infty$). Fig. 6.2 also shows that the extinction threshold depends additionally on the habitat size L, i.e., $\sigma_{extinction}(l_m, L)$. However, we will concentrate here on the dependence on the dispersal length l_m for infinite habitats ($L = \infty$). Therefore, we will study $\sigma_{extinction,\infty}(l_m) = \sigma_{extinction}(l_m, L \to \infty)$, and denote by $\sigma_\infty^\infty = \sigma_{extinction}(l_m \to \infty, L \to \infty)$ the mean field value for an infinite habitat. The mean field value for an infinite habitat can be obtained, and it is calculated here, by the mean-field approximation explained in Chapter 5. The ration of extinction threshold for infinite habitat $\sigma_{extinction,\infty}$ and its respective mean-field value σ_∞^∞ for each dispersal rate m is plotted as a function of the ratio of the dispersal length and the environmental correlation length, l_m/l_e, in Fig. 6.3. This two ratios show an approximate scaling of the form

$$\frac{\sigma_{extinction,\infty}\left(m,\frac{l_m}{l_e}\right)}{\sigma_\infty^\infty(m)} = M\left(\frac{l_m}{l_e}\right) = \left(\frac{1}{1+\left(\frac{b_M\, l_e}{l_m}\right)^{n_M}}\right)^{1/d_M} . \qquad (6.11)$$

A maximum likelihood fit (see Appendix 6.A) of this scaling form to the simulation results leads the values of the fitting parameters: d_M, n_M, and b_M indicated in Table 6.2. Plots of $\sigma_{extinction,\infty}/\sigma_\infty^\infty$ as a function of the ratios l_m/l_0 or l_m/l_K do not present this approximate scaling behavior. See Fig. 6.B in Appendix 6.B.

n_M	d_M	b_M	SE	$-\ln \mathcal{L}$	AIC_C
1.9±1.4	8.0±6.8	10.1±3.2	0.105	146	298

Table 6.2: Parameters giving the maximum likelihood fit for the 42 points in Fig. 6.3 to Eq. (6.11). Uncertainties have been calculated with a confidence Interval of 68%, i.e. at one-sigma level. Squared error SE, logarithm of the likelihood (-ln $\mathcal{L}$) and Akaike Information Criterion AIC_C are also included (See Appendix 6.A for their definitions).

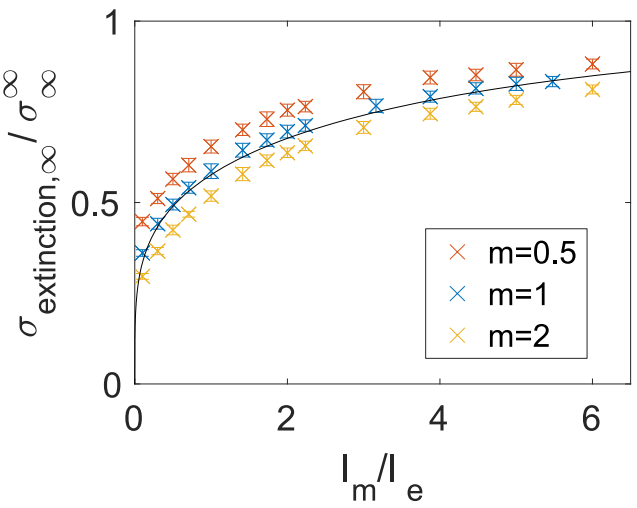

Figure 6.3: Extinction thresholds for infinite habitat $\sigma_{extinction,\infty}$ as a function of the dispersal length l_m, for various values of the migration rate m. The figure shows that the extinction threshold for infinite habitat $\sigma_{extinction,\infty}$ (divided by the respective mean-field value σ_∞^∞ for each migration rate m) is fitted by the scaling function in Eq. (6.11) with the parameter values in Table 6.2 (solid black line). The dispersal length is expressed in units of the spatial scale of environmental fluctuations l_e. Vertical bars indicate uncertainty in the simulation results (see Appendix 6.D). All simulations are for Allee threshold $A = 0.1$, carrying capacity $K = 1$, extinction rate $r = 0.1$, and spatial scale of synchrony of environmental fluctuations $l_e = 1$.

The data in Fig. 6.3 have a slight dependence in the migration rate m, showing that points with smaller migration rates are higher than those with larger dispersal rate for the same ratio l_m/l_e. Thus, the extinction threshold $\sigma_{extinction}$ divided by its respective mean-field value σ_∞^∞, has a better scaling as a function of $\left(\frac{m}{r}\right)^{s_M}\left(\frac{l_m}{l_e}\right)$, where s_M is an additional fitting parameter,

$$\frac{\sigma_{extinction,\infty}\left(m,\frac{l_m}{l_e}\right)}{\sigma_\infty^\infty(m)} = M\left(\frac{m}{r},\frac{l_m}{l_e}\right) = \left(\frac{1}{1+\left(\frac{b_M\, l_e}{l_m}\left(\frac{r}{m}\right)^{s_M}\right)^{n_M}}\right)^{1/d_M} . \qquad (6.12)$$

The fit to the numerical results of this scaling law, Eq. (6.12), is better than for the previous one, Eq. (6.11), even taking into account the AIC penalty for the additional parameter (s_M). See Fig. 6.4 and Table 6.3. The significant difference in AIC_C yielded by fitting Eqs. (6.11) and (6.12), $\Delta AIC_C = 481 \gg 10$, implies that the model with higher AIC_C, given by Eq. (6.11), can be discarded entirely (Appendix 6.A). The best-fitting model (the model with the lowest AIC_C), Eq. (6.12), indicates that the mean-field value is reached for long dispersal distances l_m, but more slowly for higher dispersal rates m.

n_M	d_M	b_M	s_M	SE	$-\ln\mathcal{L}$	AIC_C
1.26±0.21	5.0±1.1	1.57±0.36	-0.667±0.049	0.0120	-96.0	-183

Table 6.3: Parameters giving the maximum likelihood fit for the 42 points in Fig. 6.4 to Eq. (6.12). Uncertainties have been calculated with a confidence Interval of 68%, i.e. at one-sigma level. Squared error SE, logarithm of the likelihood (-ln $\mathcal{L}$) and Akaike Information Criterion AIC_C are also included (See Appendix 6.A for their definitions).

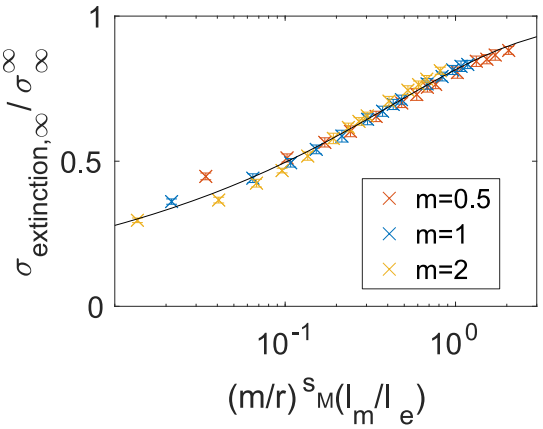

Figure 6.4: Extinction thresholds for infinite habitat $\sigma_{extinction,\infty}$ as a function of the ratio $\left(\frac{m}{r}\right)^{s_M}\left(\frac{l_m}{l_e}\right)$, with $s_M = -0.667$, as shown in table. The figure shows that the extinction threshold for infinite habitat $\sigma_{extinction,\infty}$ (divided by the respective mean-field value σ_∞^∞ for each migration rate m) is fitted by an approximate scaling described by Eq. (6.12) with the parameter values in Table 6.3 (solid black line). Vertical bars indicate uncertainty in the simulation results (see Appendix 6.D). All simulations are for Allee threshold $A = 0.1$, carrying capacity $K = 1$, extinction rate $r = 0.1$, and spatial scale of synchrony of environmental fluctuations $l_e = 1$.

6.3.2. Habitat fragmentation reduces resilience to environmental fluctuations

As we explained above, the resilience to environmental fluctuations can be characterized by the minimum amplitude of environmental fluctuations that leads to global extinction, the extinction threshold $\sigma_{extinction}(m, l_m, L)$. The extinction threshold decreases as the habitat size decreases (for example due to habitat fragmentation). We characterized in the previous

section the dependence of the extinction threshold with the dispersal length l_m for infinite habitats. Using these previous results and an analogous approach we will find the scaling behavior with the habitat size L. We consider the ratio of the extinction threshold for finite and infinite habitat size (see Fig. 6.5) and compare fits of the type

$$\frac{\sigma_{extinction}(m, l_m, L)}{\sigma_{extinction,\infty}\left(m, \frac{l_m}{l_e}\right)} = F\left(\frac{L}{l_i}\right) = \left(\frac{1}{1+\left(\frac{b_F\, l_i}{L}\right)^{n_F}}\right)^{1/d_F}, \tag{6.13}$$

where l_i can represent the spatial scale of environmental synchrony l_e, the dispersal length l_m, the spatial scale of population synchrony close to extinction $l_0 = \sqrt{l_e^2 + m l_m^2/\gamma_0}$, or the spatial scale of population synchrony close to the carrying capacity $l_K = \sqrt{l_e^2 + m l_m^2/\gamma_K}$ [as introduced in Eqs. (6.5) and (6.6) above]. The maximum likelihood fitting of Eq. (6.13) to the simulation results (Fig 6.5) gives the parameter values indicated in Table 6.4, where the AIC_C results indicate that the best fitting model is that with $l_i = l_m$, closely followed by $l_i = l_0$. The other models can be discarded as its difference in AIC_C is greater than 10 (Burnham and Anderson 2002). In particular, the model with $l_i = l_e$ is completely discarded due to the large value of AICc, the large uncertainty and instability in the parameter value determination, which is consistent with the dispersal of the values observed in Fig. 6.5 for this case.

	n_F	d_F	b_F	SE	$-\ln \mathcal{L}$	AIC_C
L/l_m	1.93±0.83	8.5±4.0	28.7±6.4	0.158	-69.4	-132
L/l_0	1.84±0.73	8.0±3.5	6.4±1.5	0.193	-68.9	-131
L/l_K	2.3±1.6	10.1±7.6	16.5±4.6	0.382	-21.6	-36.8
L/l_e	3.0±4.0	14±19	58±26	1.033	209	424

Table 6.4: Parameters giving the maximum likelihood fit for the 60 points in Fig. 6.5 to Eq. (6.13). Uncertainties have been calculated with a confidence Interval of 68%, i.e. at one-sigma level. Squared error SE, logarithm of the likelihood ($-ln\,\mathcal{L}$) and Akaike Information Criterion AIC_C are also included (See Appendix 6.A for their definitions).

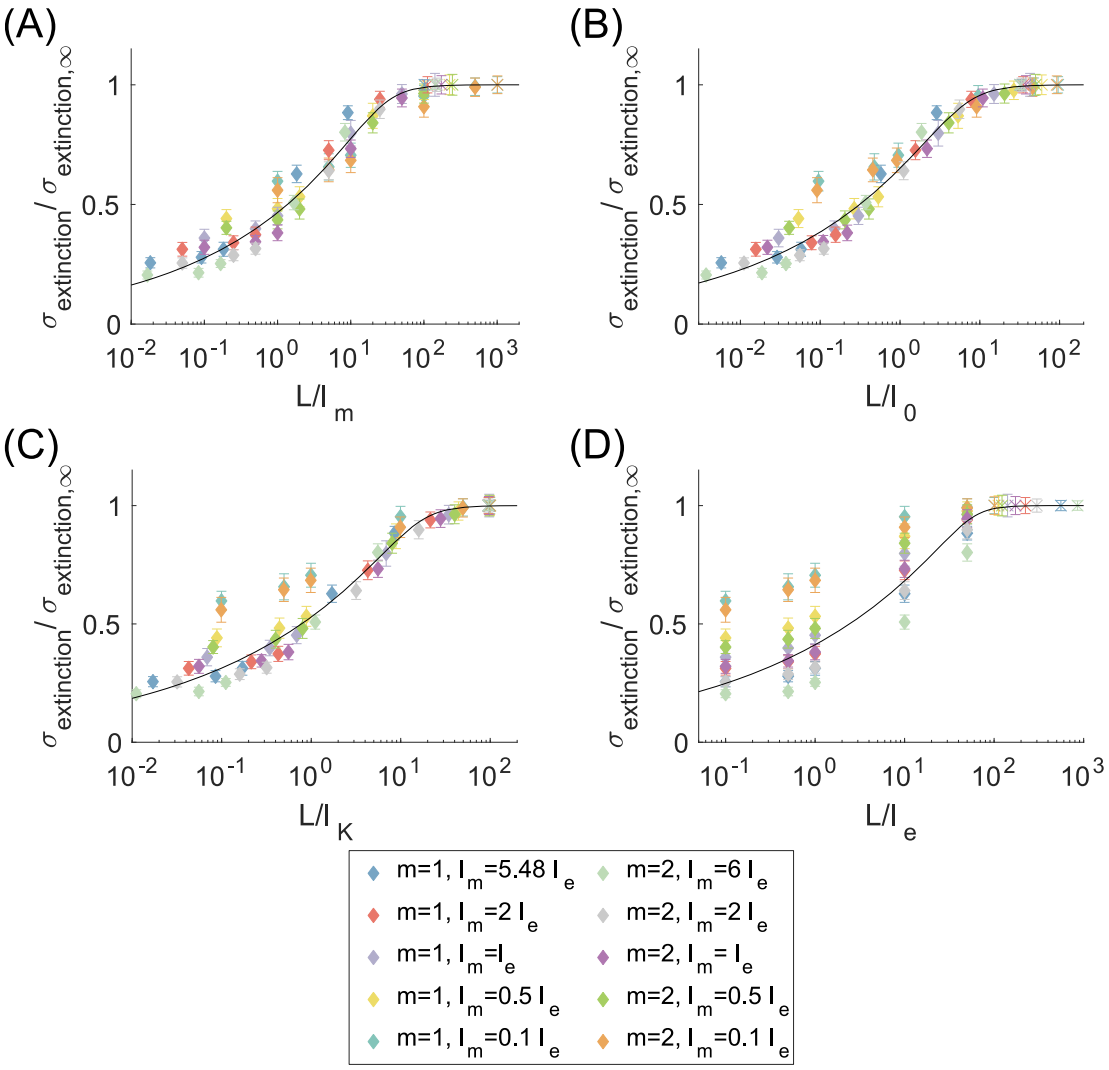

Figure 6.5: Extinction thresholds for fragmented habitats $\sigma_{extinction}$ as functions of the size of the habitat L divided by the dispersal length of the population l_m (Panel A), the spatial scale of population synchrony around extinction l_0 (Panel B), the spatial scale of population synchrony around carrying capacity l_K (Panel C), and the spatial scale of synchrony of environmental fluctuations l_e (Panel D). The figure shows that the extinction threshold for a fragmented habitat $\sigma_{extinction}$ divided by the respective infinite habitat value $\sigma_{extinction,\infty}$ (for the same dispersal rate m and dispersal length l_m) is fitted by the scaling function in Eq. (6.13) with the parameter values in Table 6.4 (solid black line). Vertical bars indicate uncertainty in the numerical results (see Appendix 6.D). All simulations are for Allee threshold A =0.1, carrying capacity K =1, extinction rate r =0.1, and spatial scale of synchrony of environmental fluctuations l_e =1.

Additionally, the improved fit found in the previous subsection for the l_m/l_e scaling introducing a dependence on the ratio between the dispersal rate m and the extinction rate r motivates us to perform a similar check for the scaling of the habitat size L. We found that the data in Fig. 6.5 scale better as a function of $\left(\frac{m}{r}\right)^{S_F}\left(\frac{L}{l_i}\right)$,

$$\frac{\sigma_{extinction}(m, l_m, L)}{\sigma_{extinction,\infty}\left(m, \frac{l_m}{l_e}\right)} = F\left(\frac{m}{r}, \frac{L}{l_i}\right) = \left(\frac{1}{1 + \left(\frac{b_F\, l_i}{L}\left(\frac{r}{m}\right)^{s_F}\right)^{n_F}}\right)^{1/d_F}, \qquad (6.14)$$

which fits the numerical results with the parameters of Table 6.5 (Fig. 6.6). We see, comparing Table 6.4 and 6.5, that the AIC_C is much lower for a maximum likelihood fit to Eq. (6.14) than to Eq.(6.13) ($\Delta AIC_C > 10$), therefore the model with more empirical support is that which follows Eq. (6.14) with $l_i = l_m$. The scaling given by Eq. (6.14) indicates that the infinite habitat value is reached for long ratios L/l_i, and that limit is reached slower for higher dispersal rates m.

	n_F	d_F	b_F	s_F	SE	$-\ln \mathcal{L}$	AIC_C
L/l_m	1.91±0.70	8.5±3.4	2.5±1.4	-0.93±0.21	0.132	-89.6	-170
L/l_0	1.87±0.72	8.2±3.5	1.6 ±1.0	-0.53±0.24	0.188	-75.5	-142
L/l_K	2.2±1.4	9.7±6.6	3.1±2.6	-0.62±0.29	0.367	-31.1	-53.5
L/l_e	2.5±2.5	11±12	2.7±3.7	-1.09±0.48	0.963	179	367

Table 6.5: Parameters giving the maximum likelihood fit (uncertainties have been calculated with a confidence Interval of 68%, i.e. at one-sigma level) for the 60 points in Fig. 6.6 to a form of Eq. (6.13). Squared error, logarithm of the likelihood and Akaike Information Criterion are also included.

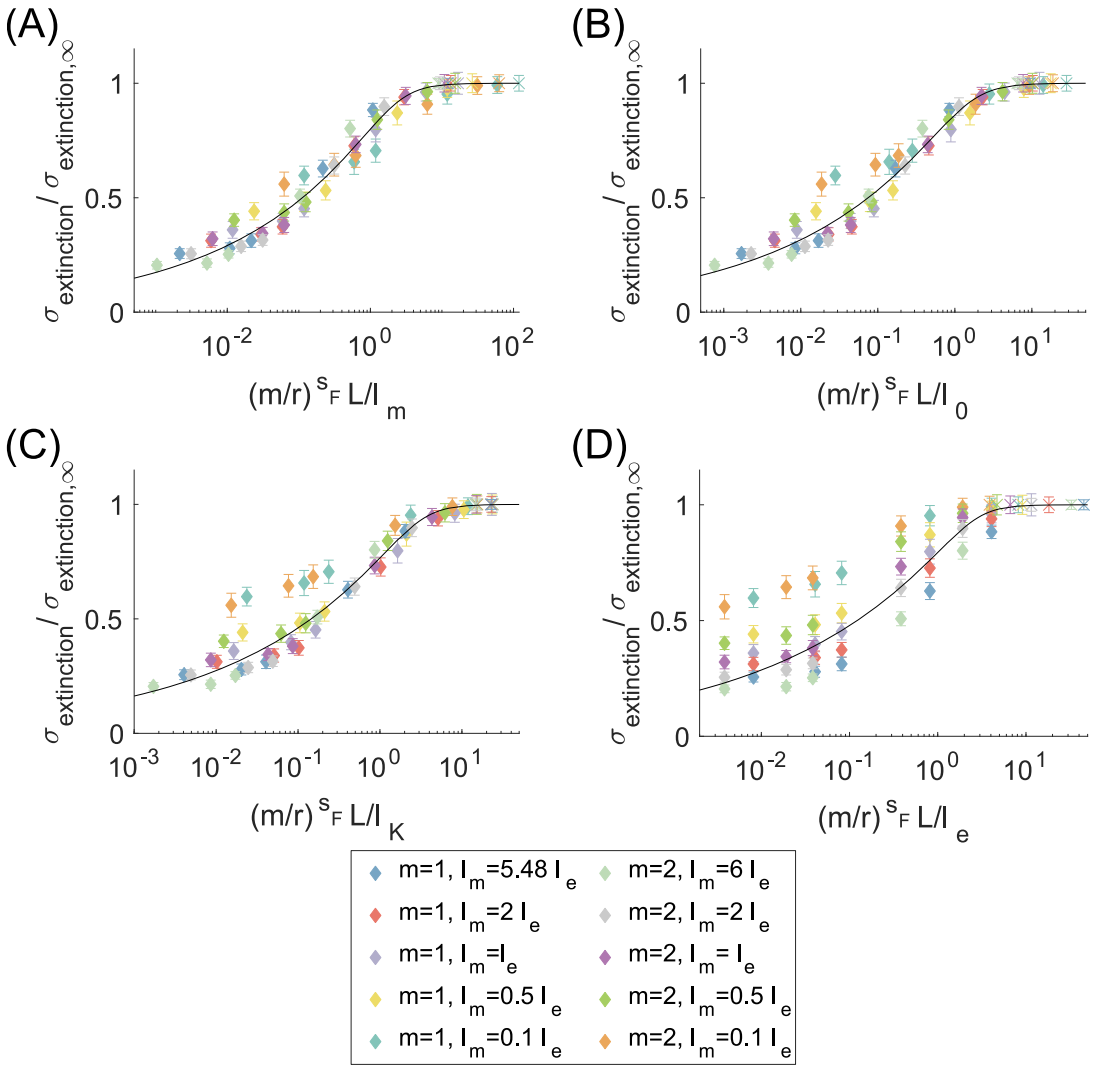

Figure 6.6: Extinction thresholds for fragmented habitats $\sigma_{extinction}$ as functions of the size of the habitat L multiplied by the ratio $\left(\frac{m}{r}\right)^{s_F}$ (value of s_F is given in table 6.5) and divided by the dispersal length of the population l_m (Panel A), the spatial scale of population synchrony around extinction l_0 (Panel B), the spatial scale of population synchrony around carrying capacity l_K (Panel C), and the spatial scale of synchrony of environmental fluctuations l_e (Panel D). The figure shows that the extinction threshold for a fragmented habitat $\sigma_{extinction}$ (divided by the respective infinite habitat value $\sigma_{extinction,\infty}$ for the same migration rate m and dispersal length l_m) is fitted by an approximate scaling described by Eq. (6.14) with the parameter values in Table 6.5 (solid black line). Vertical bars indicate uncertainty in the simulation result (see Appendix 6.D). All simulations are for Allee threshold A =0.1, carrying capacity K =1, extinction rate r =0.1, and spatial scale of synchrony of environmental fluctuations l_e =1.

Putting together the results of this subsection and of the previous one provides the complete scaling behavior of the extinction threshold $\sigma_{extinction}$

$$\sigma_{extinction}(m, l_m, L) = \sigma_{\infty}^{\infty}(m)\, M\left(\frac{m}{r}, \frac{l_m}{l_e}\right) F\left(\frac{m}{r}, \frac{L}{l_m}\right)$$
$$= \sigma_{\infty}^{\infty}(m) \left(\frac{1}{1+\left(\frac{b_M\, l_e}{l_m}\left(\frac{r}{m}\right)^{s_M}\right)^{n_M}}\right)^{1/d_M} \left(\frac{1}{1+\left(\frac{b_F\, l_m}{L}\left(\frac{r}{m}\right)^{s_F}\right)^{n_F}}\right)^{1/d_F}, \quad (6.15)$$

with the values of the parameters given in the first row of Tables 6.3 and 6.5.

6.3.3. Habitat fragmentation reduces the effective dispersal length

From the results in previous subsections, we got that habitat reduction effectively decreases the dispersal length, leading to a detriment in a population's resilience to environmental fluctuations. Thus, we can define an effective dispersal length $l_{m,eff}(m, l_m, L)$, which is the dispersal length of a non-fragmented population in an infinite habitat ($L = \infty$) that has the same extinction threshold as a population with dispersal length l_m confined in a fragmented habitat of size L, if the other parameters affecting both populations are equal. This definition is equivalent to the following equation [expanded using Eq. (6.15)]:

$$\begin{aligned} &\sigma_{extinction}\left(m, l_{m,eff}, L \to \infty\right) = \sigma_{extinction}(m, l_m, L) \\ &\Rightarrow M\left(\frac{m}{r}, \frac{l_{m,eff}}{l_e}\right) F\left(\frac{L}{l_m} \to \infty\right) = M\left(\frac{m}{r}, \frac{l_m}{l_e}\right) F\left(\frac{m}{r}, \frac{L}{l_m}\right) \\ &\Rightarrow M\left(\frac{m}{r}, \frac{l_{m,eff}}{l_e}\right) = M\left(\frac{m}{r}, \frac{l_m}{l_e}\right) F\left(\frac{m}{r}, \frac{L}{l_m}\right). \end{aligned} \quad (6.16)$$

Thus, we got the following expression for the effective dispersal length $l_{m,eff}(m, l_m, L)$,

$$l_{m,eff}(m, l_m, L) =$$
$$b_M l_e \left(\frac{r}{m}\right)^{s_M} \left(\left(1+\left(\frac{b_M\, l_e}{l_m}\left(\frac{r}{m}\right)^{s_M}\right)^{n_M}\right) \cdot \left(1+\left(\frac{b_F\, l_m}{L}\left(\frac{r}{m}\right)^{s_F}\right)^{n_F}\right)^{\frac{d_M}{d_F}} - 1 \right)^{-\frac{1}{n_M}}, \quad (6.17)$$

with the parameters given in the first row of Tables 6.3 and 6.5. The effective dispersal length, as shown in Fig. 6.7, is a monotonously increasing function with the habitat size L, and it tends to the real dispersal length l_m when the habitat size becomes sufficiently large. Thus, habitat size reduction implies a decrease in the effective dispersal length.

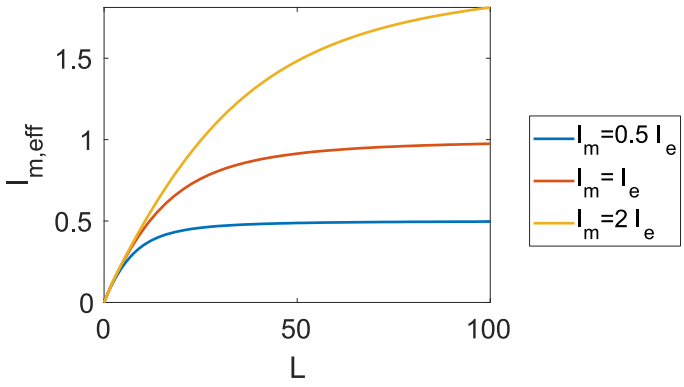

Figure 6.7: Effective dispersal length $l_{m,eff}$ as a function of the size of the habitat L for different dispersal distances $l_m = 0.5\ l_e$ (blue), $l_m = l_e$ (red) and $l_m = 2\ l_e$ (orange). All curves are for Allee threshold A =0.1, carrying capacity K =1, extinction rate r =0.1, migration rate m =1, and spatial scale of synchrony of environmental fluctuations l_e =1.

6.4. Discussion

We have shown that both habitat reduction and dispersal reduction decrease a population's resilience against environmental fluctuations. We have measured the extinction threshold $\sigma_{extinction}$, defined as the minimum amplitude of environmental fluctuations that ensures population's extinction at long times (Appendix 6.D). On the one hand, we have obtained that populations with dispersal distances larger than the scale of synchrony of environmental fluctuations are more resilient to fluctuations, and reach the largest extinction threshold for every confinement size. On the other hand, habitat reduction is found to decrease the resilience to environmental fluctuations, leading to a huge drop in the extinction threshold when the habitat size becomes of the order of the typical dispersal distances of the population.

These results imply that habitat reduction (or habitat fragmentation) causes an effective reduction in dispersal length, thus minimizing dispersal-induced resilience caused by the rescue effect. As studied in Chapter 5, dispersal is proved as an essential mechanism against extinction in populations with Allee Effect (Palmqvist and Lundberg 1998; Dennis et al. 2016; Crespo-Miguel, Jarillo, and Cao-García 2022a). However, dispersal is not so effective when a smaller habitat size truncates its range. These results further clarify that habitat reduction (or habitat fragmentation) is a problem for endangered populations. Its impact can be much more significant for species that depend on dispersal when the habitat size is reduced close to its typical dispersal length. We can apply this knowledge by making a special effort to develop conservation strategies that include active prevention of habitat destruction, so environmental fluctuations are less likely to destroy endangered species populations. Deeper knowledge of populations' dynamics helps to optimize species conservation and sustainable exploitation policies.

Synchrony plays an essential role in the regional extinction risk (Heino et al. 1997; Engen 2007; Engen, Lande, and Sæther 2002). However, we found that the decrease of the extinction threshold with habitat size scales better with the ratio of the habitat size to the dispersal length than with the ratio of the habitat size to the spatial scale of synchrony. Thus, we think that the transition to regional extinction needs further study to achieve a complete understanding of the interplays among the spatial scale of population synchrony, the dispersal length, the habitat size, and the transitions to extinction.

Here, we have studied the one-dimensional case. The extension of this study to two dimensions would be interesting because many natural ecosystems are two-dimensional. It is known that the shapes of the fragmented patches can affect the survival of many species (Diamond 1975), favoring connectivity to support recovery by internal migration. Patch shapes can also determine colonized area expansion or contraction (Lewis and Kareiva 1993; Keitt, Lewis, and Holt 2001). Additionally, habitat reduction and fragmentation per se have slightly different effects on population resilience (Fahrig 2003; 1997). Studying the one- and two-dimensional patch structure and its connectivity can also provide insight into the transitions to extinction.

These results have been obtained for one-species systems, for which dispersal is beneficial, increasing the rescue effect. However, dispersal does not always benefit the dynamics for multiple-species systems since it can homogenize the habitats, removing some local species (Mouquet and Loreau 2003). Furthermore, the diversity is expected to peak at intermediate diffusion (Gravel, Massol, and Leibold 2016). Additionally, recent work has shown that coupling between heterogeneous patches can lead to a non-monotonic behavior of the extinction probability with the dispersal (Agranov and Bunin 2021). This work also stresses that dispersal from other patches might act as a non-gaussian noise in the receiving patch, extending the noise-induced phenomena found in ecosystems (Spagnolo, Valenti, and Fiasconaro 2004).

6.A. Appendix: Maximum likelihood fit and Akaike Information Criterion (AIC_C)

The fits used in the main text have been done by maximizing likelihood (Burnham and Anderson 2002). Likelihood is defined by Equation (6.A1) for a set of n independent measures with equal standard deviation S,

$$-\ln \mathcal{L} = \frac{n}{2}\ln(2\pi) + \frac{n}{2}\ln S^2 + \frac{1}{2S^2}SE \ , \qquad (6.A1)$$

where $SE = \sum_i^n (f(x_i) - y_i)^2$ is the total squared error, $f(x_i)$ is the value of the fit function for a parameter x_i, and y_i its measured value.

This definition can be generalized for a set of measures with different uncertainties S_i (Hogg, Bovy, and Lang 2010), so that the logarithm of the likelihood in this case becomes

$$-\ln \mathcal{L} = \frac{n}{2}\ln(2\pi) + \frac{1}{2}\sum_i^n \ln S_i^2 + \frac{1}{2}\sum_i^n \frac{(f(x_i) - y_i)^2}{S_i^2} \ . \qquad (6.A2)$$

Thus, maximizing the likelihood is equal to minimizing the right-hand side of Eq. (A2). Given that $\frac{n}{2}\ln(2\pi) + \frac{1}{2}\sum_i^n \ln S_i^2$ is a constant that only depends on the data, not on the model (as a consequence, it is usually omitted when comparing models that depend on the same data, as it cancels out). Then, maximizing the likelihood is equivalent to minimizing $\sum_i^n \frac{(f(x_i)-y_i)^2}{S_i^2}$.

Comparing maximum likelihood of two models is useful if both models have the same number of free parameters. In the other case, we must compare them by the Akaike Information Criterion (Akaike 1974) defined by

$$AIC = 2k - 2\ln \mathcal{L} \ , \qquad (6.A3)$$

where k is the number of free parameters of the model. The definition of Eq. (A3) supposes a infinitely large number of points to fit by the model, so there is a correction for small size of the sample defined by

$$AIC_C = AIC + \frac{2k^2 + 2k}{n - k - 1} = 2k - 2\ln \mathcal{L} + \frac{2k^2 + 2k}{n - k - 1} \ . \qquad (6.A4)$$

Thus, given two models fitting the same set of points, the model with lower AIC_C is the best. Nonetheless, models with higher AIC_C should not always be discarded. If we define the difference between the AIC_C of the two models, this is

$$\Delta_i = AIC_{C,i} - AIC_{C,min} \ , \qquad (6.A5)$$

then, a difference Δ_i between 0 and 2 indicates that the i-th model has a substantial empirical support (Burnham and Anderson 2002), a difference between 4 and 7 indicates a considerably lesser support of the model, and a difference greater that 10 means that the i-th model has essentially no empirical support and should be completely discarded.

6.B. Appendix: Figures of extinction threshold depending on the dispersal distance shown as functions of other parameters

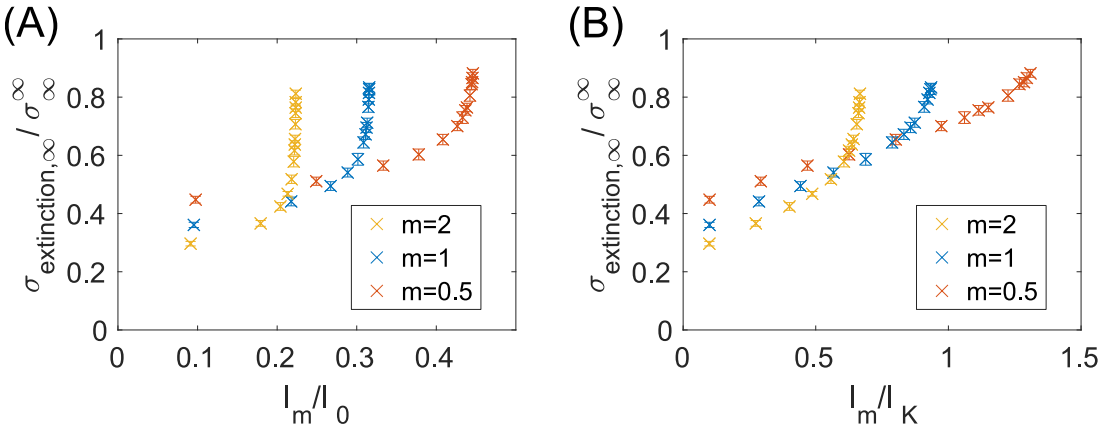

Figure 6.B: Extinction thresholds for infinite habitat $\sigma_{extinction,\infty}$ (divided by the respective mean-field value σ_{∞}^{∞} for each migration rate m) as a function of the dispersal length l_m divided by the spatial scale of population synchrony around extinction l_0 (Panel A), and the spatial scale of population synchrony around carrying capacity l_K (Panel B), for different values of the migration rate m. Vertical bars indicate uncertainty in the simulation results. All simulations are for Allee threshold $A = 0.1$, carrying capacity $K = 1$, extinction rate $r = 0.1$, and spatial scale of synchrony of environmental fluctuations $l_e = 1$. This figure does not present an approximate scaling behavior, in contrast with the scaling found for the ratio of the dispersal length l_m over the spatial scale of synchrony of environmental fluctuations l_e (see Fig. 6.3).

6.C. Appendix: Extinction threshold and extinction time

In all the paper we have estimated the extinction threshold $\sigma_{extinction}$ for a maximum simulation time, or final time for the simulation, of $t = 100r^{-1}$. At this time we considered the population is extinct if all the positions are below the Allee Threshold. To determine the extinction threshold we plotted the fraction of the positions with a population density above the Allee Threshold f_A as function of the amplitude of environmental fluctuations σ. The extinction threshold $\sigma_{extinction}$ and its uncertainty was estimated as the center and the width of the range of values where f_A makes the transition between extinct and non-extinct population. (See Panels A and B of Fig. 6.C and Appendix 6.D for further details)

Here, we show that extinction threshold mildly decreases as we increase the maximum simulation time, because the extinction time increases as the amplitude of environmental fluctuations decreases. Panel C and D show that the extinction threshold has a relative decrease of the order of 10% when the maximum simulation time is increased by a factor 10.

In the computations of this article, we have considered 10 different realizations for each value of the amplitude of environmental fluctuations σ. (See, for example, Fig. 6.C.) This number of realizations is enough for the required precision. For 5 and 10 realizations, the difference in the results for the mean of $\log_{10} t_{extinction}$ for 5 and 10 realizations is small enough (4.8% for small habitat size and 2.9% for large habitat), and even smaller for $\sigma_{extinction}$ (1% difference). In both cases, the differences are smaller than the uncertainties (See Appendix 6.D). Thus, a greater number of realizations would mean only a small difference in the final results.

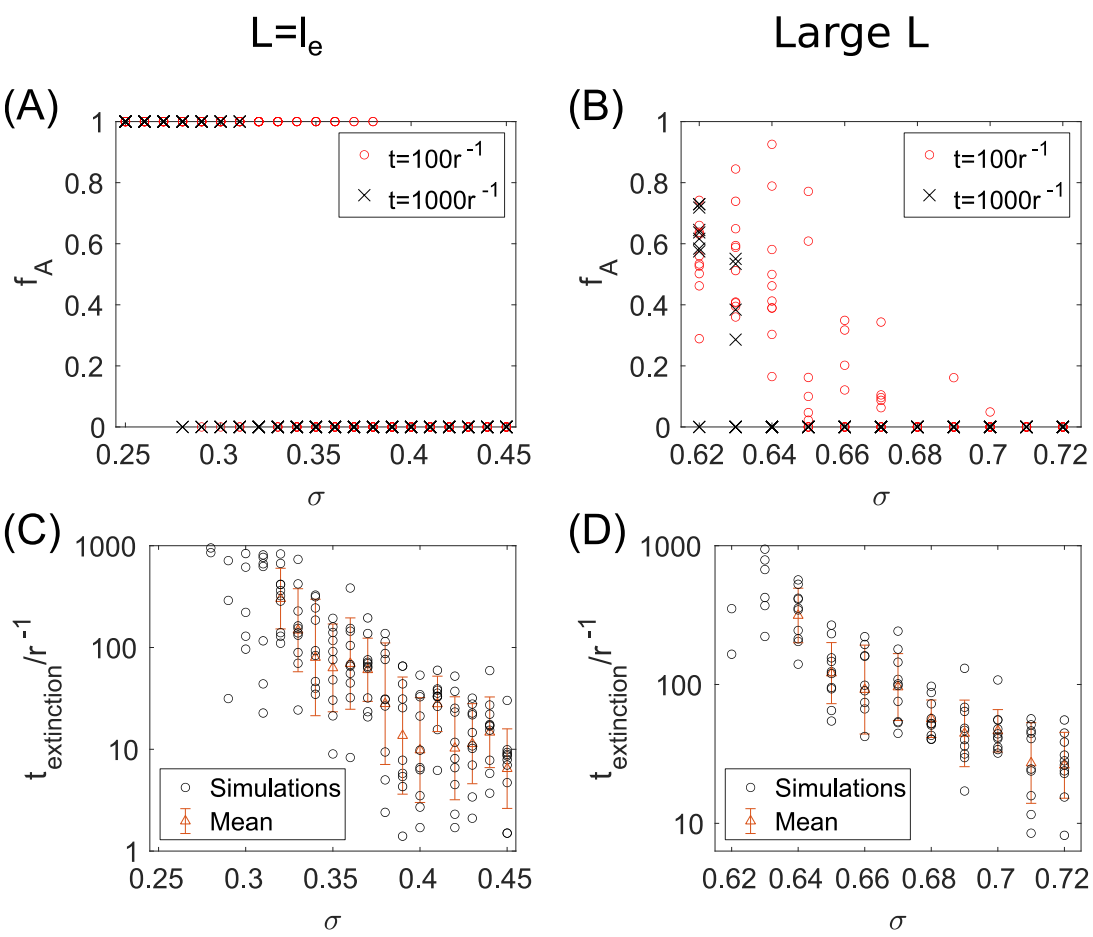

Figure 6.C: Extinction threshold for the amplitude of environmental fluctuations σ and extinction times $t_{extinction}$. Upper panels show the fraction of the positions with a population density above the Allee Threshold f_A for a small habitat size L=l_e (Panel A) and a large habitat size ($L = 187 l_e$) (Panel B) as a function of the amplitude of the environmental fluctuations σ. Bottom panels show the extinction time (in units of the inverse of the extinction rate r^{-1}) for a small habitat size (Panel C) and a large habitat size (Panel D) as a function of the amplitude of the environmental fluctuations σ. (Triangles indicate the mean and error bars the 1-standard deviation interval in $\log_{10} t_{extinction}$.) (10 simulations for each value of σ.) For all panels Allee Threshold A=0.1, carrying capacity K=1, extinction rate $r = 0.1$, dispersal rate $m = 1$, and dispersal length $l_m = 0.5\, l_e$ (with the spatial scale of environmental synchrony l_e chosen as the unit of length).

6.D. Appendix: Calculation of extinction thresholds

In order to obtain the extinction threshold and its uncertainty for given fixed values of the rest of parameters (i.e., for each point in Figs. 6.2-6.6), we have implemented the following procedure. We chose a set of amplitudes of the environmental fluctuations $\{\sigma_1, \sigma_2, \ldots, \sigma_s\}$, with $\sigma_{i+1} = \sigma_i + \Delta\sigma$, using $\Delta\sigma = 0.01$, and covering a sufficiently large range (such as realizations with the smaller σ never end in global extinction and those with the larger σ always do). Then, we perform R realizations for each σ_i, and we store the fraction of realizations k_i which finish in global extinction at the end of the simulation (i.e., those realizations with a fraction of the positions with a population density above the Allee Threshold $f_A = 0$ at $t = 100r^{-1}$). Next, we define the discrete distribution

$$p(\sigma_i) = \frac{\min(k_i, 1-k_i)}{\sum_1^S \min(k_j, 1-k_j)} \ , \tag{6.D1}$$

which satisfies $\sum_1^S p(\sigma_i) = 1$. This distribution can be used to calculate the mean extinction threshold

$$\sigma_{extinction} = \sum_1^S p(\sigma_i) \cdot \sigma_i \ , \tag{6.D2}$$

and its standard deviation

$$sd_{biased} = \sqrt{\sum_1^S p(\sigma_i) \cdot (\sigma_i - \sigma_{extinction})^2} \ . \tag{6.D3}$$

The distribution is discrete and obtained by a finite sample, so the standard deviation is biased. Only $h \cdot R$ simulations contribute to sampling the distribution $p(\sigma)$, where h is the number of σ_i with non-zero $p(\sigma_i)$ (i.e., with k_i different to 0 or 1). The unbiased standard deviation is then given by

$$sd^2_{unbiased} = \frac{h \cdot R}{h \cdot R - 1} sd^2_{biased}. \tag{6.D4}$$

Furthermore, the discretization of the σ interval in intervals of $\Delta\sigma = 0.01$ can contribute to an underestimation of the standard deviation. To correct this understimation, we computed the uncertainty S of the extinction threshold as

$$S = \sqrt{sd^2_{unbiased} + \Delta\sigma^2}. \tag{6.D5}$$

We verified that the interval value of $\Delta\sigma = 0.01$ did not contribute significantly to the uncertainty of the extinction threshold. Thus, the uncertainty S accurately represented the uncertainty in $\sigma_{extinction}$ due to the stochastic nature of the dynamics.

We first considered five realizations, $R = 5$, for each amplitude σ_i, then we compared the results with those obtained with ten realizations, $R = 10$. The average difference between $\sigma_{extinction,R=5}$ and $\sigma_{extinction,R=10}$ was less than 1% and always smaller than the uncertainty S. This result indicates that ten realizations for each environmental fluctuations amplitude σ_i (for each fixed group of value of the other parameters) are enough to accurately calculate the extinction threshold and its uncertainty in the range of parameters that we studied.

PART III: Predictability of population fluctuations

Chapter 7: Predictability of population fluctuations

Population dynamics is affected by environmental fluctuations (such as climate variations), which have a characteristic correlation time. Strikingly, the time scale of predictability can be larger for the population dynamics than for the underlying environmental fluctuations. Here, we present a general mechanism leading to this increase in predictability. We considered colored environmental fluctuations acting on a population close to equilibrium. In this framework, we derived the temporal auto and cross-correlation functions for the environmental and population fluctuations. We found a general correlation time hierarchy led by the environmental-population correlation time, closely followed by the population autocorrelation time. The increased predictability of the population fluctuations arises as an increase in its autocorrelation and cross-correlation times. These increases are enhanced by the slow damping of the population fluctuations, which has an integrative effect on the impact of correlated environmental fluctuations. Therefore, population fluctuations predictability is enhanced when the damping time of the population fluctuation is larger than the correlation time of the environmental fluctuations. This general mechanism can be quite frequent in nature, and it largely increases the perspectives of making reliable predictions of population fluctuations.

7.1. Introduction

Population dynamics is frequently affected by the randomness of the environmental fluctuations requiring the use of stochastic dynamics equations (Gotelli 2008; Lande, Engen, and Saether 2003). Environmental fluctuations have different sources including variability in resources needed by a population (e.g., food) (Fujiwara and Takada 2017); unpredictability in weather or climate (Nowicki et al. 2009; Saltz, Rubenstein, and White 2006); and natural disasters (Mangel and Tier 1993), which are usually considered extreme cases of environmental fluctuations (Shaffer 1987). Environmental fluctuations can alter the dynamics of a population, significantly impacting population fluctuations and their predictability (Luis et al. 2015), and even causing the extinction of otherwise stable populations (Schreiber 2010; Crespo-Miguel, Jarillo, and Cao-García 2022a; Mangel and Tier 1993). Random environmental fluctuations can have an appreciable time correlation, requiring models with colored (temporally correlated) noise instead of white noise. Accurate prediction of the population dynamics requires using appropriate colored noise (*i.e.*, with the correct correlation time function) to simulate the environmental fluctuations (Petchey 2000; Halley 1996). The color (or temporal correlation) of the environmental fluctuations has been shown to have relevant consequences for population dynamics and the population extinction risk (J. Ripa and Lundberg 1996; Heino, Ripa, and Kaitala 2000; Greenman and Benton 2003; Kamenev, Meerson, and Shklovskii 2008; Spanio, Hidalgo, and Muñoz 2017). The impact of colored noise on the dynamics has also been experimentally observed (Laakso, Löytynoja, and Kaitala 2003; Reuman et al. 2008; Petchey 2000).

The environmental variability is especially critical in some species. For example, ectotherms are particularly sensitive to changes in temperature (Zuo et al. 2012; Paaijmans et al. 2013). Ectotherms suffer important changes in growth (Atkinson 1994) and development (de Jong and van der Have 2009) depending on the circumstances given by the environment, and a study of the underlying mechanism describing the general effect of environmental variability can help to understand ectotherms' dynamics.

Here we are interested in using stochastic population dynamics models to get further insight into the predictability of the population fluctuations. It has been reported that the predictability of the population fluctuations can be larger than the underlying environmental fluctuations (Pimm and Redfearn 1988; Petchey 2000). In particular, primary production fluctuations have been found to be predictable at larger time scales than the underlying sea surface temperature anomalies (environmental fluctuations) (Seferian et al. 2014). In the context of the study of the impact of El Niño teleconnections on the European climate variability, it was found that the predictability of the crop yield was higher than that of the underlying atmospheric variables affecting crop yield (Capa-Morocho, Rodríguez-Fonseca, and Ruiz-Ramos 2014). Analogous results have been found for the predictability of Malaria in Africa (Diouf et al. 2021). Similarly, higher predictability has been found for the Pacific fisheries anomalies than for the underlying Pacific sea surface temperatures (SSTs) when exploiting the Atlantic-Pacific teleconnection (Gómara et al. 2021).

Here, we aim to apply stochastic population dynamics with colored environmental noise to understand population fluctuations predictability and its relations with environmental fluctuations predictability. In terms of temporal correlations, we aim to understand how the dynamics transform the temporal correlations of the environmental fluctuations into temporal correlations of the population fluctuations.

In Section 7.2, we present the population dynamics model (for small fluctuations around equilibrium) driven by colored environmental noise. In Section 7.3, we compute and compare the auto and cross-correlation functions between the environmental fluctuations and the population fluctuations. We compute their maxima and characteristic times, establishing their hierarchies, which provide insight into the propagation of the amplitude and temporal correlation of the fluctuations. Finally, the results are discussed in Section 7.4.

7.2. The model: One species with temporally correlated noise

To study how temporal autocorrelated noise affects a single species, we begin by defining the differential equation that rules the evolution of fluctuations of a species around the equilibrium. For a population with size $N(t)$ (dimensionless) at a certain time t, evolving close to the equilibrium value N_{eq} of the population dynamics, we define the population fluctuations as $\varepsilon(t) = \frac{N(t)-N_{eq}}{N_{eq}}$, which are dimensionless (Chapter 4). (When we assume small fluctuations, the effective equilibrium population size can be estimated with the average of the population size measured in a long enough time series.) Close to equilibrium, this leads to the linear evolution equation

$$d\varepsilon = -\frac{\varepsilon}{T}dt + \lambda\, A dt, \tag{7.1}$$

where T is the characteristic time of return to equilibrium (units of time), and $\gamma = 1/T$ is the rate of return to equilibrium (units of time^{-1}). λ is a coupling constant with units of ($[A]$·time)$^{-1}$. The population is affected by environmental fluctuations A. Environmental fluctuations are random variations or anomalies in an environmental variable (such as temperature, humidity, or a resource needed by the population, and the units of A depend on the kind of environmental fluctuations considered) which influence the evolution of the evolution of the population (Chapter 3). Here, we consider environmental fluctuations A described by a positively-autocorrelated (red) noise defined as an Ornstein-Uhlenbeck process (García-Ojalvo, Sancho, and Ramírez-Piscina 1992) such as

$$dA = -\frac{A}{\tau}dt + \frac{\sigma}{\tau}dW, \tag{7.2}$$

where τ is the characteristic correlation time of the noise (units of time), σ its amplitude (Units of $[A]$·time$^{1/2}$), and dW the differential increment of a normalized Wiener process (*i.e.,* $\xi = dW/dt$ is a normalized Gaussian white noise, see Chapter 2). $< dW(t)dW(t+t') >= c_{dWdW}(t') = 0$ for $t' \neq 0$ and $c_{dWdW}(t') = dt$ for $t' = 0$, with $<>$ the expectation value. All the variables used in this model are described in Table 7.1, as well as their units.

Variables	Description
$N(t)$	Population size at a given time t. Dimensionless.
$\varepsilon(t)$	Population density fluctuations around equilibrium $\varepsilon(t) = \frac{N(t)}{N_{(eq)}} - 1$. Dimensionless.
$A(t)$	Temporally autocorrelated environmental fluctuations at a given time t. Units $[A]$ depend on the kind of environmental fluctuations considered (e.g., temperature or humidity)
τ	Characteristic correlation time of the environmental fluctuations. Units of time.
T	Characteristic time of return to equilibrium of the population. Units of time.
$\gamma = 1/T$	Rate of return to equilibrium. For the logistic equation and small fluctuations, it is equal to the growth rate r. Units of time^{-1}.
$\alpha = T/\tau = 1/(\gamma\tau)$	Ratio between the characteristic damping time of the population fluctuations T and the correlation time of the environmental fluctuations τ. Dimensionless.
σ	Amplitude of the noise. Units of $[A]$·time$^{1/2}$.
λ	The coupling constant giving the impact of the environmental fluctuations A on the population dynamics ε. Units of ($[A]$·time)$^{-1}$.

Table 7.1: Variables used in this chapter, with its description and units.

Fig. 7.1 shows a typical evolution for the environmental noise A and for the population fluctuation ε. Population fluctuations are compared for a lower (red) and a higher (green) damped population dynamics. The plot illustrates that higher damped population fluctuations present a smaller amplitude of population fluctuations. It also shows that peaks in environmental fluctuations A appear delayed and smoothed in the population fluctuations. This pattern anticipates the relevant and delayed temporal cross-correlations between the environmental and population fluctuations that we find in the next section.

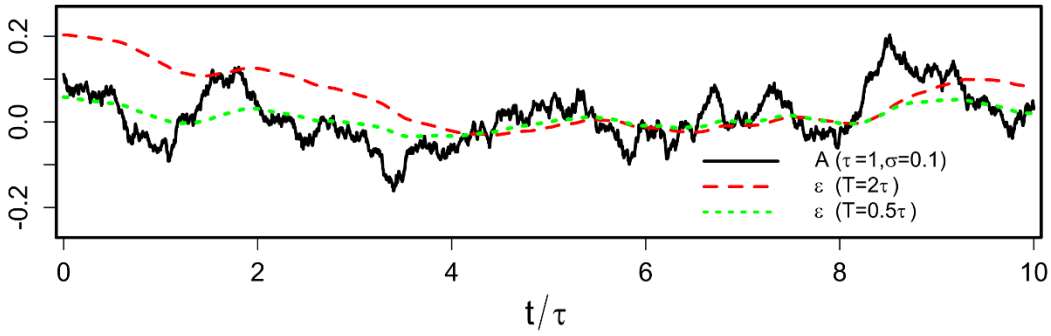

Figure 7.1: Evolution for the environmental fluctuations A (solid black line); and the population fluctuations for $T = 2\tau$ ($\Rightarrow \gamma = 0.5/\tau$) (red dashed line), and $T = 0.5\tau$ ($\Rightarrow \gamma = 2/\tau$) (green pointed line) for $\sigma = 0.1$, $\lambda = 1$ and $\tau = 1$. Population fluctuations peak a short time after environmental fluctuations peak, indicating a delayed correlation between environmental and population fluctuations.

7.3. Temporal autocorrelations and cross-correlations

Once we have seen the behavior of the evolution before, our target is to calculate temporal correlations for a single species in the presence of temporally autocorrelated noise. We want to calculate environmental (noise) autocorrelation, species autocorrelation, and environmental-species correlation, as well as a correlation time.

The correlation between two magnitudes X and Y in two instants separated by a delay t' is given by the correlation function (see Chapter 2)

$$c_{XY}(t') =< X(t)Y(t+t') >, \tag{7.3}$$

where <> means expected value. This correlation indicates how good is $X(t)$ as a predictor of $Y(t+t')$. Therefore, to understand the predictability of the population fluctuations, we have computed the correlations functions of the environmental fluctuations A and of the population fluctuations ε. See Appendix 7.A for the detail of the computations. The correlation functions are

$$c_{AA}(t') = \frac{\sigma^2}{2\tau} e^{-|t'|/\tau} \tag{7.4}$$

$$c_{\varepsilon\varepsilon}(t') = \begin{cases} \dfrac{\lambda^2\sigma^2\tau}{2}\dfrac{\alpha^2}{1-\alpha^2}\left(e^{-|t'|/\tau} - \alpha\, e^{-|t'|/T}\right), & T \neq \tau \\ \dfrac{\lambda^2\sigma^2\tau}{4}(1+|t'|/\tau)e^{-|t'|/\tau}, & T = \tau \end{cases} \tag{7.5}$$

$$c_{A\varepsilon}(t') = \begin{cases} \dfrac{\lambda\sigma^2}{2}\dfrac{\alpha}{1+\alpha} e^{t'/\tau}, & t' \leq 0 \\ \dfrac{\lambda\sigma^2}{2}\dfrac{\alpha}{1-\alpha^2}\left((1+\alpha)e^{-t'/\tau} - 2\alpha\, e^{-t'/T}\right), & t' > 0 \text{ and } T \neq \tau \\ \dfrac{\lambda\sigma^2}{4}(1+2t'/\tau)e^{-t'/\tau}, & t' > 0 \text{ and } T = \tau \end{cases} \tag{7.6}$$

$$c_{\varepsilon A}(t') = c_{A\varepsilon}(-t') \tag{7.7}$$

where $\alpha = T/\tau = 1/(\gamma\tau)$ is the dimensionless ratio between the characteristic damping time of the population fluctuations T and the correlation time of the environmental fluctuations τ. We have represented these correlation functions in Fig. 7.2A.

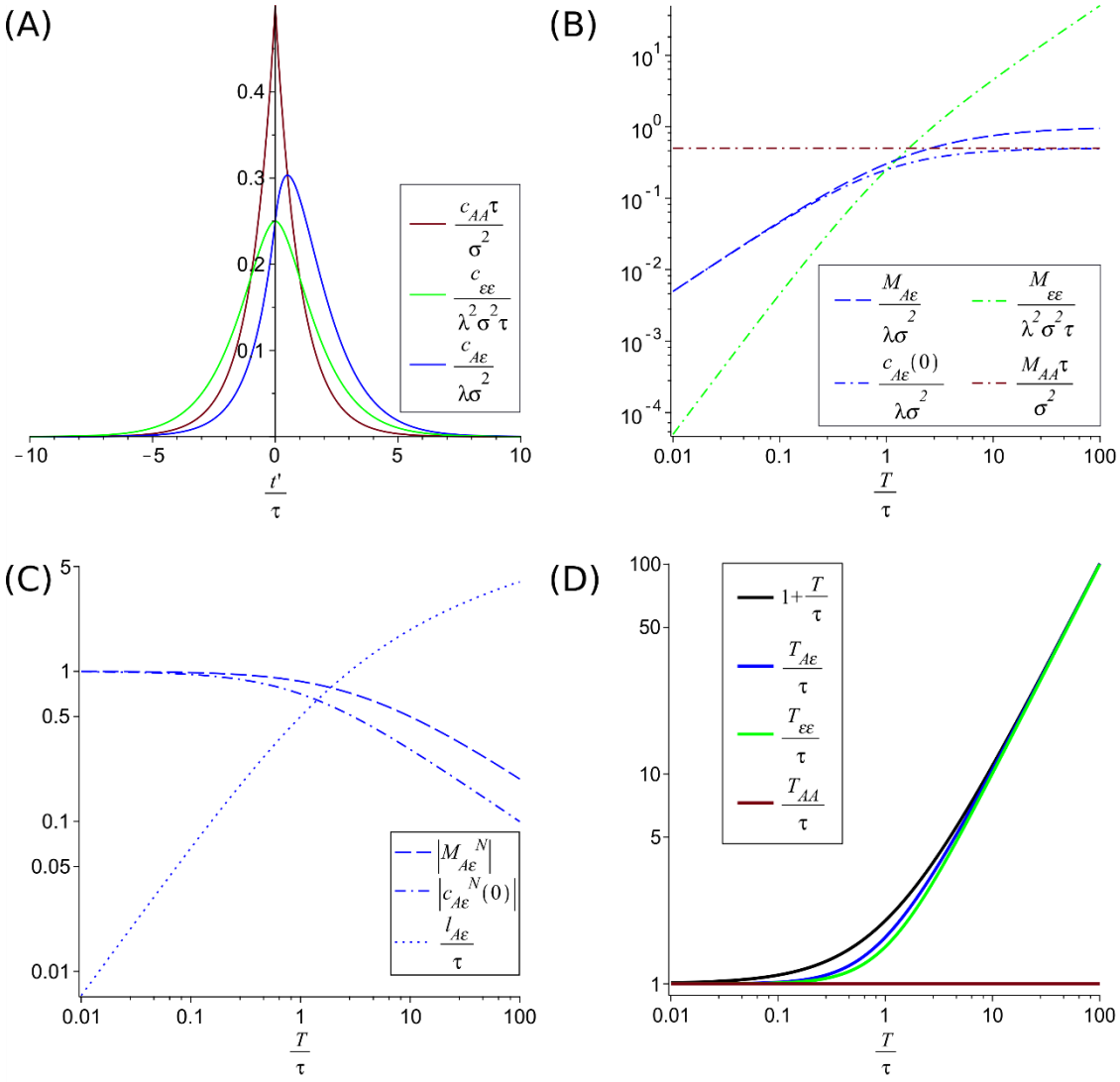

Figure 7.2: Correlation functions with their maximums and their values at t'=0 and correlation times. (A) represents the adimensionalized correlation functions $c_{\varepsilon\varepsilon}(t')$ (green), $c_{AA}(t')$ (red) and $c_{A\varepsilon}(t')$ (blue) adimensionalized for the case $\alpha = T/\tau = 1$. (B) compares the adimensionalized maxima of the autocorrelations function M_{AA} and $M_{\varepsilon\varepsilon}$ (which coincide with the value at $t' = 0$ of the respective autocorrelation) with the maxima of the adimensionalized crosscorrelation function $M_{A\varepsilon}$ and its value at zero delay $c_{A\varepsilon}(0)$. Their normalized values, $M^N_{A\varepsilon} = M_{A\varepsilon}/\sqrt{c_{AA}(0)c_{\varepsilon\varepsilon}(0)}$ and $c^N_{A\varepsilon}(0) = c_{A\varepsilon}(0)/\sqrt{c_{AA}(0)c_{\varepsilon\varepsilon}(0)}$ are shown in (C), with the delay of the cross-correlation maximum $l_{A\varepsilon}$. (D) compares the correlations times $T_{A\varepsilon}$, $T_{\varepsilon\varepsilon}$ and T_{AA}. These plots illustrate the hierarchies for temporal correlations and for the maxima of the correlations discussed in the main text. In particular, it shows that for low damping (large $\alpha = T/\tau$) the crosscorrelation time $T_{A\varepsilon}$ increases, allowing longer-term predictions, despite the decrease in accuracy that can be seen from the decay of the normalized maximum of the cross-correlation $M^N_{A\varepsilon}$.

7.3.1. Maxima of the correlation functions

The autocorrelation function of the environmental fluctuations $c_{AA}(t')$ and the autocorrelation function of the species $c_{\varepsilon\varepsilon}(t')$, which are symmetric, have their maximum at the origin, $t' = 0$,

$$M_{AA} = c_{AA}(0) = \frac{\sigma^2}{2\tau} \tag{7.8}$$

$$M_{\varepsilon\varepsilon} = c_{\varepsilon\varepsilon}(0) = \frac{\lambda^2\sigma^2\tau}{2}\frac{\alpha^2}{1+\alpha} \tag{7.9}$$

The cross-correlation $c_{A\varepsilon}(t')$, has a value at the origin of

$$c_{A\varepsilon}(0) = \frac{\lambda\,\sigma^2}{2}\frac{\alpha}{1+\alpha}. \tag{7.10}$$

But the cross-correlation $c_{A\varepsilon}(t')$ has a lagged maximum (a minimum for negative coupling λ), see Fig. 7.2A, situated at a time displacement ($t' = l_{A\varepsilon}$)

$$l_{A\varepsilon} = \begin{cases} \tau\dfrac{\alpha}{1-\alpha}\ln\left(\dfrac{2}{1+\alpha}\right), & T \neq \tau \\ \dfrac{\tau}{2}, & T = \tau \end{cases} \tag{7.11}$$

This lag means that the population is more affected by the environmental fluctuations after a certain time instead of instantly. Because of the basic property of correlations $c_{XY}(t') = c_{YX}(-t')$, the correlation function $c_{A\varepsilon}(t')$ has the maximum in $t' = -l_{A\varepsilon}$. This maximum, $l_{A\varepsilon}$, is at $t' > 0$ for any $\alpha = T/\tau > 0$, and approaches the origin (smaller lag) as T/τ decreases. This dependence on T/τ causes the lag to tend to zero if the characteristic time of return to equilibrium of the population T is very short.

The cross-correlation $c_{A\varepsilon}(t')$ at this maximum located at $t' = l_{A\varepsilon}$ has a value

$$M_{A\varepsilon} = \begin{cases} \dfrac{1}{2}\lambda\,\sigma^2\alpha\left(\dfrac{2}{1+\alpha}\right)^{\frac{\alpha}{\alpha-1}}, & T \neq \tau \\ \dfrac{1}{2}\lambda\,\sigma^2 e^{-1/2}, & T = \tau \end{cases} \tag{7.12}$$

It can be shown that the maximum correlation $M_{A\varepsilon}$ at most doubles the correlation at the origin $c_{A\varepsilon}(0)$, *i.e.*, $1 \leq \frac{M_{A\varepsilon}}{c_{A\varepsilon}(0)} \leq 2$.

The maxima values can be adimensionalized and compared as in Fig. 7.2B. This shows the following hierarchy

$$\begin{aligned} &\frac{M_{\varepsilon\varepsilon}}{\sigma^2\tau} < \frac{M_{A\varepsilon}}{\lambda\,\sigma^2} < \frac{M_{AA}\tau}{\lambda^2\sigma^2} && \text{for } T < \tau \\ &\frac{M_{\varepsilon\varepsilon}}{\sigma^2\tau} \gtrsim \frac{M_{A\varepsilon}}{\lambda\,\sigma^2} \gtrsim \frac{M_{AA}\tau}{\lambda^2\sigma^2} && \text{for } T \gtrsim \tau \end{aligned} \tag{7.13}$$

This hierarchy means that when the characteristic time scale of population fluctuations damping T is greater than the environmental fluctuations correlation time τ, the magnitude of the adimensionalized maxima increases as the fluctuation propagates (from the environment to the population). Conversely, when the population fluctuations dampen faster than the environmental fluctuations correlations time ($T < \tau$), the maxima decrease as the fluctuation propagates. Only in this later regime and when $T \ll \tau$ (*i.e.*, on the constant environmental fluctuation limit) the normalized environment-population cross-correlation maximum reaches full correlation $M_{A\varepsilon}^N = 1$ (but at zero delay, $l_{A\varepsilon} = 0$). See Fig. 7.2C. The normalized environment-population cross-correlation maximum and value at the origin are given by

$$M_{A\varepsilon}^N = \frac{M_{A\varepsilon}}{\sqrt{c_{AA}(0)c_{\varepsilon\varepsilon}(0)}} = \begin{cases} \text{sign}(\lambda)\sqrt{2}\left(\frac{2}{1+\alpha}\right)^{\frac{1+\alpha}{2(\alpha-1)}}, & T \neq \tau \\ \text{sign}(\lambda)\sqrt{2}\,e^{-1/2}, & T = \tau \end{cases} \tag{7.14}$$

$$c_{A\varepsilon}^N(0) = \frac{c_{A\varepsilon}(0)}{\sqrt{c_{AA}(0)c_{\varepsilon\varepsilon}(0)}} = \frac{\text{sign}(\lambda)}{\sqrt{1+\alpha}}. \tag{7.15}$$

7.3.2. Temporal correlations

The characteristic time of temporal correlations gives the time extension of the predictability. For simple exponential decays of the correlation, the correlation time is just given by the characteristic decay factor in the exponential. For more general cases, we define the correlation time as

$$T_{XY} = \frac{\int_0^\infty t'|c_{XY}(t')|dt'}{\int_0^\infty |c_{XY}(t')|dt'}. \tag{7.16}$$

The absolute value allows incorporating the effects of negative correlations as predictors. For the autocorrelations and cross-correlations, we get

$$T_{AA} = T_{\varepsilon A} = \tau \tag{7.17}$$

$$T_{\varepsilon\varepsilon} = \tau\left[1 + \frac{\alpha^2}{1+\alpha}\right] = \tau + T\frac{1}{1+1/\alpha} \tag{7.18}$$

$$T_{A\varepsilon} = \tau\left[1 + \frac{2\alpha^2}{1+2\alpha}\right] = \tau + T\frac{1}{1+1/(2\alpha)} \tag{7.19}$$

In Fig. 7.2D, these correlation times are plotted as functions of $\alpha = T/\tau$, the ratio between the damping time of the population fluctuations T and the correlation time of the environmental fluctuations τ. Fig. 7.2D suggests a hierarchy of correlation times that can be proven from the previous expressions [Eqs. (7.17)-(7.19)]

$$T_{AA} = T_{\varepsilon A} = \tau < T_{\varepsilon\varepsilon} < T_{A\varepsilon} < \tau + T \tag{7.20}$$

The difference between the last two is bounded by $0 < (T_{A\varepsilon} - T_{\varepsilon\varepsilon}) < \frac{\tau}{2}$.

This hierarchy of correlation times implies a longer correlation time, and therefore a larger scale of predictability, for population fluctuations than for environmental fluctuations.

7.4. Discussion

We aimed to understand the predictability of population fluctuations compared to environmental fluctuations predictability. To get insight into the question, we computed the correlation functions of a population close to an equilibrium state in the presence of environmental colored noise. This computation allowed us to compute the correlation times and the maxima of the correlation functions, finding hierarchies for them, which gives general relations.

We found that the predictability of the population fluctuations is always higher than for the environmental fluctuations. Because of that, we have determined that the correlation time of the population fluctuations is always greater than the correlation time of the environmental fluctuations. The difference in correlation time increases with increased characteristic damping time of population fluctuations T. For example, for $T = 10\,\tau$ we have $T_{\varepsilon\varepsilon} = 10.1\,\tau$ and $T_{A\varepsilon} = 10.5\,\tau$; we also have that the maximum of the population-environment cross-correlation is at $l_{A\varepsilon} = 1.9\,\tau$ with a normalized correlation $M^N_{A\varepsilon} = 0.5$, showing a clear increase with respect to the correlation time for the environmental fluctuations T_{AA}. The underlying mechanism is analogous to the one described by Hasselmann for the integration of the fast weather components leading to the slow climate dynamics (Hasselmann 1976). Our model stresses that the mechanism is general and time-scale independent. In practical cases times scales can range from days (for pest populations in agriculture) to years (for large species or ecosystems).

This study was inspired by our previous results on spatial population synchrony (Jarillo et al. 2018; 2020; Lee et al. 2022; Fernández-Grande and Cao-Garcia 2020) and motivated by the findings that population fluctuations showed larger predictability than the underlying environmental variables. This was shown to happen for a wide range of systems: primary production in oceans (Seferian et al. 2014), crop yield (Capa-Morocho, Rodríguez-Fonseca, and Ruiz-Ramos 2014), malaria (Diouf et al. 2021) and fisheries (Gómara et al. 2021). This higher predictability increases the prospects of predicting climatic variability effects on populations (Iizumi et al. 2014; Watters et al. 2003; Christensen et al. 2015; Capa-Morocho, Rodríguez-Fonseca, and Ruiz-Ramos 2014; Diouf et al. 2021; Gómara et al. 2021).

The determination of the effective equilibrium can be challenging in practical cases (Pimm and Redfearn 1988). In general, the effective equilibrium is obtained from the time-average of the data in long-enough time series. However, sometimes the equilibrium can have seasonal oscillations or long-term trends. In these cases, these variations in the equilibrium have to be taken into account substracting them to obtain the correct fluctuations around equilibrium. Several model extensions are possible to get insight on the scope of the results. The results have been obtained for a single-environmental variable acting on a single-species in the small fluctuation regime, which allows the linearization of the dynamical equations around the equilibrium. This model can be extended including several interacting species and several environmental variables (which may also interact as wind stress and sea surface temperature). Other extension is including the division of species populations into distinct life stages, with some of them particularly affected by environmental fluctuations (Lowe et al. 2021). Our model considers small enough environmental fluctuations (which implies the population is close to equilibrium). This can be extended studying larger environmental fluctuations in

particularly relevant ecological models, which would clarify how the results in the present work are affected by the presence of nonlinearities.

The present study raises the question of how the propagation of fluctuations through the food webs impacts the predictability of the different species' population fluctuations. This more profound understanding of the population predictability will help to design improved conservation policies, particularly useful for species especially sensitive to environmental variability (represented in our model with great couplings λ), such as ectotherms.

7.A. Appendix: Computation of temporal correlation functions and times.

As the dynamics are time invariant, the asymptotic time correlations are stationary. The stationarity condition is

$$< X(t)Y(t+t') >=< X(t+dt)Y(t+t'+dt) >$$

where $X(t+dt) = X(t) + dX(t)$ and $Y(t+t'+dt) = Y(t+t') + dY(t+t')$. The application of this stationary condition provides relationships between time correlation, which allow computing them.

7.A.1. Wiener process temporal autocorrelation

The temporal autocorrelation of the Wiener process (whose derivative gives the white noise) is known to be

$$c_{dWdW}(t') = \begin{cases} dt, & \text{for } t' = 0, \\ 0, & \text{for } t' \neq 0. \end{cases} \qquad (7.A1)$$

7.A.2. Wiener – colored-noise temporal cross-correlation

We know that $c_{dWA}(t') =< dW(t)A(t+t') >$ is zero for $t' \leq 0$, as there is no fluctuation propagation to the past. Therefore, we just have to make the computation for positive time displacement.

We compute $c_{dWA}(t') =< dW(t)A(t+t') >$ for $t' = dt$, $t' = 2dt$, $t' = 3dt$, ...

$$< dW(t)A(t+dt) > =< dW(t)\left(A(t) - \frac{A(t)}{\tau}dt + \frac{\sigma}{\tau}dW(t)\right) > = \frac{\sigma}{\tau}\, dt$$

$$< dW(t)A(t+2dt) > =< dW(t)\left(A(t+dt) - \frac{A(t+dt)}{\tau}dt + \frac{\sigma}{\tau}dW(t+dt)\right) >$$

$$= \frac{\sigma}{\tau}\left(1 - \frac{dt}{\tau}\right)\, dt$$

$$< dW(t)A(t+3dt) > =< dW(t)\left(A(t+2dt) - \frac{A(t+2dt)}{\tau}dt + \frac{\sigma}{\tau}dW(t+2dt)\right) >$$

$$= \frac{\sigma}{\tau}\left(1 - \frac{dt}{\tau}\right)^2\, dt$$

These results allow us to get the general expression

$$c_{dWA}(ndt) =< dW(t)A(t+ndt) > = \frac{\sigma}{\tau}\left(1 - \frac{dt}{\tau}\right)^{n-1}\, dt$$

In the large n limit, we get the exponential expression

$$c_{dWA}(t') = \frac{\sigma}{\tau}e^{-t'/\tau}dt \text{ if } t' > 0$$

Therefore, we have

$$c_{dWA}(t') = \begin{cases} 0 & \text{if } t' \leq 0 \\ \frac{\sigma}{\tau}e^{-t'/\tau}\, dt & \text{if } t' > 0 \end{cases} \qquad (7.A2)$$

7.A.3. Wiener – population temporal cross-correlation

There is no propagation of the fluctuations to the past. Thus, $c_{dW\varepsilon}(t') =< dW(t)\varepsilon(t+t') >$ is zero for $t' \leq 0$, and we only have to compute the correlation for positive time displacement.

The same procedure used for $c_{dWA}(t')$ allows obtaining $c_{dW\varepsilon}(t')$

$$< dW(t)\varepsilon(t+dt) > =< dW(t)\cdot(\varepsilon(t) - \gamma\varepsilon(t)dt + \lambda A(t)dt) > = 0$$

$$< dW(t)\varepsilon(t+2dt) > =< dW(t)\cdot(\varepsilon(t+dt) - \gamma\varepsilon(t+dt)dt + \lambda A(t+dt)dt) > = \frac{\lambda\sigma}{\tau}dt^2$$

$$\begin{aligned} < dW(t)\varepsilon(t+3dt) > &=< dW(t)\cdot(\varepsilon(t+2dt) - \gamma\varepsilon(t+2dt)dt + \lambda A(t+2dt)dt) > \\ &= \frac{\lambda\sigma}{\tau}(1-\gamma dt)dt^2 + \frac{\lambda\sigma}{\tau}\left(1-\frac{dt}{\tau}\right)dt^2 \end{aligned}$$

$$\begin{aligned} < dW(t)\varepsilon(t+4dt) > &=< dW(t)\cdot(\varepsilon(t+3dt) - \gamma\varepsilon(t+3dt)dt + \lambda A(t+3dt)dt) > \\ &= \frac{\lambda\sigma}{\tau}(1-\gamma dt)^2dt^2 + \frac{\lambda\sigma}{\tau}(1-\gamma dt)\left(1-\frac{dt}{\tau}\right)dt^2 + \frac{\lambda\sigma}{\tau}\left(1-\frac{dt}{\tau}\right)^2 dt^2 \end{aligned}$$

$$\begin{aligned} < dW(t)\varepsilon(t+ndt) > &= \frac{dt^2}{\tau}\lambda\sigma\sum_{i=0}^{n-2}(1-\gamma dt)^{n-2-i}\left(1-\frac{dt}{\tau}\right)^i \\ &= \frac{\lambda\sigma}{\tau}dt^2(1-\gamma dt)^{n-2}\sum_{i=1}^{n-1}\left(\frac{1-\frac{dt}{\tau}}{1-\gamma dt}\right)^{i-1} \end{aligned}$$

The later expression gives, when $\gamma\tau = 1$

$$\frac{\lambda\sigma}{\tau}dt^2(1-\gamma dt)^{n-2}\sum_{i=1}^{n-1}1 = \frac{\lambda\sigma}{\tau}dt^2(1-\gamma dt)^{n-2}\cdot(n-1) \approx \frac{\lambda\sigma}{\tau}t'e^{-\gamma t'}dt = \frac{\lambda\sigma}{\tau}t'e^{-t'/\tau}dt,$$

while for $\gamma\tau \neq 1$

$$\begin{aligned} \frac{\lambda\sigma}{\tau}dt^2(1-\gamma dt)^{n-2}\sum_{i=1}^{n-1}\left(\frac{1-\frac{dt}{\tau}}{1-\gamma dt}\right)^{i-1} &= \frac{\lambda\sigma}{\tau}dt^2(1-\gamma dt)^{n-2}\cdot\frac{1-\left(\frac{1-\frac{dt}{\tau}}{1-\gamma dt}\right)^{n-1}}{1-\frac{1-\frac{dt}{\tau}}{1-\gamma dt}} \\ &= \frac{\lambda\sigma dt}{1-\gamma\tau}\left((1-\gamma dt)^{n-1} - \left(1-\frac{dt}{\tau}\right)^{n-1}\right) \approx \frac{\lambda\sigma}{1-\gamma\tau}\left(e^{-\gamma t'} - e^{-t'/\tau}\right)dt. \end{aligned}$$

(Note that in the limit $\gamma\tau \to 1$, the results for $\gamma\tau = 1$ are recovered, indicating the continuity of the solution on $\gamma\tau$.)

Therefore, we have the temporal correlation

$$c_{dW\varepsilon}(t') = \begin{cases} 0 & \text{if } t' < 0 \\ \frac{\lambda\sigma}{1-\gamma\tau}\left(e^{-\gamma t'} - e^{-t'/\tau}\right)dt & \text{if } t' > 0 \text{ and } \gamma\tau \neq 1 \\ \frac{\lambda\sigma}{\tau}t'e^{-t'/\tau}dt & \text{if } t' > 0 \text{ and } \gamma\tau = 1 \end{cases} \qquad (7.A3)$$

7.A.4. Colored-noise autocorrelations

The computation of this (and the following) temporal correlations relies on the time invariance of the dynamics, which leads to the stationarity of the asymptotic temporal correlations.

We begin calculating the temporal autocorrelation for the environmental autocorrelations, $c_{AA}(t') =< A(t)A(t+t') >$, whose stationary condition implies

$$< A(t)A(t+t') > = < \big(A(t) + dA(t)\big) \cdot \big(A(t+t') + dA(t+t')\big) > =$$

$$< (A(t) - A(t)/\tau\, dt + \sigma/\tau\, dW(t)) \cdot (A(t+t') - A(t+t')/\tau\, dt + \sigma/\tau\, dW(t+t')) >$$

Expanding up to the first order in dt we get

$$< A(t)A(t+t') > = < A(t)A(t+t') > - \frac{2}{\tau} < A(t)A(t+t') > dt$$

$$+ \frac{\sigma}{\tau}\left(1 - \frac{dt}{\tau}\right) < A(t)dW(t+t') > + \frac{\sigma}{\tau}\left(1 - \frac{dt}{\tau}\right) < dW(t)A(t+t') >$$

$$+ \frac{\sigma^2}{\tau^2} < dW(t)dW(t+t') >,$$

which gives the equation

$$\frac{2}{\tau} c_{AA}(t')dt = \frac{\sigma}{\tau}\left(1 - \frac{dt}{\tau}\right) c_{AdW}(t') + \frac{\sigma}{\tau}\left(1 - \frac{dt}{\tau}\right) c_{dWA}(t') + \frac{\sigma^2}{\tau^2} c_{dWdW}(t').$$

As we have shown that $c_{dWA} \sim dt$ and $c_{dW\epsilon} \sim dt$ [Eqs. (7.A2) and (7.A3)], which indicates that there are still terms of second order in the previous equation. Keeping only the first order terms in dt and using $c_{AdW}(t') = c_{dWA}(-t')$, the equation becomes

$$c_{AA}(t') = \frac{\sigma}{2\, dt}\left(c_{dWA}(t') + c_{dWA}(-t')\right) + \frac{\sigma^2}{2\tau} \frac{c_{dWdW}(t')}{dt}$$

This later equation gives $c_{AA}(t')$, in terms of the cross-correlations of the white noise with the colored noise and with the population fluctuations.

Substituting Eq. (7.A2), we get environmental autocorrelation

$$c_{AA}(t') = \frac{\sigma^2}{2\tau} e^{-|t'|/\tau} \qquad (7.A4)$$

7.A.5. Colored-noise – population cross-correlation

We continue with the environment-species temporal cross-correlation $c_{A\varepsilon}(t') = < A(t)\varepsilon(t+t') >$, whose stationary condition gives

$$< A(t)\varepsilon(t+t') > = < \big(A(t) + dA(t)\big) \cdot \big(\varepsilon(t+t') + d\varepsilon(t+t')\big) > =$$

$$< (A(t) - A(t)/\tau\, dt + \sigma/\tau\, dW(t)) \cdot (\varepsilon(t+t') - \gamma\varepsilon(t+t')dt + \lambda A(t+t')\, dt) >$$

Again, up to the first order in dt, we get

$$< A(t)\varepsilon(t+t') > = < A(t)\varepsilon(t+t') > - \left(\gamma + \frac{1}{\tau}\right) < A(t)\varepsilon(t+t') > dt$$

$$+ \frac{\sigma}{\tau}(1 - \gamma dt) < dW(t)\varepsilon(t+t') > + \lambda < A(t)A(t+t') > dt + \frac{\lambda\sigma}{\tau} < dW(t)A(t+t') > dt,$$

resulting in the second relation,

$$-\left(\gamma+\frac{1}{\tau}\right)c_{A\varepsilon}(t')dt+\frac{\sigma}{\tau}(1-\gamma dt)c_{dW\varepsilon}(t')+\lambda c_{AA}(t')dt+\frac{\lambda\sigma}{\tau}c_{dWA}(t')dt=0.$$

Recalling again that $c_{dWA}\sim dt$ and $c_{dW\varepsilon}\sim dt$, fewer terms are of the first order in dt, leading to

$$c_{A\varepsilon}(t')=\frac{1}{\gamma+1/\tau}\left(\frac{\sigma}{\tau}\frac{c_{dW\varepsilon}(t')}{dt}+\lambda c_{AA}(t')\right)$$

Substituting Eqs. (7.A3) and (7.A4), we can calculate the environmental-population fluctuations cross-correlation

$$c_{A\varepsilon}(t')=\begin{cases}\dfrac{\lambda\sigma^2}{2(1+\gamma\tau)}e^{t'/\tau}, & t'\le 0\\ \dfrac{\lambda\sigma^2}{2((\gamma\tau)^2-1)}\left((1+\gamma\tau)e^{-t'/\tau}-2e^{-\gamma t'}\right), & t'>0 \text{ and } \gamma\tau\neq 1\\ \dfrac{\lambda\sigma^2}{4\tau}(\tau+2t')e^{-t'/\tau}, & t'>0 \text{ and } \gamma\tau=1\end{cases} \qquad (7.A5)$$

while $c_{\varepsilon A}(t')=c_{A\varepsilon}(-t')$.

7.A.6. Autocorrelations of the population fluctuations

We finally compute the temporal autocorrelation for the population fluctuations of the species $c_{\varepsilon\varepsilon}(t')=<\varepsilon(t)\varepsilon(t+t')>$, whose stationary condition implies

$$<\varepsilon(t)\varepsilon(t+t')>=<\big(\varepsilon(t)+d\varepsilon(t)\big)\cdot\big(\varepsilon(t+t')+d\varepsilon(t+t')\big)>=$$

$$<(\varepsilon(t)-\gamma\varepsilon(t)dt+\lambda A(t)\,dt)\cdot(\varepsilon(t+t')-\gamma\varepsilon(t+t')dt+\lambda A(t+t')\,dt)>.$$

Keeping terms up to first order in dt, we obtain the following expression:

$$<\varepsilon(t)\varepsilon(t+t')>=<\varepsilon(t)\varepsilon(t+t')>-2\gamma<\varepsilon(t)\varepsilon(t+t')>dt$$

$$+\lambda<\varepsilon(t)A(t+t')>dt\ +\lambda<A(t)\varepsilon(t+t')>dt$$

In terms of correlations and using the relation $c_{XY}(t')=c_{YX}(-t')$, we have

$$c_{\varepsilon\varepsilon}(t')=\frac{\lambda}{2\gamma}\left(c_{A\varepsilon}(t')+c_{A\varepsilon}(-t')\right).$$

Substituting Eq. (7.A5), we get for the population fluctuations autocorrelation

$$c_{\varepsilon\varepsilon}(t')=\begin{cases}\dfrac{\lambda^2\sigma^2\tau}{2\gamma\tau((\gamma\tau)^2-1)}\left(\gamma\tau e^{-\frac{|t'|}{\tau}}-e^{-\gamma|t'|}\right), & \gamma\tau\neq 1\\ \dfrac{\lambda^2\sigma^2}{4}(\tau+|t'|)e^{-|t'|/\tau}, & \gamma\tau=1\end{cases} \qquad (7.A6)$$

7.A.7. Maxima

The environmental noise autocorrelation $c_{AA}(t')$ and of the population fluctuations autocorrelation $c_{\varepsilon\varepsilon}(t')$ have their maximum at the origin $t'=0$. The environment-population cross-correlation has a lagged maximum at a time $t'=l_{A\varepsilon}$ with

$$l_{A\varepsilon}=\begin{cases}\dfrac{\ln\left(\frac{2\gamma\tau}{\gamma\tau+1}\right)}{\gamma\tau-1}\tau, & \gamma\tau\neq 1\\ \dfrac{\tau}{2}, & \gamma\tau=1\end{cases} \qquad (7.A7)$$

with a magnitude $M_{A\varepsilon}=c_{A\varepsilon}(l_{A\varepsilon})$ given by

$$M_{A\varepsilon}=\begin{cases}\dfrac{\lambda\sigma^2\left(\frac{2\gamma\tau}{1+\gamma\tau}\right)^{\frac{1}{1-\gamma\tau}}}{2\gamma\tau}, & \gamma\tau\neq 1\\ \lambda\,\sigma^2 e^{-\frac{1}{2}}/2, & \gamma\tau=1.\end{cases} \qquad (7.A8)$$

These expressions are also given in the main text in terms of $\alpha=\frac{T}{\tau}=\frac{1}{\gamma\tau}$, the ratio of the population relaxation time T and the correlation time of environmental fluctuations τ.

7.A.8. Correlation times

The previous explicit expression for the time correlation function allows computing their respective correlation times

$$T_{AA}=\frac{\int_0^\infty t' c_{AA}(t')dt'}{\int_0^\infty c_{AA}(t')dt'}=\frac{\int_0^\infty t'\frac{\sigma^2}{2\tau}e^{-t'/\tau}dt'}{\int_0^\infty \frac{\sigma^2}{2\tau}e^{-t'/\tau}dt'}=\frac{\int_0^\infty t' e^{-t'/\tau}dt'}{\int_0^\infty e^{-t'/\tau}dt'}=\tau, \qquad (7.A9)$$

$$T_{\varepsilon A}=\tau, \qquad (7.A10)$$

$$T_{\varepsilon\varepsilon}=\tau\,\frac{(\gamma\tau)^2+\gamma\tau+1}{\gamma\tau(\gamma\tau+1)}=\tau\left[1+\frac{1}{\gamma\tau(\gamma\tau+1)}\right]=\tau\left[1+\frac{\alpha^2}{1+\alpha}\right]=\tau+T\frac{\alpha}{1+\alpha}, \qquad (7.A11)$$

$$T_{A\varepsilon}=\tau\,\frac{(\gamma\tau)^2+2\gamma\tau+2}{\gamma\tau(\gamma\tau+2)}=\tau\left[1+\frac{2}{\gamma\tau(\gamma\tau+2)}\right]=\tau\left[1+\frac{2\alpha^2}{1+2\alpha}\right]=\tau+T\frac{2\alpha}{1+2\alpha}, \qquad (7.A12)$$

where $\alpha=\frac{T}{\tau}=\frac{1}{\gamma\tau}$ is the ratio of the population relaxation time T and the correlation time of environmental fluctuations τ.

PART IV: Conclusions, discussion and future work

Conclusions and discussion

Deterministic models are just approximations of reality. Random events are present in many real systems. Then, stochastic models become necessary to describe these systems consistently (Gardiner 2009). In this way, fluctuations or noise are included in the model to represent variability. In particular, when we study populations of living beings, the inclusion in the model of a stochastic term becomes essential to accurately study natural ecosystems (Lande, Engen, and Saether 2003).

Stochastic analysis is necessary because each individual differs from other population members and may have a different behavior over time. For example, even under similar circumstances, there may be individual variability from the average age of death of the species or in the number of offspring given in every breeding season. While important, individual (non-environmental) variability can be averaged out for sufficiently large populations.

Besides, environmental conditions, such as weather, affect an entire population and vary randomly in time. In these cases, simply taking the average of the random variations so that they deterministically affect the population evolution causes a loss of information. This approximation may be completely wrong if the variability is large enough (Engen, Bakke, and Islam 1998; Lande, Engen, and Saether 2003; Cabrerizo and Marañón 2021).

Specifically, the deterministic part of the evolution of many populations has been classically modeled as logistic growth, i.e., exponential growth at low populations with a density regulation term (Verhulst 1838; Cotgreave and Gotelli 2006). The regulation term implies that the population saturates near an equilibrium population that we call carrying capacity. Besides, we have focused on a variation of this model, which describes the difficulty of recovery (or tendency to extinction) of low-density populations, known as the Allee effect (Allee and Rosenthal 1949). The model is obtained by adding a term so that the effective growth rate is negative for populations below a certain threshold. This negative growth rate implies that, in general, populations suffering from the Allee effect are less resilient to adverse effects.

Moreover, to study a system with greater precision, it is necessary to consider that individuals are not in a single point of space. Movements between different habitat areas can rescue the population in areas affected by local extinction or depletion. Dispersal of individuals within the ecosystem has been studied as a mechanism that significantly increases the population's resilience (Engen, Lande, and Sæther 2002). This thesis shows how this is done in systems with Allee Effect: A species' tendency to disperse and repopulate areas with low population densities is one of the main factors affecting species' resilience. Dispersals with greater range and intensity are more effective in increasing the population's resilience.

As we have just mentioned, the deterministic treatment is incorrect in most cases since the parameters that describe it can vary randomly over time. Therefore, population density must be treated as a stochastic process whose dynamics are affected by environmental fluctuations. These fluctuations are represented as white (temporally uncorrelated) or colored (temporally autocorrelated) noise. Environmental fluctuations are spatially correlated, which means that weather events extend across space, and this correlation, as well as dispersal, synchronizes the population across space (Moran 1953; Lande, Engen, and Sæther 1999). The typical correlation distances (spatial scale of synchrony of the population) increase with the spatial scale of

environmental synchrony, the typical dispersal distance, and its intensity (the dispersal rate). Spatial scales of population synchrony are approximately the size of the areas where the species is found in abundance, or on the contrary, of the local extinction areas.

In our work about Allee effect and dispersal, we want to know which are the main factors that affect a spatially extended population's resilience, given Allee effect dynamics. We have simulated the evolution of populations and studied their distribution at long times (chapter 5) to obtain which are the parameters that influence resilience: The dispersal distances, the scale of synchrony of environmental fluctuations, the Allee threshold of the minimum viable population compared to the carrying capacity, and the dispersal rate compared to the growth rate.

More precisely, we are interested in determining how the environmental and population characteristics affect the extinction risk. The results about variations in the minimum viable population threshold (Allee threshold) show that populations with more significant difficulties of recovery at low population densities (greater Allee threshold compared to the carrying capacity) are much more vulnerable to climatic variability.

We also study the extinction risk's dependence on the dispersal intensity and scope. The study shows the great importance of dispersal in preventing the extinction of a population: Specifically, we get that the population's resilience grows proportionally to the root of the dispersal rate and that populations always get extinct in the absence of dispersal. Moreover, longer dispersal distances compared to the scale of synchrony of environmental fluctuations allow populations to recolonize farther locations. Thus, the rescue effect is enhanced, providing more resilience against environmental variability.

In our work about habitat size and dispersal, we wanted to understand how the reduction of habitat size affects the population's resilience. In chapter 6, we have got the extinction risk’s dependence on the confinement size by simulating a population that disperses inside a finite space. In so doing, we have obtained that a reduction in habitat size implies a drastic increase in extinction risk since the dispersal-induced rescue effect's effectiveness is minimized. Consequently, individuals will be unable to re-colonize distant areas if their mobility capability is truncated (Collingham and Huntley 2000; Dullinger et al. 2015). Extinction risk is even higher if the habitat becomes much smaller compared to the dispersal distance.

Nonetheless, it is important to clarify how much dispersal can increase population resilience. As said before, longer dispersal implies enhanced population resilience, but this increase is not unlimited. Each habitat size determines a maximum resilience reached at a certain dispersal distance, again supporting that habitat fragmentation reduces the effectiveness of the rescue effect. This change in the extinction risk with the habitat size indicates that habitat preservation is a crucial point in population conservation and tells us the cases for which we need a special effort to protect a certain population's habitat.

Next, in Chapter 7, we have studied a population close to equilibrium. This population is influenced by temporally autocorrelated environmental fluctuations (colored noise). From the equations that describe population dynamics, we obtained expressions for the autocorrelation and cross-correlation functions of the population and the environment. Those correlation functions depend on the amplitude of the environmental noise, the coupling between environment and population, and the characteristic time of environmental and population fluctuations.

Correlation functions allow us to obtain valuable properties of the population dynamics. The value of the autocorrelation function for the population fluctuations at time zero measures the population variability. Moreover, the correlation time of the studied variables is a measure of the time extension of their predictability. For any set of dynamic parameters, the autocorrelation time of the population is longer than that of the environmental fluctuations. Lastly, the delayed maximum of the cross-correlation function indicates when and how intensely the environmental variable has the greatest influence on population fluctuations.

The results presented in this thesis are helpful in adequately understanding the resilience of a population to adverse environmental conditions. Our results also allow us to predict an ecosystem's proximate evolution with a certain degree of accuracy. Besides, given that human action can be studied as an agent that affects the ecosystem's dynamic parameters, these results allow us to assess how to exploit a population without causing irreversible damage to the ecosystem. Thereby, this deeper understanding allows to develop more optimal repopulation strategies or harmless ways to exploit natural resources.

Future work

The results presented for the spatially extended population model with Allee effect (Part II) open the door to investigating other relevant effects, such as external migration, harvesting, repopulation, and habitat shape. This model can be also extended to study interspecific interactions or how other external factors affect the ecosystem, to obtain new results and applications.

External migration has already been studied (Dennis et al. 2016), showing that it reduces the extinction risk. However, a study of a population with Allee effect considering both external migration and dispersal within the ecosystem is still to be made. This model may be especially relevant as it allows us to describe human action in the ecosystem. Specifically, we can add the possibility of harvesting, which clearly affects extinction risk (Jarillo et al. 2018). Understanding this dependence on populations with Allee effect can help advance effective species conservation strategies or enhance sustainable exploitation methods. Similarly, repopulation can also be added so that the human factor's effect on the species' resilience can be quantified.

Moreover, our works on spatially extended population dynamics (Part II) have taken a one-dimensional space as a first approximation. Nonetheless, previous studies such as (Diamond 1975) show that the habitats' shape is determinant in the species' evolution. In two dimensions, besides the size of the habitat, other factors must be taken into account. For example, circular-like habitats easily allow dispersal throughout due to the propagation front of individuals. Then, habitats with more circular forms are more optimal for the survival of a species than those with elongated forms or penínsulas. Therefore, seeking a generalization for two dimensions seems necessary to study other natural systems with enough precision.

Our study on the predictability of a population affected by temporally autocorrelated environmental fluctuations (Part III) considers a uniform population near equilibrium. This study can be extended by considering larger fluctuations, which may invalidate the linear approximation around equilibrium. This extension would allow us to study systems under more extreme conditions.

To conclude, species are not isolated but are part of an ecosystem. In the studies included in this thesis (Chapters 5-7), we have not explicitly considered the effects of other species. Those effects can be relevant in the dynamics of other populations interacting with them. Then, these studies should be extended to include several interacting species. Specifically, we are working on an extension of our models to understand food chains under the influence of temperature variations in several fishing areas in the Atlantic Ocean (TRIATLAS Project). Understanding those ecosystems would contribute to a better managing of fisheries.

The extensions presented in this section to previously included models in this thesis allow a more accurate description of a wider variety of ecosystems. Thus, we would get a deeper understanding of how species interact with the other components of the ecosystem, both the physical ones (such as climate) and the other species present in the same habitat. Consequently, present and future results in this line can potentially provide better tools to protect locally endangered populations. Additionally, these results allow planning more efficient and less damaging strategies for exploiting natural resources (including harvested species) in the future.

Conclusiones y discusión

Los modelos deterministas son solo aproximaciones de la realidad en la mayoría de las situaciones. En muchos sistemas reales aparecen eventos aleatorios, por lo que los procesos estocásticos se vuelven una herramienta necesaria para describir consistentemente estos sistemas (Gardiner 2009). De esta manera, se introducen fluctuaciones (o ruido) en el modelo para representar variabilidad. En concreto, cuando estudiamos poblaciones de seres vivos, la inclusión en el modelo de un término estocástico se vuelve imprescindible si queremos hacer un estudio preciso de los ecosistemas (Lande, Engen y Saether 2003).

El tratamiento estocástico es necesario ya que cada individuo es diferente de sus congéneres y puede tener un comportamiento distinto con el paso del tiempo: Por ejemplo, incluso en circunstancias similares, puede existir variaciones individuales respecto a la edad de muerte promedio de la población, o en el número de crías en cada época de cría. Esta variabilidad individual (no ambiental), aunque importante, puede ser promediada para poblaciones suficientemente grandes.

Además, las condiciones ambientales, como el tiempo atmosférico, que afectan a toda una población, también varían aleatoriamente a lo largo del tiempo. En estos casos, simplemente tomar el promedio de las variaciones aleatorias de tal manera que afecten de forma determinista a la evolución de la población hace que se pierda información. Si dicha variabilidad es suficientemente grande, esta aproximación puede ser completamente errónea (Engen, Bakke e Islam 1998; Lande, Engen y Saether 2003; Cabrerizo y Marañón 2021).

En concreto, la parte determinista de la evolución de una población para muchas especies ha sido clásicamente modelada como un crecimiento logístico, esto es, crecimiento exponencial a poblaciones bajas con un término de regulación de densidad (Verhulst 1838; Cotgreave y Gotelli 2006). Este término de regulación implica que la población sature cerca de una población de equilibrio que llamamos capacidad de carga. Además, nosotros nos hemos centrado en una variación de este modelo que sirve para describir la dificultad de recuperación (o tendencia a la extinción) de poblaciones con baja densidad, lo que se conoce como efecto Allee (Allee y Rosenthal 1949). El modelo se consigue añadiendo un término adicional de manera que el ratio de crecimiento efectivo es negativo para poblaciones debajo de un cierto umbral, lo que implica que en general las poblaciones que sufren de efecto Allee son menos resilientes a efectos adversos.

Por otro lado, para estudiar un sistema con mayor precisión, es necesario tener en cuenta que los individuos no se encuentran en un único punto del espacio y los movimientos entre distintas zonas del habitat pueden rescatar a la población de zonas afectadas por una extinción local o deterioro del tamaño de la población. Así, la dispersión de individuos dentro del ecosistema ha sido estudiada como un mecanismo que aumenta en gran manera la resiliencia de la población (Engen, Lande y Sæther 2002). En esta tesis hemos demostrado de qué manera lo hace en sistemas con Efecto Allee: La tendencia de una especie a dispersarse y repoblar zonas con densidades de población bajas es una de las principales circunstancias que afectan a la resiliencia de la especie. Esta dispersión es más efectiva aumentando la resiliencia de la población cuanto mayor alcance e intensidad tiene.

Como acabamos de comentar, el tratamiento determinista no es correcto en la mayor parte de los casos, ya que los parámetros que lo describen pueden variar aleatoriamente con el tiempo.

Por tanto, la densidad de población ha de ser tratada como un proceso estocástico cuya dinámica es afectada por fluctuaciones ambientales, que son representadas en forma de ruido blanco (temporalmente no autocorrelacionado) o de color (temporalmente autocorrelacionado). Las fluctuaciones ambientales están espacialmente correlacionadas, lo que significa que algunos eventos climáticos se extienden a lo largo del espacio, y esta correlación, así como la dispersión, sincroniza la población a lo largo del espacio (Moran 1953; Lande, Engen y Sæther 1999). Las distancias de correlación típicas (escala espacial de sincronía) de la población aumentan con la escala espacial de sincronía ambiental, la distancia típica de dispersión y la intensidad de esta (el ratio de dispersión), y estas distancias son aproximadamente el tamaño de las zonas donde la especie se halla en abundancia o, por el contrario, de las zonas que presentan extinción local.

En nuestro trabajo sobre efecto Allee y dispersión queremos saber cuáles son los factores principales que afectan a la resiliencia de una población extendida espacialmente con dinámica dada por efecto Allee. Hemos simulado la evolución de poblaciones y estudiado su distribución a tiempos largos (capítulo 5) para obtener cuáles son aquellos parámetros que influyen sobre la resiliencia: La distancia de dispersión, la escala espacial de sincronía de las fluctuaciones ambientales, el umbral Allee de mínima población viable comparado con la capacidad de carga, y el ratio de dispersión comparado con el ratio de crecimiento.

En concreto, estamos interesados en determinar como el riesgo de extinción es afectado por estas características de la población y del ambiente. Los resultados sobre variaciones en el umbral de mínima población viable (umbral Allee) muestran que las poblaciones con mayores dificultades de recuperación a densidades de poblaciones bajas (mayor umbral Allee respecto a la capacidad de carga) son mucho más vulnerables a la variabilidad climática.

Adicionalmente hemos estudiado la dependencia del riesgo de extinción según la intensidad y alcance de la dispersión. El estudio muestra la gran importancia de la dispersión previniendo la extinción de una población. Específicamente, tenemos que la resiliencia de la población crece de forma proporcional a la raíz del ratio de dispersión, y que las poblaciones siempre acaban extinguiéndose en la ausencia de dispersión. Además, distancias de dispersión más largas comparadas con la escala de sincronía de las fluctuaciones ambientales permiten a las poblaciones recolonizar localizaciones más lejanas. Así se mejora el efecto rescate, propiciando mayor resiliencia frente a la variabilidad ambiental.

En nuestro trabajo acerca de tamaño del hábitat y dispersión buscamos entender cómo la resiliencia de la población se ve afectada por reducciones en el tamaño de su hábitat. En el Capítulo 6 hemos encontrado una dependencia del riesgo de extinción con el tamaño del confinamiento a partir de simulaciones en las cuales una pobración se dispersa en un espacio finito. Haciendo esto, hemos obtenido que una reducción del tamaño del hábitat implica un incremento drástico en el riesgo de extinción, ya que el efecto rescate inducido por dispersión pierde efectividad. Esto significa que los individuos no son capaces de recolonizar áreas muy distantes si su capacidad de movilización se ve truncada (Collingham y Huntley 2000; Dullinger et al. 2015). El riesgo de extinción es aún más alto si el tamaño del hábitat disminuye respecto a la distancia de dispersión.

Sin embargo, es importante dejar claro hasta qué punto puede la dispersión aumentar la resiliencia de la población. Como dijimos antes, dispersiones más largas implican un incremento en la resiliencia de la población, pero ese aumento no es ilimitado. Cada tamaño del hábitat determina una resiliencia máxima que se da a partir de cierta distancia de

dispersión, lo que de nuevo apoya que la fragmentación del hábitat reduce la efectividad del efecto rescate. Este cambio del riesgo de extinción con el tamaño del hábitat nos indica que la preservación del hábitat es un punto clave en la conservación de poblaciones y nos dice los casos para los cuales necesitamos dedicar un mayor esfuerzo en proteger los hábitats de una determinada población.

A continuación, en el Capítulo 7 hemos estudiado una población cercana al equilibrio. La población se encuentra influenciada fluctuaciones ambientales autocorrelacionadas temporalmente (ruido de color). A partir de las ecuaciones que describen la dinámica de la población, hemos obtenido expresiones para las funciones de autocorrelación y correlación cruzada de la población y el ambiente. Estas funciones de correlación dependen de la amplitud del ruido, el acoplo entre ambiente y población, y los tiempos característicos de las fluctuaciones (ambientales y de población).

Las funciones de correlación permiten obtener propiedades útiles de la dinámica de la población. El valor de la función de autocorrelación de las fluctuaciones poblacionales a tiempo cero indica la variabilidad de la población. Por otro lado, el tiempo de correlación de las variables estudiadas es una medida del alcance temporal de su predictibilidad. Para cualquier grupo de parámetros, el tiempo de autocorrelación de la población es mayor que el de las fluctuaciones ambientales. Por último, el máximo retardado de la función de correlación cruzada nos indica cuándo, y con cuánta intensidad, se da la mayor influencia de la variable ambiental sobre las fluctuaciones de la población.

Los resultados presentados en esta tesis nos permiten conocer de forma eficaz la resiliencia de una población frente a condiciones ambientales adversas, así como predecir la evolución próxima de un ecosistema con cierto grado de precisión. Además, dado que la acción humana puede ser estudiada como un agente que afecta los parámetros dinámicos del ecosistema, estos resultados nos permiten evaluar cómo explotar una población sin causar daños irreversibles al ecosistema. Así, este conocimiento más profundo permitirá desarrollar estrategias de repoblación más óptima o formas menos dañinas de explotar los recursos naturales.

Trabajo futuro

Los resultados presentados para modelos de poblaciones espacialemente extendida con efecto Allee (Parte II) dan pie a investigar otros efectos relevantes, como migración externa, explotación, repoblación y forma del hábitat. Nuestro modelo también puede extenderse para estudiar interacciones interespecíficas o como otros factores externos afectan a la población, para así obtener nuevos resultados y aplicaciones.

La migración externa ya ha sido estudiada (Dennis et al. 2016), mostrando que reduce el riesgo de extinción. No obstante, aún está pendiente un estudio de una población con Efecto Allee que considere tanto migración externa como dispersion dentro del ecosistema. Este modelo puede ser especialmente relevante al permitirnos describir la acción humana sobre el ecosistema. En concreto puede añadirse la posibilidad de explotación, que tiene un claro efecto en el riesgo de extinción (Jarillo et al. 2018). Entender claramente cuál es esta dependencia en poblaciones con efecto Allee puede servir para avanzar en estrategias eficaces de conservación de especies, o desarrollar mejores métodos de explotación sostenible. De igual manera, también puede añadirse la repoblación, de modo que podrá cuantificarse claramente el efecto del factor humano en la resiliencia de la especie.

Por otro lado, nuestros trabajos sobre dinámica de poblaciones espacialmente extendidas (Parte II) han tomado un espacio unidimensional como primera aproximación. No obstante, estudios anteriores como (Diamond 1975) muestran que la forma de los hábitats es determinante en la evolución de la especie. En dos dimensiones, además del tamaño del hábitat, hay que tener en cuenta otros factores. Por ejemplo, debido al frente de propagación de individuos, hábitats circulares permiten fácilmente la dispersion a lo largo del mismo. Por tanto, hábitats con formas más circulares son más óptimos para la supervivencia de una especie que aquellos con formas alargadas o con peninsulas. Entonces, buscar una generalización para dos dimensiones parece una necesidad para estudiar sistemas reales con mayor precisión.

Nuestro estudio sobre predictibilidad de una población afectada por fluctuaciones ambientales temporalmente autocorrelacionadas (Parte III) tiene en cuenta una población uniforme cerca del equilibrio. Este estudio puede ser ampliado considerando fluctuaciones mayores, que invaliden la aproximación lineal en torno al equilibrio. Con esta ampliación se podrá estudiar sistemas en condiciones más extremas.

Para concluir, las especies no están aisladas, sino que forman parte de un ecosistema. En los estudios incluidos en esta tesis (Capítulos 5-7) no hemos tenido en cuenta explícitamente los efectos de otras especies. Estos efectos pueden ser relevantes en la dinámica de otras poblaciones con las que interactúan. Por tanto, estos estudios pueden ampliarse incluyendo varias especies en interacción. En concreto, estamos trabajando en una ampliación de nuestros modelos para entender las dinámicas de cadenas tróficas bajo la influencia de variaciones de temperatura en varias zonas pesqueras del Océano Atlántico (Proyecto TRIATLAS). Entender estos ecosistemas contribuirá a una mejor gestión de pesquerías.

Las ampliaciones presentadas en esta sección a los modelos incluidos en esta tesis permiten describir una variedad más amplia de ecosistemas con mayor precisión. Así, se podrá entender mejor cómo interactúan dichas poblaciones con los demás componentes del ecosistema, tanto las físicas (como el clima) como las otras especies presentes en el mismo. Por tanto, los

presentes y futuros resultados en esta dirección podrán proporcionar herramientas para proteger mejor poblaciones con mayor riesgo de extinción regional. Adicionalmente, estos resultados permiten desarrollar estrategias de explotación de recursos naturales (entre ellos especies capturadas o cosechadas) más eficientes y menos dañinas para los ecosistemas.

References

Agranov, Tal, and Guy Bunin. 2021. “Extinctions of Coupled Populations, and Rare Event Dynamics under Non-Gaussian Noise.” *Physical Review E* 104 (2): 1–14. https://doi.org/10.1103/PhysRevE.104.024106.

Akaike, Hirotugu. 1974. “A New Look at the Statistical Model Identification.” *IEEE Transactions on Automatic Control*. https://doi.org/10.1109/TAC.1974.1100705.

Allee, W. C. 1931. *Animal Aggregations. A Study in General Sociology.* Chicago: The University of Chicago Press. https://doi.org/10.5962/bhl.title.7313.

Allee, W. C., and G.M. Rosenthal. 1949. “Group Survival Value for Philodina Rosola, A Rotifer.” *Ecology*. https://doi.org/10.2307/1932623.

Allee, W. C., and J. F. Schuett. 1927. “Studies in Animal Aggregations: The Relation between Mass of Animals and Resistance to Colloidal Silver.” *The Biological Bulletin* 53 (5): 301–17. https://doi.org/10.2307/1537055.

Angulo, Elena, Gary W. Roemer, Luděk Berec, Joanna Gascoigne, and Franck Courchamp. 2007. “Double Allee Effects and Extinction in the Island Fox.” *Conservation Biology*. https://doi.org/10.1111/j.1523-1739.2007.00721.x.

Antolin, Michael F., Beatrice Van Horne, Michael D. Berger, Jr., Alisha K. Holloway, Jennifer L. Roach, and Ronald D. Weeks, Jr. 2001. “Effective Population Size and Genetic Structure of a Piute Ground Squirrel (*Spermophilus Mollis*) Population.” *Canadian Journal of Zoology* 79 (1): 26–34. https://doi.org/10.1139/cjz-79-1-26.

Araújo, Márcio S., R. Brian Langerhans, Sean T. Giery, and Craig A. Layman. 2014. “Ecosystem Fragmentation Drives Increased Diet Variation in an Endemic Livebearing Fish of the Bahamas.” *Ecology and Evolution*. https://doi.org/10.1002/ece3.1140.

Atkinson, D. 1994. “Temperature and Organism Size—A Biological Law for Ectotherms?” In , 1–58. https://doi.org/10.1016/S0065-2504(08)60212-3.

Barghathi, Hatem, Skye Tackkett, and Thomas Vojta. 2017. “Extinction Phase Transitions in a Model of Ecological and Evolutionary Dynamics.” *European Physical Journal B* 90 (7): 129. https://doi.org/10.1140/epjb/e2017-80220-7.

Bjørnstad, Ottar N., Rolf A. Ims, and Xavier Lambin. 1999. “Spatial Population Dynamics: Analyzing Patterns and Processes of Population Synchrony.” *Trends in Ecology and Evolution* 14 (11): 427–32. https://doi.org/10.1016/S0169-5347(99)01677-8.

Blasius, Bernd, Amit Huppert, and Lewi Stone. 1999. “Complex Dynamics and Phase Synchronization in Spatially Extended Ecological Systems.” *Nature* 399 (6734): 354–59. https://doi.org/10.1038/20676.

Bonsall, Michael B., Claire A. Dooley, Anna Kasparson, Tom Brereton, David B. Roy, and Jeremy A. Thomas. 2014. “Allee Effects and the Spatial Dynamics of a Locally Endangered Butterfly, the High Brown Fritillary (Argynnis Adippe).” *Ecological Applications* 24 (1): 108–20. https://doi.org/10.1890/13-0155.1.

Brassil, Chad E. 2001. “Mean Time to Extinction of a Metapopulation with an Allee Effect.” *Ecological Modelling* 143 (1–2): 9–16. https://doi.org/10.1016/S0304-3800(01)00351-9.

Braumann, Carlos A. 2007. “Harvesting in a Random Environment: Itô or Stratonovich

Calculus?" *Journal of Theoretical Biology*. https://doi.org/10.1016/j.jtbi.2006.08.029.

Brown, James H, and Astrid Kodric-Brown. 1977. "Turnover Rates in Insular Biogeography: Effect of Immigration on Extinction." *Ecology* 58 (2): 445–49. http://www.jstor.org/stable/1935620.

Brown, Robert. 1828. " XXVII. A Brief Account of Microscopical Observations Made in the Months of June, July and August 1827, on the Particles Contained in the Pollen of Plants; and on the General Existence of Active Molecules in Organic and Inorganic Bodies ." *The Philosophical Magazine*. https://doi.org/10.1080/14786442808674769.

Bruggeman, Douglas J., Thorsten Wiegand, and Néstor Fernández. 2010. "The Relative Effects of Habitat Loss and Fragmentation on Population Genetic Variation in the Red-Cockaded Woodpecker (Picoides Borealis)." *Molecular Ecology*. https://doi.org/10.1111/j.1365-294X.2010.04659.x.

Burnham, KP, and DR Anderson. 2002. "Model Selection and Multimodel Inference: A Practical Information-Theoretic Approach. 2nd Edn. Springer, Berlin." *Bayesian Data Analysis in Ecology Using Linear Models with R, BUGS, and STAN*.

Cabrerizo, Marco J, and Emilio Marañón. 2021. "Temperature Fluctuations in a Warmer Environment: Impacts on Microbial Plankton." *Faculty Reviews*. https://doi.org/10.12703/r/10-9.

Capa-Morocho, Mirian, Belén Rodríguez-Fonseca, and Margarita Ruiz-Ramos. 2014. "Crop Yield as a Bioclimatic Index of El Niño Impact in Europe: Crop Forecast Implications." *Agricultural and Forest Meteorology*. Elsevier B.V. https://doi.org/10.1016/j.agrformet.2014.07.012.

Cazelles, Bernard, and Gérard Boudjema. 2001. "The Moran Effect and Phase Synchronization in Complex Spatial Community Dynamics." *The American Naturalist* 157 (6): 670–76. https://doi.org/10.1086/320624.

Christensen, Villy, Marta Coll, Joe Buszowski, William W.L. Cheung, Thomas Frölicher, Jeroen Steenbeek, Charles A. Stock, Reg A. Watson, and Carl J. Walters. 2015. "The Global Ocean Is an Ecosystem: Simulating Marine Life and Fisheries." *Global Ecology and Biogeography* 24 (5): 507–17. https://doi.org/10.1111/geb.12281.

Clark, Francis, Barry W. Brook, Steven Delean, H. Reşit Akçakaya, and Corey J. A. Bradshaw. 2010. "The Theta-Logistic Is Unreliable for Modelling Most Census Data." *Methods in Ecology and Evolution*. https://doi.org/10.1111/j.2041-210x.2010.00029.x.

Collingham, Yvonne C., and Brian Huntley. 2000. "Impacts of Habitat Fragmentation and Patch Size upon Migration Rates." *Ecological Applications*. https://doi.org/10.1890/1051-0761(2000)010[0131:IOHFAP]2.0.CO;2.

Cotgreave, Peter, and Nicholas J. Gotelli. 2006. "A Primer of Ecology." *The Journal of Animal Ecology*. https://doi.org/10.2307/5745.

Crates, Ross, Laura Rayner, Dejan Stojanovic, Matthew Webb, and Robert Heinsohn. 2017. "Undetected Allee Effects in Australia's Threatened Birds: Implications for Conservation." *Emu - Austral Ornithology* 117 (3): 207–21. https://doi.org/10.1080/01584197.2017.1333392.

Crespo-Miguel, Rodrigo, and Francisco J. Cao-García. 2022. "Predictability of Population Fluctuations." *Mathematics* 10 (17): 3176. https://doi.org/10.3390/math10173176.

Crespo-Miguel, Rodrigo, Javier Jarillo, and Francisco Javier Cao-García. 2022a. “Dispersal-Induced Resilience to Stochastic Environmental Fluctuations in Populations with Allee Effect.” *Physical Review E* 105 (1): 014413. https://doi.org/10.1103/PhysRevE.105.014413.

———. 2022b. “Scaling of Population Resilience with Dispersal Length and Habitat Size.” *Journal of Statistical Mechanics: Theory and Experiment* 2022 (2): 023501. https://doi.org/10.1088/1742-5468/ac4982.

Dennis, Brian. 2002. “Allee Effects in Stochastic Populations.” *Oikos*. https://doi.org/10.1034/j.1600-0706.2002.960301.x.

Dennis, Brian, Laila Assas, Saber Elaydi, Eddy Kwessi, and George Livadiotis. 2016. “Allee Effects and Resilience in Stochastic Populations.” *Theoretical Ecology*. https://doi.org/10.1007/s12080-015-0288-2.

Diamond, Jared M. 1975. “The Island Dilemma: Lessons of Modern Biogeographic Studies for the Design of Natural Reserves.” *Biological Conservation*. https://doi.org/10.1016/0006-3207(75)90052-X.

Dias, Paula C. 1996. “Sources and Sinks in Population Biology.” *Trends in Ecology and Evolution* 11 (8): 326–30. https://doi.org/10.1016/0169-5347(96)10037-9.

Diouf, Ibrahima, Roberto Suárez-Moreno, Belen Rodríguez-Fonseca, Cyril Caminade, Malick Wade, Wassila M. Thiaw, Abdoulaye Deme, et al. 2021. “Oceanic Influence on Seasonal Malaria Incidence in West Africa.” *Weather, Climate, and Society* 14 (1): 287–302. https://doi.org/10.1175/wcas-d-20-0160.1.

Dullinger, Stefan, Nicolas Dendoncker, Andreas Gattringer, Michael Leitner, Thomas Mang, Dietmar Moser, Caspar A. Mücher, et al. 2015. “Modelling the Effect of Habitat Fragmentation on Climate-Driven Migration of European Forest Understorey Plants.” *Diversity and Distributions*. https://doi.org/10.1111/ddi.12370.

Einstein, A. 1905. “Über Die von Der Molekularkinetischen Theorie Der Wärme Geforderte Bewegung von in Ruhenden Flüssigkeiten Suspendierten Teilchen.” *Annalen Der Physik*. https://doi.org/10.1002/andp.19053220806.

Engen, Steinar. 2007. “Stochastic Growth and Extinction in a Spatial Geometric Brownian Population Model with Migration and Correlated Noise.” *Mathematical Biosciences* 209 (1): 240–55. https://doi.org/10.1016/j.mbs.2006.08.011.

Engen, Steinar, Oyvind Bakke, and Aminul Islam. 1998. “Demographic and Environmental Stochasticity-Concepts and Definitions.” *Biometrics*. https://doi.org/10.2307/2533838.

Engen, Steinar, Russell Lande, and Bernt-Erik Sæther. 2002. “The Spatial Scale of Population Fluctuations and Quasi-Extinction Risk.” *The American Naturalist* 160 (4): 439–51. https://doi.org/10.1086/342072.

Engen, Steinar, Russell Lande, and Bernt Erik Sæther. 2003. “Demographic Stochasticity and Allee Effects in Populations with Two Sexes.” *Ecology*. https://doi.org/10.1890/02-0123.

Eriksson, Anders, Federico Elías-Wolff, Bernhard Mehlig, and Andrea Manica. 2014. “The Emergence of the Rescue Effect from Explicit Within- and between-Patch Dynamics in a Metapopulation.” *Proceedings of the Royal Society B: Biological Sciences* 281 (1780): 20133127. https://doi.org/10.1098/rspb.2013.3127.

Fahrig, Lenore. 1997. “Relative Effects of Habitat Loss and Fragmentation on Population

Extinction." *The Journal of Wildlife Management*. https://doi.org/10.2307/3802168.

———. 2003. "Effects of Habitat Fragmentation on Biodiversity." *Annual Review of Ecology, Evolution, and Systematics*. https://doi.org/10.1146/annurev.ecolsys.34.011802.132419.

Fernández-Grande, Miguel Ángel, and Francisco Javier Cao-Garcia. 2020. "Spatial Scales of Population Synchrony Generally Increases as Fluctuations Propagate in a Two Species Ecosystem," December. http://arxiv.org/abs/2012.11043.

Frankham, Richard, and Katherine Ralls. 1998. "Inbreeding Leads to Extinction." *Nature*. https://doi.org/10.1038/33022.

Fujiwara, Masami, and Takenori Takada. 2017. "Environmental Stochasticity." In *ELS*, 1–8. Wiley. https://doi.org/10.1002/9780470015902.a0021220.pub2.

García-Ojalvo, J., J. M. Sancho, and L. Ramírez-Piscina. 1992. "Generation of Spatiotemporal Colored Noise." *Physical Review A* 46 (8): 4670–75. https://doi.org/10.1103/PhysRevA.46.4670.

Gardiner, Crispin W. 2009. "Handbook of Stochastic Methods: For Physics,Chemistry and the Natural Sciences（second Edition）." *Book*.

Gilpin, M. E., and F. J. Ayala. 1973. "Global Models of Growth and Competition." *Proceedings of the National Academy of Sciences of the United States of America*. https://doi.org/10.1073/pnas.70.12.3590.

Gómara, Iñigo, Belén Rodríguez-Fonseca, Elsa Mohino, Teresa Losada, Irene Polo, and Marta Coll. 2021. "Skillful Prediction of Tropical Pacific Fisheries Provided by Atlantic Niños." *Environmental Research Letters* 16 (5): 054066. https://doi.org/10.1088/1748-9326/abfa4d.

Gotelli, Nicholas J. 1991. "Metapopulation Models: The Rescue Effect, the Propagule Rain, and the Core-Satellite Hypothesis." *The American Naturalist*. https://doi.org/10.1086/285249.

Gotelli, Nicholas J., and Walter G. Kelley. 1993. "A General Model of Metapopulation Dynamics." *Oikos*. https://doi.org/10.2307/3545306.

Gotelli, Nicholas J. 2008. *A Primer of Ecology, 4th Ed. Sinauer Associates, Sunderland, Massachusetts.* Gotelli2008.

Gravel, Dominique, François Massol, and Mathew A. Leibold. 2016. "Stability and Complexity in Model Meta-Ecosystems." *Nature Communications* 7 (1): 12457. https://doi.org/10.1038/ncomms12457.

Greenman, J. V., and T. G. Benton. 2003. "The Amplification of Environmental Noise in Population Models: Causes and Consequences." *The American Naturalist* 161 (2): 225–39. https://doi.org/10.1086/345784.

Hackney, E. E., and J. B. McGraw. 2001. "Experimental Demonstration of an Allee Effect in American Ginseng." *Conservation Biology*. https://doi.org/10.1046/j.1523-1739.2001.98546.x.

Hagberg, Aric, and Ehud Meron. 1994. "Complex Patterns in Reaction-diffusion Systems: A Tale of Two Front Instabilities." *Chaos: An Interdisciplinary Journal of Nonlinear Science* 4 (3): 477–84. https://doi.org/10.1063/1.166047.

Halley, John M. 1996. "Ecology, Evolution and 1f-Noise." *Trends in Ecology & Evolution* 11 (1): 33–37. https://doi.org/10.1016/0169-5347(96)81067-6.

Hansen, Brage B., Vidar Grøtan, Ivar Herfindal, and Aline M. Lee. 2020. “The Moran Effect Revisited: Spatial Population Synchrony under Global Warming.” *Ecography*. https://doi.org/10.1111/ecog.04962.

Hanski, I., and M. Gyllenberg. 1993. “Two General Metapopulation Models and the Core-Satellite Species Hypothesis.” *American Naturalist*. https://doi.org/10.1086/285527.

Hasselmann, K. 1976. “Stochastic Climate Models Part I. Theory.” *Tellus* 28 (6): 473–85. https://doi.org/10.3402/tellusa.v28i6.11316.

Heino, Mikko. 1998. “Noise Colour, Synchrony and Extinctions in Spatially Structured Populations.” *Oikos*. https://doi.org/10.2307/3546851.

Heino, Mikko, Veijo Kaitala, Esa Ranta, and Jan Lindstrom. 1997. “Synchronous Dynamics and Rates of Extinction in Spatially Structured Populations.” *Proceedings of the Royal Society B: Biological Sciences* 264 (1381): 481–86. https://doi.org/10.1098/rspb.1997.0069.

Heino, Mikko, Jörgen Ripa, and Veijo Kaitala. 2000. “Extinction Risk under Coloured Environmental Noise.” *Ecography*. https://doi.org/10.1111/j.1600-0587.2000.tb00273.x.

Herbener, Kathy W., Simon J. Tavener, and Thompson T. Hobbs. 2010. “The Distinct Effects of Habitat Fragmentation on Population Size.” *Theoretical Ecology*. https://doi.org/10.1007/s12080-010-0097-6.

Hogg, David W, Jo Bovy, and Dustin Lang. 2010. “Data Analysis Recipes: Fitting a Model to Data.” arXiv.org. https://arxiv.org/pdf/1008.4686.pdf.

Iizumi, Toshichika, Jing Jia Luo, Andrew J. Challinor, Gen Sakurai, Masayuki Yokozawa, Hirofumi Sakuma, Molly E. Brown, and Toshio Yamagata. 2014. “Impacts of El Niño Southern Oscillation on the Global Yields of Major Crops.” *Nature Communications* 5 (May): 1–7. https://doi.org/10.1038/ncomms4712.

IPCC. 2012. *Managing the Risks of Extreme Events and Disasters to Advance Climate Change Adaptation*. Edited by Christopher B. Field, Vicente Barros, Thomas F. Stocker, Qin Dahe, David Jon Dokken, Kristie L. Ebi, Michael D. Mastrandrea, et al. *Managing the Risks of Extreme Events and Disasters to Advance Climate Change Adaptation*. https://doi.org/10.1017/cbo9781139177245.

Jager, Henriette I., Eric A. Carr, and Rebecca A. Efroymson. 2006. “Simulated Effects of Habitat Loss and Fragmentation on a Solitary Mustelid Predator.” *Ecological Modelling*. https://doi.org/10.1016/j.ecolmodel.2005.05.025.

Jarillo, Javier, Bernt-Erik Sæther, Steinar Engen, and Francisco Javier Cao-García. 2020. “Spatial Scales of Population Synchrony in Predator-Prey Systems.” *American Naturalist* 195 (2): 216–30. https://doi.org/10.1086/706913.

Jarillo, Javier, Bernt Erik Sæther, Steinar Engen, and Francisco J. Cao. 2018. “Spatial Scales of Population Synchrony of Two Competing Species: Effects of Harvesting and Strength of Competition.” *Oikos* 127 (10): 1459–70. https://doi.org/10.1111/oik.05069.

Jong, G. de, and T. M. van der Have. 2009. “Temperature Dependence of Development Rate, Growth Rate and Size: From Biophysics to Adaptation.” In *Phenotypic Plasticity of Insects: Mechanisms and Consequence*, 461–526. Plymouth, UK: Science Publishers, Inc.

Kamenev, Alex, Baruch Meerson, and Boris Shklovskii. 2008. “How Colored Environmental Noise Affects Population Extinction.” *Physical Review Letters* 101 (26): 268103. https://doi.org/10.1103/PhysRevLett.101.268103.

Kanarek, Andrew R., Colleen T. Webb, Michael Barfield, and Robert D. Holt. 2015. “Overcoming Allee Effects through Evolutionary, Genetic, and Demographic Rescue.” *Journal of Biological Dynamics* 9 (1): 15–33. https://doi.org/10.1080/17513758.2014.978399.

Karlin, Samuel, and Howard M Taylor. 1967. *A First Course in Stochastic Processes 2nd Ed. SIAM Review*. https://doi.org/10.1137/1009056.

Keitt, Timothy H, Mark A Lewis, and Robert D Holt. 2001. “Allee Effects , Invasion Pinning , and Species ’ Borders.” *The American Naturalist* 157 (2): 203–16.

Kent, Adam, C. Patrick Doncaster, and Tim Sluckin. 2003. “Consequences for Predators of Rescue and Allee Effects on Prey.” *Ecological Modelling* 162 (3): 233–45. https://doi.org/10.1016/S0304-3800(02)00343-5.

Kenward, R. E. 2006. “Hawks and Doves: Factors Affecting Success and Selection in Goshawk Attacks on Woodpigeons.” *The Journal of Animal Ecology*. https://doi.org/10.2307/3793.

Kessler, David A., Zvi Ner, and Leonard M. Sander. 1998. “Front Propagation: Precursors, Cutoffs, and Structural Stability.” *Physical Review E* 58 (1): 107. https://doi.org/10.1103/PhysRevE.58.107.

Kumar, Ankit, and Balram Dubey. 2020. “Dynamics of Prey–Predator Model with Strong and Weak Allee Effect in the Prey with Gestation Delay.” *Nonlinear Analysis: Modelling and Control* 25 (3). https://doi.org/10.15388/namc.2020.25.16663.

Kuparinen, Anna, and Jeffrey A. Hutchings. 2014. “Increased Natural Mortality at Low Abundance Can Generate an Allee Effect in a Marine Fish.” *Royal Society Open Science*. https://doi.org/10.1098/rsos.140075.

Laakso, Jouni, Katja Löytynoja, and Veijo Kaitala. 2003. “Environmental Noise and Population Dynamics of the Ciliated Protozoa Tetrahymena Thermophila in Aquatic Microcosms.” *Oikos*. https://doi.org/10.1034/j.1600-0706.2003.12319.x.

Lande, R. 1993. “Risks of Population Extinction from Demographic and Environmental Stochasticity and Random Catastrophes.” *American Naturalist*. https://doi.org/10.1086/285580.

Lande, Russell, Steinar Engen, and Bernt-Erik Saether. 2003. *Stochastic Population Dynamics in Ecology and Conservation*. Oxford University Press. https://doi.org/10.1093/acprof:oso/9780198525257.001.0001.

Lande, Russell, Steinar Engen, and Bernt-Erik Sæther. 1999. “Spatial Scale of Population Synchrony: Environmental Correlation versus Dispersal and Density Regulation.” *The American Naturalist* 154 (3): 271–81. https://doi.org/10.1086/303240.

Law, R, U Dieckmann, and JAJ Metz. 2000. “Introduction.” In *The Geometry of Ecological Interactions: Simplifying Spatial Complexity,* edited by U Dieckmann, R Law, and JAJ Metz, 1–6. Cambridge University Press.

Lee, Aline Magdalena, Bernt-Erik Sæther, and Steinar Engen. 2011. “Demographic Stochasticity, Allee Effects, and Extinction: The Influence of Mating System and Sex Ratio.” *The American Naturalist*. https://doi.org/10.1086/658344.

Lee, AM, Javier Jarillo, Bart Peeters, BB Hansen, FJ Cao-García, Bernt-erik Sæther, and Steinar Engen. 2022. “Population Responses to Harvesting in Fluctuating Environments.” *Climate Research* 86 (January): 79–91. https://doi.org/10.3354/cr01656.

Levins, Richard. 1970. “Some Mathematical Questions in Biology.” In *Some Mathematical*

Questions in Biology.

Lewis, M. A., and P. Kareiva. 1993. "Allee Dynamics and the Spread of Invading Organisms." *Theoretical Population Biology*. https://doi.org/10.1006/tpbi.1993.1007.

Liebhold, Andrew, and Jordi Bascompte. 2003. "The Allee Effect, Stochastic Dynamics and the Eradication of Alien Species." *Ecology Letters*. https://doi.org/10.1046/j.1461-0248.2003.00405.x.

Liebhold, Andrew, Walter D. Koenig, and Ottar N. Bjørnstad. 2004. "Spatial Synchrony in Population Dynamics." *Annual Review of Ecology, Evolution, and Systematics* 35 (1): 467–90. https://doi.org/10.1146/annurev.ecolsys.34.011802.132516.

Liz, Eduardo, and Alfonso Ruiz-Herrera. 2015. "Delayed Population Models with Allee Effects and Exploitation." *Mathematical Biosciences and Engineering* 12 (1): 83–97. https://doi.org/10.3934/mbe.2015.12.83.

Lotze, Heike K., Marta Coll, Anna M. Magera, Christine Ward-Paige, and Laura Airoldi. 2011. "Recovery of Marine Animal Populations and Ecosystems." *Trends in Ecology and Evolution*. https://doi.org/10.1016/j.tree.2011.07.008.

Lowe, Winsor H., Thomas E. Martin, David K. Skelly, and H. Arthur Woods. 2021. "Metamorphosis in an Era of Increasing Climate Variability." *Trends in Ecology & Evolution* 36 (4): 360–75. https://doi.org/10.1016/J.TREE.2020.11.012.

Luis, Angela D., Richard J. Douglass, James N. Mills, and Ottar N. Bjørnstad. 2015. "Environmental Fluctuations Lead to Predictability in Sin Nombre Hantavirus Outbreaks." *Ecology* 96 (6): 1691–1701. https://doi.org/10.1890/14-1910.1.

Malthus, Thomas Robert. 1798. "An Essay on the Principle of Population." *Library*. https://doi.org/10.1093/fmls/cqi148.

Mangel, M., and C. Tier. 1993. "Dynamics of Metapopulations with Demographic Stochasticity and Environmental Catastrophes." *Theoretical Population Biology* 44 (1): 1–31. https://doi.org/10.1006/tpbi.1993.1016.

Mannella, Riccardo, and Peter V.E. McClintock. 2012. "ITÔ versus Stratonovich: 30 Years Later." In *Fluctuation and Noise Letters*. https://doi.org/10.1142/S021947751240010X.

May, R. M. 1973. "Stability and Complexity in Model Ecosystems." *Monographs in Population Biology*. https://doi.org/10.2307/3743.

McDermott, Shana M., and David C. Finnoff. 2016. "Impact of Repeated Human Introductions and the Allee Effect on Invasive Species Spread." *Ecological Modelling* 329 (June): 100–111. https://doi.org/10.1016/j.ecolmodel.2016.03.001.

Méndez, Vicenç, Michael Assaf, Axel Masó-Puigdellosas, Daniel Campos, and Werner Horsthemke. 2019. "Demographic Stochasticity and Extinction in Populations with Allee Effect." *Physical Review E*. https://doi.org/10.1103/PhysRevE.99.022101.

Méndez, Vicenç, Daniel Campos, and Frederic Bartumeus. 2014. *Stochastic Foundations in Movement Ecology*. *Stochastic Foundations in Movement Ecology*. https://doi.org/10.1007/978-3-642-39010-4.

Molnár, Péter K., Andrew E. Derocher, Mark A. Lewis, and Mitchell K. Taylor. 2008. "Modelling the Mating System of Polar Bears: A Mechanistic Approach to the Allee Effect." *Proceedings of the Royal Society B: Biological Sciences*. https://doi.org/10.1098/rspb.2007.1307.

Moran, Patrick Alfred Pierce. 1953. “The Statistical Analysis of the Canadian Lynx Cycle. II. Synchronization and Meteorology.” *Australian Journal of Zoology* 1 (3): 291–98. https://doi.org/10.1071/ZO9530291.

Morozov, Andrew, and Jean Christophe Poggiale. 2012. “From Spatially Explicit Ecological Models to Mean-Field Dynamics: The State of the Art and Perspectives.” *Ecological Complexity* 10: 1–11. https://doi.org/10.1016/j.ecocom.2012.04.001.

Mouquet, Nicolas, and Michel Loreau. 2003. “Community Patterns in Source-Sink Metacommunities.” *The American Naturalist* 162 (5): 544–57. https://doi.org/10.1086/378857.

Moynihan, Martin H., and H. Kruuk. 2010. “Predators and Anti-Predator Behaviour of the Black-Headed Gull (Larus Ridibundus L.).” *Bird-Banding*. https://doi.org/10.2307/4511169.

Nowicki, Piotr, Simona Bonelli, Francesca Barbero, and Emilio Balletto. 2009. “Relative Importance of Density-Dependent Regulation and Environmental Stochasticity for Butterfly Population Dynamics.” *Oecologia* 161 (2): 227–39. https://doi.org/10.1007/s00442-009-1373-2.

Odum, Howard T., and W. C. Allee. 2006. “A Note on the Stable Point of Populations Showing Both Intraspecific Cooperation and Disoperation.” *Ecology*. https://doi.org/10.2307/1931412.

Paaijmans, Krijn P., Rebecca L. Heinig, Rebecca A. Seliga, Justine I. Blanford, Simon Blanford, Courtney C. Murdock, and Matthew B. Thomas. 2013. “Temperature Variation Makes Ectotherms More Sensitive to Climate Change.” *Global Change Biology* 19 (8): 2373–80. https://doi.org/10.1111/gcb.12240.

Palmqvist, Eva, and Per Lundberg. 1998. “Population Extinctions in Correlated Environments.” *Oikos* 83 (2): 359. https://doi.org/10.2307/3546850.

Panja, Debabrata. 2004. “Effects of Fluctuations on Propagating Fronts.” *Physics Reports* 393 (2): 87–174. https://doi.org/10.1016/j.physrep.2003.12.001.

Petchey, Owen L. 2000. “Environmental Colour Affects Aspects of Single-Species Population Dynamics.” *Proceedings of the Royal Society of London. Series B: Biological Sciences* 267 (1445): 747–54. https://doi.org/10.1098/RSPB.2000.1066.

Pimm, Stuart L., and Andrew Redfearn. 1988. “The Variability of Population Densities.” *Nature* 334 (6183): 613–14. https://doi.org/10.1038/334613a0.

Pires, Marcelo A., and Sílvio M. Duarte Queirós. 2019. “Optimal Dispersal in Ecological Dynamics with Allee Effect in Metapopulations.” Edited by Sergio Gómez. *PLOS ONE* 14 (6): e0218087. https://doi.org/10.1371/journal.pone.0218087.

Pulliam, H. Ronald. 1988. “Sources, Sinks, and Population Regulation.” *The American Naturalist* 132 (5): 652–61. https://doi.org/10.1086/284880.

Ralls, Katherine, Richard Frankham, and Jonathan D. Ballou. 2013. “Inbreeding and Outbreeding.” In *Encyclopedia of Biodiversity: Second Edition*. https://doi.org/10.1016/B978-0-12-384719-5.00073-3.

Ranta, E., V. Kaitala, J. Lindstrom, and H. Linden. 1995. “Synchrony in Population Dynamics.” *Proceedings of the Royal Society B: Biological Sciences*. https://doi.org/10.1098/rspb.1995.0184.

Ranta, Esa, Veijo Kaitala, Jan Lindström, Eero Helle, and Jan Lindstrom. 1997. “The Moran Effect and Synchrony in Population Dynamics.” *Oikos*. https://doi.org/10.2307/3545809.

Reuman, Daniel C., Robert F. Costantino, Robert A. Desharnais, and Joel E. Cohen. 2008. “Colour of Environmental Noise Affects the Nonlinear Dynamics of Cycling, Stage-Structured Populations.” *Ecology Letters*. https://doi.org/10.1111/j.1461-0248.2008.01194.x.

Ribeiro, Fabiano L., and Kayo N. Ribeiro. 2015. “A One Dimensional Model of Population Growth.” *Physica A: Statistical Mechanics and Its Applications* 434 (September): 201–10. https://doi.org/10.1016/j.physa.2015.03.021.

Ripa, J., and P. Lundberg. 1996. “Noise Colour and the Risk of Population Extinctions.” *Proceedings of the Royal Society B: Biological Sciences*. https://doi.org/10.1098/rspb.1996.0256.

Ripa, Jörgen, and Esa Ranta. 2007. “Biological Filtering of Correlated Environments: Towards a Generalised Moran Theorem.” *Oikos* 116 (5): 783–92.

Sæther, Bernt-Erik, Thor Harald Ringsby, and Eivin Røskaft. 1996. “Life History Variation, Population Processes and Priorities in Species Conservation: Towards a Reunion of Research Paradigms.” *Oikos* 77 (2): 217. https://doi.org/10.2307/3546060.

Saltz, David, Daniel I. Rubenstein, and Gary C. White. 2006. “The Impact of Increased Environmental Stochasticity Due to Climate Change on the Dynamics of Asiatic Wild Ass.” *Conservation Biology* 20 (5): 1402–9. https://doi.org/10.1111/j.1523-1739.2006.00486.x.

Schreiber, Sebastian J. 2010. “Interactive Effects of Temporal Correlations, Spatial Heterogeneity and Dispersal on Population Persistence.” In *Proceedings of the Royal Society B: Biological Sciences*. https://doi.org/10.1098/rspb.2009.2006.

Seferian, R., Laurent Bopp, Marion Gehlen, Didier Swingedouw, Juliette Mignot, Eric Guilyardi, and Jérôme Servonnat. 2014. “Multiyear Predictability of Tropical Marine Productivity.” *Proceedings of the National Academy of Sciences* 111 (32): 11646–51. https://doi.org/10.1073/pnas.1315855111.

Shaffer, Mark. 1987. “Minimum Viable Populations: Coping with Uncertainty.” In *Viable Populations for Conservation*, 69–86. Cambridge University Press. https://doi.org/10.1017/CBO9780511623400.006.

Spagnolo, B., D. Valenti, and A. Fiasconaro. 2004. “Noise in Ecosystems: A Short Review.” *Mathematical Biosciences and Engineering* 1 (1): 185–211. https://doi.org/10.3934/mbe.2004.1.185.

Spanio, Tommaso, Jorge Hidalgo, and Miguel A. Muñoz. 2017. “Impact of Environmental Colored Noise in Single-Species Population Dynamics.” *Physical Review E* 96 (4): 042301. https://doi.org/10.1103/PhysRevE.96.042301.

Surendran, Anudeep, Michael J. Plank, and Matthew J. Simpson. 2020. “Population Dynamics with Spatial Structure and an Allee Effect.” *Proceedings of the Royal Society A: Mathematical, Physical and Engineering Sciences* 476 (2242): 20200501. https://doi.org/10.1098/rspa.2020.0501.

Vercken, E., A. M. Kramer, P. C. Tobin, and J. M. Drake. 2011. “Critical Patch Size Generated by Allee Effect in Gypsy Moth, Lymantria Dispar (L.).” *Ecology Letters*. https://doi.org/10.1111/j.1461-0248.2010.01569.x.

Verhulst, P F. 1838. “Notice Sur La Loi Que La Population Suit Dans Son Accroissement.” *Correspondance Mathématique et Physique*.

Villa Martín, Paula, Juan A. Bonachela, Simon A. Levin, and Miguel A. Muñoz. 2015. “Eluding Catastrophic Shifts.” *Proceedings of the National Academy of Sciences* 112 (15): E1828–36. https://doi.org/10.1073/pnas.1414708112.

Wagenius, Stuart, Eric Lonsdorf, and Claudia Neuhauser. 2007. “Patch Aging and the S-Allee Effect: Breeding System Effects on the Demographic Response of Plants to Habitat Fragmentation.” *American Naturalist*. https://doi.org/10.1086/511313.

Watters, George M., Robert J. Olson, Robert C. Francis, Paul C. Fiedler, Jeffrey J. Polovina, Stephen B. Reilly, Kerim Y. Aydin, et al. 2003. “Physical Forcing and the Dynamics of the Pelagic Ecosystem in the Eastern Tropical Pacific: Simulations with ENSO-Scale and Global-Warming Climate Drivers.” *Canadian Journal of Fisheries and Aquatic Sciences* 60 (9): 1161–75. https://doi.org/10.1139/f03-100.

Way, M. J., and C. J. Banks. 1967. “Intra-specific Mechanisms in Relation to the Natural Regulation of Numbers of Aphis Fabae Scop.” *Annals of Applied Biology*. https://doi.org/10.1111/j.1744-7348.1967.tb04428.x.

Weissmann, Haim, and Nadav M. Shnerb. 2014. “Stochastic Desertification.” *Epl* 106 (2): 28004. https://doi.org/10.1209/0295-5075/106/28004.

Windus, Alastair, and Henrik Jeldtoft Jensen. 2007. “Allee Effects and Extinction in a Lattice Model.” *Theoretical Population Biology*. https://doi.org/10.1016/j.tpb.2007.07.006.

Zuo, Wenyun, Melanie E. Moses, Geoffrey B. West, Chen Hou, and James H. Brown. 2012. “A General Model for Effects of Temperature on Ectotherm Ontogenetic Growth and Development.” *Proceedings of the Royal Society B: Biological Sciences* 279 (1734): 1840–46. https://doi.org/10.1098/rspb.2011.2000.